The Physics of Galaxy Clusters

Prof. Dr. Christoph Pfrommer
Leibniz-Institut für Astrophysik Potsdam (AIP)
University of Potsdam

Contents

Chapter 1

Overview and Background

1.1 Why are Galaxy Clusters Interesting?

1.1.1 General Syllabus

Galaxy clusters are fascinating objects as they lie at the *cross-roads of astrophysics and cosmology,* which makes them unique tools for answering questions that reach into both areas. Let me explain to you why this is by lying out the general syllabus.

1. **Overview and background.** We will become familiar with the various appearances of clusters in a number of different observational windows; each of which allows us to probe physics that is either specific to a waveband or probes a common feature of a given cluster. We will encounter a vast range of (length and time) scales as well as physical processes. To master this problem, we need to introduce the powerful technique of *order of magnitude estimates,* a very useful tool for contemporary research in astrophysics that we will frequently use in the course of these lectures.

2. **Evolution of the dark component.** Most of the matter in the universe is in form of dark matter that interacts primarily gravitationally with baryonic matter (that is described by the standard model of particle physics). Galaxy clusters are the largest gravitationally collapsed objects. Hence, they represent a fair sample of the universe and are also dominated by dark matter. We will first learn how (the dark component of) a cluster forms and grows. This knowledge is the basis for using clusters as cosmological tools.

3. **Evolution of the baryonic component.** We will then encounter the rich and interesting astrophysics that governs the assembly and evolution of baryons in clusters. This chapter starts with basic thermodynamics and conservation laws and ends with plasma and high-energy astrophysics.

4. **Cluster physics across wavelengths.** We will see how we can take advantage of these physical processes to observe clusters and deepen our understanding of the underlying fundamental (astro-) physics.

I will briefly introduce and overview the main motivation to study clusters and present the concepts that we will develop in these lectures. I hope that those concepts will be of good use for you in your further career as (astro-)physicist (even if you won't be studying galaxy clusters).

1.1.2 Tools for Cosmology

- Galaxy clusters are the largest and most massive gravitationally bound structures known in the Universe. As such, they represent the latest stage of the structure formation, presently assembling through mergers of smaller groups of galaxies and gas accretion. Hence they provide us with the opportunity to study an "ecosystem" – a volume that is a high-density microcosm of the rest of the Universe.

- At the same time, clusters are extremely rare events, forming at sites of constructive interference of long waves in the primordial density fluctuations. Hence, they are very sensitive tracers of the growth of structure in the universe and the cosmological parameters governing it, which puts them into focus of constraining the properties of Dark Energy or to test whether our understanding of gravity is complete.

- What are the most basic questions one could ask about clusters? And what are the concepts that we will develop to answer those?

    1. **When and where do clusters form?** We will learn how structures grow from tiny perturbations to non-linear structures and how we describe these by appropriate statistics, in particular correlation functions and power spectra.
    2. **How do clusters form?** We will develop a simplified model of the spherical collapse of a perturbation into a (dark matter) halo that defines all characteristic halo parameters.
    3. **How many clusters are there?** We will study the statistics of collapsed halos giving rise to the Press-Schechter mass function.
    4. **What is the structure of a cluster?** We will analyze halo density profiles and the concept of virial masses.

- These concepts are presented in Chapter 2 and enable us to build the dark matter backbone of clusters – by understanding the structure of the gravitational potential of an individual cluster as well as understanding the distribution of the cluster population as a whole. The next chapter asks what happens if we fill baryons into clusters and addresses the beautiful physics associated with this.

1.1.3 Laboratories for Physics

- Galaxy clusters are excellent laboratories for studying the rich astrophysics of dark matter and baryons. In particular, they allow us to study plasma and high-energy astrophysics under conditions

that are unique and not reproducible anywhere else, especially not in Earth-bound laboratories.

- In Chapter 3, we will "assemble" clusters by starting simple and consecutively adding more complicated physics. First (in Sect. 3.1), we consider only non-radiative physics: what is a stable thermodynamic configuration of the gas in a stratified atmosphere and how do perturbations propagate? Clusters are dynamically evolving systems that are shaken by merging groups and gas accretions, which has two consequences: 1. perturbations of an otherwise stable atmosphere can induce vortical motions that feed turbulence and 2. shock waves can be excited that irreversibly change the thermodynamical cluster state, building a new equilibrium configuration that we will characterize. We finally develop powerful cluster scaling relations that link cluster observables to fundamental cluster properties such as its mass. Its evolution differs for different cosmologies and as such, allows to solve for cosmological parameters. However, the scaling relations are intertwined with cluster physics which causes significant modifications of the scaling laws. While this enables us to infer details about complex baryonic processes in clusters, it also complicates the inference of cosmological parameters.

- In a second step (Sect. 3.2), we explore radiative gas physics, namely radiative cooling, star formation, and energy feedback by exploding stars in galaxies (supernovae) and accreting supermassive black holes that are thought to exist at the center of every galaxy. Detailed physical processes close to the Schwarzschild horizon are able to launch relativistic outflows that carry enormous momentum and energy to macroscopic scales in clusters, thereby modifying its thermodynamical structure in an important way. How this exactly works is currently under intense investigation. We will learn about the strength and weaknesses of various promising suggestions, some of which include transport processes of gas (turbulence, conduction).

- Last but certainly not least (Sect. 3.3), we will discover the physics of non-thermal processes such as magnetic fields and relativistic particle populations in galaxy clusters. We discuss proposals for the origin and transport of cluster magnetic fields and how magnetic fields modify hydrodynamic turbulence. Moreover, I present basic concepts how particles get accelerated to relativistic energies and how they interfere with the thermal plasma of a cluster, an exciting cutting-edge topic in cluster research. Those can be directly observed in form of giant radio relics and halos that constitute a puzzling glow of the outer fringes as well as entire galaxy clusters and enable us to watch powerful shocks and plasma physics at work.

1.1.4 Galaxy Formation under a Magnifying Glass

- Observing galaxies in the optical wavelength regime and realizing that they like to cluster together was the first window to galaxy clusters (not surprisingly as the name suggests). Even today, there are many interesting questions about galaxy formation that take advantage of the increased density of a cluster environment, which accelerates the formation time of galaxies and enables us look at ancient relics of galaxy formation.
- However, a cluster does not simply represent a museum that conserves galaxy properties and supports a passive aging of the stellar populations within them. Instead, the high galaxy density in a cluster environment transforms galaxy populations via different effects, including ram pressure, tidal effects, and dynamical friction, which we will all study.
- We will learn how the virial theorem can be used to weight a galaxy cluster. It is interesting to compare the masses obtained from this method to another approach that assumes the equation of hydrostatic equilibrium of the cluster gas.
- Finally, galaxy clusters literally act as magnifying glasses for very distant galaxies that happen to be in projection behind a massive cluster. The processes of gravitational lensing not only magnifies the galaxies' surface brightness but also increases their solid angle on the sky. We will review the theory of gravitational lensing, derive the lens equation, and discuss the lensing potential. This represents a third, independent method of weighting clusters.

1.1.5 General Remarks

This is a course in the Masters program. The lectures aim at students who

- wish to extend and deepen their understanding of theoretical physics;
- are interested in astronomy and astrophysics; or
- (intend to) carry out a masters thesis or Ph.D. dissertation on an astronomical or astrophysical subject.

I assume basic knowledge of *Cosmology*. While this is not absolutely necessary to follow most of the lectures, I recommand working through the *Cosmology* lecture notes by Prof. Bartelmann. You can download a revised version freely from my home page if you want to refresh your memory.

1.2 What Characterizes a Galaxy Cluster?

A galaxy cluster looks different, depending on how you look at it. Using observations at various wavelengths, we get a wealth of diverse insights into physics. This section is meant to provide a general overview of the various appearances of clusters in a number of different observational windows. Rather than lying out the most complete and accurate description, I try to convene the basic concepts by using the powerful technique of *order of magnitude estimates*, and leave the detailed discussion of the physics to later chapters.

1.2.1 Optical Window

- In a rich galaxy cluster, there are $\sim 10^3$ galaxies that have to good approximation a Gaussian velocity distribution with a dispersion $\sigma_v \approx 1200\,\mathrm{km\ s^{-1}}$. The typical radius of such a cluster is

$$r_{\rm cl} \approx 3\ \mathrm{Mpc} \approx 10^7\ \mathrm{lyr} \approx 10^{25}\ \mathrm{cm}. \tag{1.1}$$

  This defines a dynamical cluster timescale, $t \approx r_{\rm cl}/\sigma_v \approx 2$ Gyr.

- Assuming that the cluster is a closed system in dynamical equilibrium, the virial theorem relates the kinetic energy, $E_{\rm kin}$, of a galaxy of mass $M_{\rm gal}$ to its potential energy, $E_{\rm pot}$,

$$2E_{\rm kin} + E_{\rm pot} = 0, \tag{1.2}$$

$$M_{\rm gal}\sigma_v^2 - \frac{GM_{\rm cl}M_{\rm gal}}{r_{\rm cl}} = 0, \tag{1.3}$$

  where G is Newtons gravitational constant. Solving for the the gravitating mass of a cluster, $M_{\rm cl}$, we get

$$\begin{aligned} M_{\rm cl} = \frac{r_{\rm cl}\sigma_v^2}{G} &\approx \frac{10^{25}\,\mathrm{cm}\,1.4\times10^{16}\,\mathrm{cm^2 s^{-2}}}{7\times10^{-8}\,\mathrm{erg\ cm\ g^{-2}}} \\ &\approx 2\times10^{48}\,\mathrm{g} \approx 10^{15}\,\mathrm{M_\odot} \end{aligned} \tag{1.4}$$

  Note that $M_{\rm cl}$ sources the high velocity dispersion of galaxies. A typical mass range for clusters is $(10^{14}\ldots10^{15})\,\mathrm{M_\odot}$.

- However, by adding up the all the luminous stellar mass within the galaxies, we only get

$$M_* \approx \frac{1}{50}\,M_{\rm cl}. \tag{1.5}$$

  This discrepancy of the gravitating and luminous mass in galaxy clusters was already noted by Fritz Zwicky in the 1930s and led him to postulate the existence of dark matter more than 80 years ago! To be precise, back then the "dark matter" could have been baryonic in form of compact objects (such as planets) or in form of diffuse gas.

1.2.2 X-ray Regime

- With the onset of X-ray astronomy in the 1970s, it was discovered, that galaxy clusters are among the brightest X-ray emitting sources. Improved angular resolution demonstrated that the X-rays were not emitted by individual point sources but instead the entire galaxy cluster is glowing in X-rays, filling in the volume in between the galaxies. What emission process could produce X-rays? There are three possibilities:

  1. bremsstrahlung emission of hot thermal electrons,
  2. line emission from recombination of atoms, or
  3. inverse Compton emission: if relativistic electrons interact with low-energy photons (such as those from the cosmic microwave background), they can cool by upscattering these photons into the X-ray regime. This would typically produce power-law spectra that are imprinted by the power-law spectra of the underlying non-thermal relativistic electrons.

- The observed X-ray spectrum instead shows a flat spectrum with an exponential decline that is characteristic of thermal bremsstrahlung emission. Additionally, there were lines imprinted on the spectrum. The bremsstrahlung emissivity scales as $j_\mathrm{X} \propto n_\mathrm{e} n_\mathrm{i} \sqrt{T_\mathrm{e}}$, where T_e, n_e, and n_i are the electron temperature, density and the ion density, respectively. The amount of X-rays and the location of the exponential break (as well as the location of the individual lines) enable to characterize the properties of the emitting gas,

$$n \approx (10^{-4} \ldots 10^{-3})\,\mathrm{cm}^{-3}, \tag{1.6}$$

$$T \approx (10^{7} \ldots 10^{8})\,\mathrm{K}, \tag{1.7}$$

  i.e., a hot, dilute, and thermal gas (as inferred from the exponential shape of the bremsstrahlung spectrum).

- We usually talk about the temperature of a gas in terms of particle energies,

$$k_\mathrm{B} T \approx (1 \ldots 10)\,\mathrm{keV} = (10^{3} \ldots 10^{4})\,\mathrm{eV}, \tag{1.8}$$

  where k_B is the Boltzmann factor. At these temperatures, most of the elements are fully ionized, except for highly-ionized iron, e.g., hydrogen-like iron which is an iron nucleus with one bound electron, Fe XXVI. The transition energy of such highly ionized iron is

$$\begin{aligned} \text{Fe XXV}: &\quad h\nu \approx Z(Z-1)\,\mathrm{Ry} = 26 \times 25 \times 13.6\,\mathrm{eV} \approx 8.8\,\mathrm{keV} \\ \text{Fe XXVI}: &\quad h\nu \approx Z^2\,\mathrm{Ry} = 26^2 \times 13.6\,\mathrm{eV} \approx 9\,\mathrm{keV}, \end{aligned} \tag{1.9}$$

  i.e., the higher the temperature, the higher the ionization state.

- Assuming that this hot gas with energy $E_{\rm th}$ is in hydrostatic equilibrium with the cluster potential, we have

$$E_{\rm th} = E_{\rm pot}, \tag{1.10}$$

$$\frac{3}{2} k_{\rm B} T = \mu m_{\rm p} \frac{G M_{\rm cl}}{r_{\rm cl}}, \tag{1.11}$$

  where $m_{\rm p}$ is the proton mass and the mean molecular weight of primordial gas is given by $\mu = 4/(5X_{\rm H} + 3) \approx 0.588$ for a primordial hydrogen fraction $X_{\rm H} = 0.24$ (see Appendix A.1). Solving for the gravitating mass of a cluster with $k_{\rm B}T = 6$ keV yields

$$\begin{aligned} M_{\rm cl} &= \frac{3}{2} \frac{k_{\rm B} T r_{\rm cl}}{\mu m_{\rm p} G} \approx \frac{1.5 \times 10^{-8}\,{\rm erg}\, 10^{25}\,{\rm cm}}{0.6 \times 1.7 \times 10^{-24}\,{\rm g}\, 0.7 \times 10^{-8}\,{\rm erg\,cm\,g^{-2}}} \\ &\approx 2 \times 10^{48}\,{\rm g} \approx 10^{15}\,{\rm M}_\odot. \end{aligned} \tag{1.12}$$

- Resolved X-ray imaging of a galaxy cluster produces an X-ray surface brightness map. Deprojection enables us to back out the mass density profile. Integrating that over the cluster volume yields the total gas mass,

$$M_{\rm gas} \approx \frac{1}{7} M_{\rm cl}. \tag{1.13}$$

  Hence, we found some of the matter that was "dark" in the optical by looking at a different waveband. The rest cannot be directly seen in any other waveband (at least no significant amounts). It only can be indirectly inferred through its gravitational interaction. We call this "dark matter", which reflects our ignorance of the composition. It dominates the total cluster mass and is mostly responsible for the gravitational cluster potential.

- We can now summarize an inventory of cluster mass

$$\begin{aligned} M_* &\approx \ \ 2\% : && \text{stars in galaxies,} \\ M_{\rm gas} &\approx 13\% : && \text{hot gas } (1 - 10\,{\rm keV}), \\ M_{\rm dm} &\approx 85\% : && \text{dark matter.} \end{aligned} \tag{1.14}$$

  The value of the baryon fraction in a cluster of $f_{\rm b,clus} \approx 0.15$ is somewhat smaller than the cosmic mean of $f_{\rm b,clus} \approx 0.166$. This points to interesting physics, including non-gravitational energy input from supernovae and super-massive black holes. Interestingly, $f_{\rm b,clus}$ declines toward less massive clusters in which those feedback processes have a comparably larger impact because of the shallower cluster potential.

1.2.3 Gravitational Lensing

- Galaxy clusters or galaxies act as gravitational lenses for galaxies behind them. The processes of gravitational lensing not only magnifies the surface brightness of the source galaxies but also increases their solid angle on the sky. According to general relativity, light travels on geodesics (straightest possible lines) through curved space time. Mass acts as a source of gravity, curving space time at the location of a lensing galaxy cluster or galaxy and causing the light rays to be deflected by the gravitational potential of the lensing object. This causes a single galaxy to be mapped onto multiple images (or even a so-called Einstein ring, provided that we have a very symmetric configuration and a point-like source). We define the angular diameter distance to the light-deflecting cluster or galaxy, D_l, the distance to the source galaxy, D_s, and the angular diameter distance between deflector and source, D_ls. The drawing on the right explains the geometry of a lensing system.

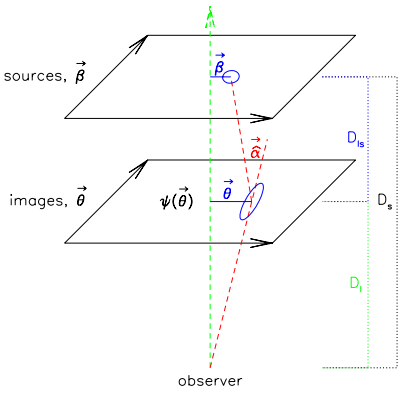

Geometry of a gravitational lensing system.

- Later on in the lectures, we will derive the Einstein radius θ_E. We state the result and insert some values to get an idea about the involved angular scales.

$$\theta_\mathrm{E} = \left[\frac{4GM(\theta_\mathrm{E})}{c^2}\frac{D_\mathrm{ls}}{D_\mathrm{l}D_\mathrm{s}}\right]^{1/2} \tag{1.15}$$

$$\approx 3'' \left(\frac{M}{10^{12}\,M_\odot}\right)^{1/2}\left(\frac{D}{1\,\mathrm{Gpc}}\right)^{-1/2} \quad \text{(galaxy lensing)} \tag{1.16}$$

$$\approx 30'' \left(\frac{M}{10^{14}\,M_\odot}\right)^{1/2}\left(\frac{D}{1\,\mathrm{Gpc}}\right)^{-1/2} \quad \text{(cluster lensing).} \tag{1.17}$$

  Here, $D = D_\mathrm{l}D_\mathrm{s}/D_\mathrm{ls}$ is the lensing efficiency distance. In the case of galaxy lensing, the approximation of a point lens is justified whereas for cluster lensing, the size of the lens is much larger than the size of the source. This makes a detailed mass modeling necessary since only a fraction of the cluster mass is contained within the Einstein radius and will contribute to the lensing potential. The inferred values of $\theta_\mathrm{E} \approx 30''$ correspond to angular scales of observed giant (tangential) arcs.

- We distinguish two types of lensing:

  1. **Strong lensing** is sensitive to the projected mass within θ_E and leads to radial arcs that are clearly visible in optical images. In this regime, a source can be imaged onto multiple different images.
  2. **Weak lensing** causes weaker distortions of a galaxy image in the tangential direction than cannot be detected on a individual basis because the effect is very small. We need

to assume that orientation of the of neighboring galaxies is random and average over an aperture to detect a weak shear signal that is induced by the gravitational tidal field of the cluster lens.

1.2.4 Sunyaev-Zel'dovich Effect

- The universe is filled with 2.75 K photons of the cosmic microwave background (CMB), which is radiation left behind from the early universe when hydrogen recombined at a redshift of $z \approx 1100$. If such a "cold" photon passes through a galaxy cluster that is filled with "hot" electrons there is the chance that this photon experiences Compton scattering off an electron:

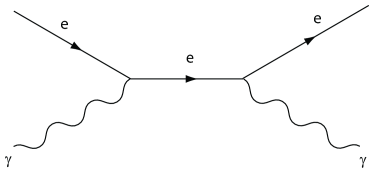

This elastic scattering event conserves the number of CMB photons. However, during this reaction there is a mean energy transfer from the "hot" electron to the "cold" photon (which is the reason why this is called *inverse* Compton scattering). This causes a unique distortion of the CMB spectrum, a decrement in thermodynamic temperature at frequencies below $\nu_0 \approx 220$ GHz, and an excess above. As a result, galaxy clusters appear as holes in the CMB sky at $\nu < \nu_0$ and as extended sources above. This Sunyaev-Zel'dovich (SZ) effect provides a complementary method for detecting and characterizing galaxy clusters.

- How many CMB photons experience inverse Compton scattering on passing through a cluster? To answer this, we compute the optical depth,

$$\tau = \int_0^L n_\mathrm{e} \sigma_\mathrm{T} \mathrm{d}l \approx n_\mathrm{e} \sigma_\mathrm{T} L, \tag{1.18}$$

where L is the effective path length through the hot intracluster medium and σ_T is the Thomson cross section,

$$\begin{aligned} \sigma_\mathrm{T} &\approx 2\pi r_0^2 = 2\pi \left(\frac{e^2}{m_\mathrm{e} c^2} \right)^2 \approx 6 \left[\frac{\left(4.8 \times 10^{-10}\right)^2}{10^{-27}\, 10^{21}} \right] \mathrm{cm}^2 \\ &\approx 6 \left(3 \times 10^{-13}\right)^2 \mathrm{cm}^2 \approx 6 \times 10^{-25}\, \mathrm{cm}^2, \end{aligned} \tag{1.19}$$

where r_0 is the classical electron radius. Hence, we obtain an optical depth

$$\tau = n_\mathrm{e} \sigma_\mathrm{T} L \approx 10^{-4}\, \mathrm{cm}^{-3}\, 6 \times 10^{-25}\, \mathrm{cm}^2\, 10^{25}\, \mathrm{cm} \approx 6 \times 10^{-4} \ll 1. \tag{1.20}$$

This means that on average only one photon in 2000 experiences a scattering event.

- What is the amplitude of the SZ effect? To answer this, we integrate the typical energy gain experienced by a photon in a Compton interaction ($k_\mathrm{B}T_\mathrm{e}/m_\mathrm{e}c^2$) times the differential scattering probability of a photon ($\mathrm{d}\tau = n_\mathrm{e}\sigma_\mathrm{T}\mathrm{d}l$) over the photon path length, D. This is the exact definition of the Compton-y parameter,

$$y = \int_0^D \frac{k_\mathrm{B}T_\mathrm{e}}{m_\mathrm{e}c^2} n_\mathrm{e}\sigma_\mathrm{T}\mathrm{d}l \approx 10^{-2} \times 6 \times 10^{-4} = 6 \times 10^{-6}. \quad (1.21)$$

  Here, we adopted a line-of-sight averaged temperature of our massive ($10^{15}\,\mathrm{M}_\odot$) cluster with $k_\mathrm{B}T_\mathrm{e} \approx 6$ keV. As we can see, the SZ signal is proportional to the integrated electron pressure ($P_\mathrm{e} = k_\mathrm{B}T_\mathrm{e}n_\mathrm{e}$), so the hot gas of the galaxy clusters dominates the effect. This implies that only the path length L through the cluster contributes significantly to the integral that formally extends over the light travel distance, D, from us to the release of the CMB photons. The resulting small value for y implies a small change in intensity that is challenging to detect.

- The thermal SZ effect directly observes the integrated Compton-y parameter which is a measure of the cluster's global gas heat-energy content, a volume-average of the thermal gas pressure,

$$Y = \frac{\sigma_\mathrm{T}}{m_\mathrm{e}c^2} \int_0^{r_\mathrm{cl}} P_\mathrm{e}\mathrm{d}V \propto E_\mathrm{th}(< r_\mathrm{cl}), \quad (1.22)$$

  and this is related to gravitational energy through the virial relation.

- The SZ surface brightness is independent of the redshift a specific cluster is at. This can be easily understood by the following consideration: CMB photon are continuously redshifted from the surface-of-last-scattering to us as the Universe expands. Irrespective of when exactly the inverse-Compton scattering event happened, that energized the photon by a fixed amount of energy, the CMB photons still experience continuous redshifting. This independence on redshift makes the SZ effect a prime candidate for cluster cosmology since it allows for an almost flat selection of cluster at a given mass with redshift. Note that this is quite different for X-ray selected clusters that suffer from the strong flux dimming as the square of the distance.

1.2.5 Synthesis of Observational Windows

Different cluster observables have different strengths and weaknesses. Hence the various windows to clusters are complementary: combining observations of different wavelengths is essential to learn more about clusters. Here is a short (and possibly incomplete) summary about the most important (dis-)advantages of different cluster observables:

- **X-ray window.**
  - It is well-suited for observing cluster centers since $j_X \propto n^2$ which emphasizes dense cluster gas.
  - It allows for high-resolution (arcsec) observations (because of the use of Bragg reflection for focusing X-rays).
  - It is difficult to observe X-ray clusters at large distances due to flux dimming, $F_X \propto L_X/D^2$.
  - If the X-rays are emitted by an inhomogeneous medium, data analyses need to be aware of the bias of the inferred density. In this case, $\bar{n}^2 = \langle n \rangle^2$ is biased high by the clumping factor $C = \langle n^2 \rangle / \langle n \rangle^2$ which is in general not known.
- **Sunyaev-Zel'dovich effect.**
  - It is an excellent tool for studying cluster outskirts as $y \propto P_e = n_e k_B T_e$ and declines less steeply with radius in comparison to the X-ray emission.
  - It is well adapted to detect and observe clusters at large distances because y is independent of redshift (since CMB photons experience continuous redshifting from the surface-of-last-scattering to us as the Universe expands).
  - The comparably small signal-to-noise ratio makes it difficult to detect small clusters and groups.
  - Current resolutions (typically arcmin) preclude the study of detailed cluster physics.
- **Optical window.**
  - Galaxies are collisionless tracers of the gravitational potential and its dynamical state. However, the method needs many galaxies to sample the velocity distribution well enough (which is only possible for large clusters).
  - Gravitational lensing is an invaluable tool for directly probing the total cluster mass which is dominated by dark matter. However, projection of structures along the line-of-sight needs to be accounted for carefully.

1.2.6 Relation to Average Universe

- How does a galaxy cluster relate to the average Universe around us? The critical density of the universe today is

$$\rho_{\rm cr,0} = \frac{3H_0^2}{8\pi G} \approx 10^{-29}\ {\rm g\ cm^{-3}}, \tag{1.23}$$

  where $H_0 \approx 70\ {\rm km\ s^{-1}\ Mpc^{-1}}$ is the Hubble constant that defines the recession velocity of local galaxies, which are at distance d, from us according to Hubble's law, $v = H_0 d$. Using the critical density, we can define the density parameters of total matter, $\Omega_{\rm m}$, and baryons, $\Omega_{\rm b}$,

$$\Omega_{\rm m,0} \equiv \frac{\bar\rho_{\rm m,0}}{\rho_{\rm cr,0}} \approx 0.27, \quad \text{and} \quad \Omega_{\rm b,0} \equiv \frac{\bar\rho_{\rm b,0}}{\rho_{\rm cr,0}} \approx 0.045. \tag{1.24}$$

- Hence the mean matter density of the Universe is

$$\bar\rho_{\rm m,0} \approx 4\times10^{10}\,{\rm M_\odot\ Mpc^{-3}} \approx 10^{9}\,{\rm M_\odot\ Mlyr^{-3}}. \tag{1.25}$$

  Compare this to typical cluster masses $M_{\rm cl} \sim 10^{15}\,{\rm M_\odot}$. In order to form clusters, you need large chunks of volume that contain $10^{15}\,{\rm M_\odot}$. As we will learn during the lectures, only less than 1% of cosmic matter forms an aggregation that makes a large clusters. Hence clusters are extremely rare!

- **Collapse of a cluster.** Typically, we find $\bar\rho_{\rm cl} \sim 10^3\bar\rho_{\rm m,0}$, hence cluster collapse roughly by a factor of 10 in radius. Let's check whether this is consistent with what we have already learned. The mean baryon density of the universe at the present time is

$$\bar n_{\rm b,0} = \frac{\rho_{\rm cr}\Omega_{\rm b}}{\mu m_{\rm p}} \approx \frac{10^{-29}\,{\rm g\,cm^{-3}}\,0.045}{0.6\times1.7\times10^{-24}\,{\rm g}} \approx 4\times10^{-7}\ {\rm cm^{-3}}. \tag{1.26}$$

  Upon collapsing this chunk of baryons by a radial factor of 10, we obtain a mean cluster density of

$$\bar n_{\rm cl} \approx 4\times10^{-4}\ {\rm cm^{-3}}, \tag{1.27}$$

  which is perfectly consistent with the densities inferred by X-ray observations of clusters.

Chapter 2

Evolution of the Dark Component

2.1 The Growth of Perturbations

2.1.1 Newtonian Equations

- There are pronounced structures in the universe on scales from galaxies to galaxy clusters and cosmic large-scale filaments. While filaments and the voids they surround can reach sizes of $\sim 50\,\mathrm{Mpc}$, they are still small compared to the Hubble radius. In this chapter, we only describe the concepts of the basic theory for structure growth in the expanding universe for the matter-dominated epoch, i.e., we only consider the conservation laws for non-relativistic fluids. A detailed derivation and more complete discussion can be found in Sect. 2.1 of the *Cosmology* lecture notes by Prof. Bartelmann.

- Strictly, this theory should be worked out in the framework of general relativity, which is a complicated exercise. With the inhomogeneities being "small", i.e. much smaller than the typical scale of the universe, we can neglect effects of curvature and the finite speed of information propagation and work within the framework of Newtonian dynamics. We will see that structure grows from small-amplitude seed fluctuations through gravitational instability and determine the rate of growth.

- We describe inhomogeneities in a cosmic fluid which contains at least radiation, dark matter, and baryonic matter and which moves according to Newtonian gravity.

- We begin with the continuity equation, which formulates mass conservation,
$$\frac{\partial\rho}{\partial t} + \boldsymbol{\nabla}_{\boldsymbol{r}} \cdot (\rho \boldsymbol{v}) = 0 \,, \tag{2.1}$$
where $\rho(t, \boldsymbol{r})$ and $\boldsymbol{v}(t, \boldsymbol{r})$ are the density and velocity of the cosmic fluid at position $\boldsymbol{r}$ and time t.

- The second equation is Euler's equation which formulates the conservation of momentum,
$$\frac{\partial\boldsymbol{v}}{\partial t} + (\boldsymbol{v} \cdot \boldsymbol{\nabla}_{\boldsymbol{r}})\boldsymbol{v} = -\frac{\boldsymbol{\nabla}_{\boldsymbol{r}} P}{\rho} - \boldsymbol{\nabla}_{\boldsymbol{r}}\Phi \,. \tag{2.2}$$
The terms on the right-hand side represent the pressure-gradient and gravitational forces.

- The Newtonian gravitational potential Φ satisfies the Poisson equation
$$\nabla_{\boldsymbol{r}}^2 \Phi = 4\pi G\rho \,. \tag{2.3}$$

2.1.2 Density Perturbations

- The next steps consist in decomposing density and velocity fields into their homogeneous background values $\bar{\rho}$ and $\bar{\boldsymbol{v}}$ and small perturbations $\delta\rho$ and $\delta\boldsymbol{v}$,

$$\rho(t,\boldsymbol{r}) = \bar{\rho}(t) + \delta\rho(t,\boldsymbol{r}) \ , \quad \boldsymbol{v}(t,\boldsymbol{r}) = \bar{\boldsymbol{v}}(t) + \delta\boldsymbol{v}(t,\boldsymbol{r}) \ . \tag{2.4}$$

- The evolution of the homogeneous background quantities are governed by the expansion of the universe. Physical coordinates, $\boldsymbol{r}$, are related to comoving coordinates, $\boldsymbol{x}$, via the equation $\boldsymbol{r} = a\boldsymbol{x}$. Here, $a(t)$ is the cosmic scale factor whose dynamics is governed by Friedmann's equations:

$$\left(\frac{\dot{a}}{a}\right)^2 = \frac{8\pi G}{3}\rho - \frac{Kc^2}{a^2} + \frac{\Lambda c^2}{3} \ , \tag{2.5}$$

$$\frac{\ddot{a}}{a} = -\frac{4\pi G}{3}\left(\rho + \frac{3p}{c^2}\right) + \frac{\Lambda c^2}{3} \ . \tag{2.6}$$

  Here, K is a constant parameterising the curvature of spatial hypersurfaces and Λ is the cosmological constant. The scale factor is uniquely determined once its value at a fixed time t is chosen. We set $a = 1$ today.

- The *critical* density at scale factor a and today are defined as

$$\rho_{\rm cr}(a) \equiv \frac{3H^2(a)}{8\pi G} \ , \quad \rho_{\rm cr0} \equiv \frac{3H_0^2}{8\pi G} \ , \quad \text{and} \tag{2.7}$$

$$H^2(a) \equiv \left(\frac{\dot{a}}{a}\right)^2 = H_0^2\left[\Omega_{\rm r0}a^{-4} + \Omega_{\rm m0}a^{-3} + \Omega_{\Lambda 0} + \Omega_{\rm K}a^{-2}\right] \tag{2.8}$$

  is the Hubble function that derives from Friedmann's equation (2.5) and describes the expansion rate of the universe. Quantities at the present time are denoted with a subscript 0. The density parameters of radiation, matter, the cosmological constant, and curvature are defined by

$$\Omega_{\rm r0} = \frac{\rho_{r0}}{\rho_{\rm cr0}}, \ \ \Omega_{\rm m0} = \frac{\rho_{m0}}{\rho_{\rm cr0}}, \ \ \Omega_{\Lambda 0} = \frac{\Lambda c^2}{3H_0^2}, \ \text{and} \ \Omega_K = \frac{-Kc^2}{H_0^2}. \tag{2.9}$$

- After this short cosmological detour, we return to the derivation of the density perturbations. To this end we transform the governing equations (2.1) through (2.3) from physical coordinates, $\boldsymbol{r}$, to comoving coordinates, $\boldsymbol{x}$, which are related by $\boldsymbol{r} = a\boldsymbol{x}$. To understand the concept of comoving coordinates, imagine a set of particles that are slightly displaced from a uniform grid. In the Eulerian point of view, the expanding universe causes the grid points to move apart from each other homogeneously and gravitational attraction increases the degree of irregularity. In the comoving frame, the large-scale homogeneous expansion is divided

out. This leaves only the dynamics of the gravitational attraction to increase the irregularity. We are hence seeking an equation for the time evolution of the density perturbations in this comoving frame, $\delta\rho(t, \boldsymbol{x})$.

- We define the density contrast,

$$\delta \equiv \frac{\delta\rho}{\bar{\rho}} \,, \tag{2.10}$$

and adopt an equation of state linking the pressure fluctuation to the density fluctuation,

$$\delta p = \delta p(\delta) \equiv c_\mathrm{s}^2 \delta\rho \tag{2.11}$$

with the sound speed c_s.

- We obtain an expression for the velocity,

$$\boldsymbol{v} = \dot{\boldsymbol{r}} = \dot{a}\boldsymbol{x} + a\dot{\boldsymbol{x}} = H\boldsymbol{r} + a\dot{\boldsymbol{x}} = \bar{\boldsymbol{v}} + \delta\boldsymbol{v}, \tag{2.12}$$

where $\bar{\boldsymbol{v}} = H\boldsymbol{r}$ is the Hubble velocity and $\delta\boldsymbol{v} = a\dot{\boldsymbol{x}}$ is the peculiar velocity that deviates from the Hubble flow. The equations (2.1) through (2.3) can be combined to yield a single equation for the density contrast

$$\ddot{\delta} + 2H\dot{\delta} = \left(4\pi G\bar{\rho}\delta + \frac{c_\mathrm{s}^2 \nabla_x^2 \delta}{a^2}\right) . \tag{2.13}$$

- We can decompose δ into plane waves,

$$\delta(\boldsymbol{x}, t) = \int \frac{\mathrm{d}^3 k}{(2\pi)^3} \hat{\delta}(\boldsymbol{k}, t) \mathrm{e}^{-\mathrm{i}\boldsymbol{k}\cdot\boldsymbol{x}} \,, \tag{2.14}$$

introducing the time-dependent Fourier amplitudes $\hat{\delta}(\boldsymbol{k}, t)$ and decoupling the time evolution from the spatial dependence. Inserted into (2.13), this yields

$$\ddot{\hat{\delta}} + 2H\dot{\hat{\delta}} = \hat{\delta}\left(4\pi G\bar{\rho} - \frac{c_\mathrm{s}^2 k^2}{a^2}\right) . \tag{2.15}$$

- On a static background, $H = 0$, and (2.15) becomes the oscillator equation

$$\ddot{\hat{\delta}} + \omega_0^2 \hat{\delta} = 0 \,, \quad \omega_0 \equiv \sqrt{\frac{c_\mathrm{s}^2 k^2}{a^2} - 4\pi G\bar{\rho}} \,. \tag{2.16}$$

The oscillation frequency is real for sufficiently large comoving wave numbers k,

$$k \geq k_\mathrm{J} \equiv \frac{2\sqrt{\pi G\bar{\rho}}\, a}{c_\mathrm{s}} \,. \tag{2.17}$$

k_J defines the comoving Jeans length

$$\lambda_\mathrm{J} \equiv \frac{2\pi}{k_\mathrm{J}} = \frac{c_\mathrm{s}}{a}\sqrt{\frac{\pi}{G\bar{\rho}}}\,. \tag{2.18}$$

Perturbations smaller than the Jeans length oscillate. Others grow or decay. The Jeans length can be heuristically derived by balancing the sound crossing time, $t_\mathrm{s} = a\lambda_\mathrm{J}/c_\mathrm{s} = 2\pi a/(k_\mathrm{J}c_\mathrm{s})$, with the gravitational free-fall time, $t_\mathrm{ff} = \sqrt{\pi/(G\bar{\rho})}$, which yields the desired result (2.17).

- We now study the behavior of perturbations on scales much larger than the Jeans length, or in pressure-less fluids. If $\Omega = 1$, we get $\rho_\mathrm{cr} = \bar{\rho} = 3H^2/(8\pi G)$ and the perturbation equation reads

$$\ddot{\hat{\delta}} + 2H\dot{\hat{\delta}} = \frac{3}{2}H^2\hat{\delta}\,. \tag{2.19}$$

Note that this is only valid for the matter-dominated epoch because we only considered the conservation laws for non-relativistic fluids. In this case, the Hubble rate is given by (see (1.54) of the *Cosmology* lecture notes by Prof. Bartelmann)

$$a \propto t^{2/3} \quad \Rightarrow \quad \frac{\dot{a}}{a} = H(t) = \frac{2}{3t}\,. \tag{2.20}$$

- The *ansatz* $\hat{\delta}(\boldsymbol{k}, t) \propto t^n$ yields

$$n^2 + \frac{n}{3} - \frac{2}{3} = 0 \tag{2.21}$$

hence $n = -1, 2/3$, which translates to

$$\hat{\delta} \propto \begin{cases} a\,, \\ a^{-3/2}\,. \end{cases} \tag{2.22}$$

Decaying modes are irrelevant for cosmic structure growth, so $\delta \propto a$ during the matter-dominated era. The phases of the waves determine whether a given cosmological patch develops into an underdense region (i.e., a void) or a galaxy cluster. Constructive interference of the growing modes causes the development of overdensities, which then collapse into galaxies (in the case of small-scale modes) or clusters (for large-scale modes). Destructive interference leads to the growth of voids.

- The sound speed defines the Jeans length, below which perturbations cannot grow, but oscillate. For dark matter consisting of weakly interacting massive particles, for instance, the concept of a sound speed makes no sense because the dark matter behaves

like an ensemble of collision-less particles. In that case, one can show that the comoving Jeans length (2.20) is replaced by

$$\lambda_{\mathrm{J}} = \frac{\left\langle v^{-2} \right\rangle^{-1/2}}{a} \sqrt{\frac{\pi}{G\bar{\rho}}} \,, \tag{2.23}$$

where v is the velocity dispersion of the particles. Perturbations in collision-less matter smaller than the Jeans length are thus prevented from growing because their gravity is insufficient for keeping their particles bound.

2.2 Statistics and Non-linear Evolution

2.2.1 Power Spectra

- We have seen before (2.14) that it is convenient to decompose the density contrast δ into plane waves. We introduce the Fourier transform $\hat{\delta}$ of the density contrast δ as

$$\delta(\boldsymbol{x}) = \int \frac{\mathrm{d}^3 k}{(2\pi)^3}\,\hat{\delta}(\boldsymbol{k})\mathrm{e}^{-\mathrm{i}\boldsymbol{k}\cdot\boldsymbol{x}}\,, \quad \hat{\delta}(\boldsymbol{k}) = \int \mathrm{d}^3 x\,\delta(\boldsymbol{x})\mathrm{e}^{\mathrm{i}\boldsymbol{k}\cdot\boldsymbol{x}}\,. \quad (2.24)$$

- The density contrast is a random field, which must be isotropic and homogeneous in order to comply with the fundamental cosmological assumptions. This means that the statistical properties of δ, e.g. its mean or variance, do not change under rotations and translations.

- By definition, the mean of the density contrast vanishes,

$$\langle\delta\rangle = \left\langle\frac{\rho-\rho_0}{\rho_0}\right\rangle = \frac{\langle\rho\rangle}{\rho_0} - 1 = 0\,. \quad (2.25)$$

  The variance of δ *in Fourier space* defines the power spectrum $P(k)$,

$$\langle\hat{\delta}(\boldsymbol{k})\hat{\delta}^*(\boldsymbol{k}')\rangle \equiv (2\pi)^3 P(k)\delta_{\mathrm{D}}(\boldsymbol{k}-\boldsymbol{k}')\,, \quad (2.26)$$

  where δ_{D} is Dirac's delta distribution, which ensures that modes of different wave vector $\boldsymbol{k}$ are uncorrelated in Fourier space in order to ensure homogeneity. The power spectrum cannot depend on the direction of $\boldsymbol{k}$ because of isotropy.

- The correlation function of δ in real space is defined as

$$\xi(y) \equiv \langle\delta(\boldsymbol{x})\delta(\boldsymbol{x}+\boldsymbol{y})\rangle\,, \quad (2.27)$$

  where the average extends over all positions $\boldsymbol{x}$ and orientations of $\boldsymbol{y}$. The correlation function measures the coherence of the density contrast between all points on the sky separated by a distance $|\boldsymbol{y}|$. Again, ξ cannot depend on the direction of $\boldsymbol{y}$ because of isotropy.

- Inserting the Fourier integrals for $\delta(\boldsymbol{x})$ in (2.27), we find

$$\begin{aligned}\xi(y) &= \left\langle\int\frac{\mathrm{d}^3k}{(2\pi)^3}\int\frac{\mathrm{d}^3k'}{(2\pi)^3}\hat{\delta}(\boldsymbol{k})\hat{\delta}(\boldsymbol{k}')\mathrm{e}^{-\mathrm{i}\boldsymbol{k}\cdot\boldsymbol{x}}\mathrm{e}^{-\mathrm{i}\boldsymbol{k}'\cdot(\boldsymbol{x}+\boldsymbol{y})}\right\rangle \\ &= \int\frac{\mathrm{d}^3k}{(2\pi)^3}\int\frac{\mathrm{d}^3k'}{(2\pi)^3}\langle\hat{\delta}(\boldsymbol{k})\hat{\delta}^*(\boldsymbol{k}')\rangle\mathrm{e}^{-\mathrm{i}\boldsymbol{k}\cdot\boldsymbol{x}}\mathrm{e}^{+\mathrm{i}\boldsymbol{k}'\cdot(\boldsymbol{x}+\boldsymbol{y})} \\ &= \int\frac{\mathrm{d}^3k}{(2\pi)^3}P(k)\mathrm{e}^{\mathrm{i}\boldsymbol{k}\cdot\boldsymbol{y}}\,, \quad (2.28)\end{aligned}$$

which states that the correlation function is the Fourier transform of the power spectrum (and vice versa). Hence, both statistical measures carry an equivalent amount of information. Simplifying furthermore, we obtain

$$\begin{aligned}\xi(y) &= 2\pi \int \frac{k^2 \mathrm{d}k}{(2\pi)^3} P(k) \int_0^\pi \sin\theta \mathrm{d}\theta \mathrm{e}^{-\mathrm{i}ky\cos\theta} \\ &= 4\pi \int \frac{k^2 \mathrm{d}k}{(2\pi)^3} P(k) \frac{\sin ky}{ky} \,, \end{aligned} \tag{2.29}$$

where θ was the angle between vectors $\boldsymbol{k}$ and $\boldsymbol{y}$. Obviously, the variance of δ is the correlation function at $y = 0$,

$$\sigma^2 = 4\pi \int \frac{k^2 \mathrm{d}k}{(2\pi)^3} P(k) \,. \tag{2.30}$$

- The variance in real space depends on the scale which we are considering. Let us introduce

$$\bar{\delta}(\boldsymbol{x}) := \int \mathrm{d}^3 y \delta(\boldsymbol{x}) W_R(|\boldsymbol{x} - \boldsymbol{y}|) \,, \tag{2.31}$$

  i.e. the density contrast field averaged on the scale R with a *window function* W_R. The idea of the window function is that it approaches a finite constant well within R, and drops to zero outside R.

- The Fourier convolution theorem says $\widehat{f * g} = \hat{f}\hat{g}$, i.e. the Fourier transform of a convolution is the product of the Fourier transforms of the convolved functions. Applying this to (2.30) yields $\hat{\bar{\delta}} = \hat{\delta}\hat{W}_R$. thus, the power spectrum of the density contrast filtered on the scale R is $\bar{P}(k) = P(k)\hat{W}_R^2(k)$. Using (2.30), the variance of the filtered density-contrast field is

$$\sigma_R^2 = 4\pi \int \frac{k^2 \mathrm{d}k}{(2\pi)^3} P(k) \hat{W}_R^2(k) \,. \tag{2.32}$$

  The variance on a scale of $8\,h^{-1}$ Mpc, σ_8, is often used for characterizing the amplitude of the power spectrum.

2.2.2 Hierarchical Structure Formation

- A detailed study of how modes of different wave numbers grow in the radiation- and matter-dominated era allows to infer the shape of the power spectrum. In the linear regime of small-amplitude perturbations this can be worked out analytically (see e.g., Sect. 2.2.2 of the *Cosmology* lecture notes by Prof. Bartelmann). For a

cold dark matter (CDM) cosmology, the resulting power spectrum reads

$$P(k) \propto \begin{cases} k & (k < k_0) \\ k^{-3} & (k \gg k_0). \end{cases} \tag{2.33}$$

Here, $k_0 = 2\pi a_{\rm eq}/\lambda_0$ is the comoving wave number of the particle horizon at matter-radiation equality.

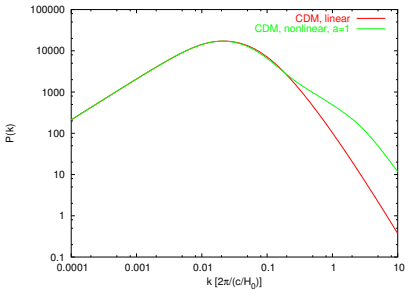

Linear and non-linear CDM power spectra.

- We use this result to understand when galaxy clusters form in comparison to elliptical or dwarf galaxies. To this end, we define the *non-linear mass* M_*, as the mass contained in a sphere of radius R_* on which the variance becomes unity.

$$\sigma_*^2 = \int_0^{k_*} \frac{{\rm d}^3 k}{(2\pi)^3} P(k) \stackrel{!}{=} 1, \tag{2.34}$$

where $k_* = 2\pi/R_*$.

- We assume that the power spectrum can be approximated locally by a power law of the form $P(k) = Ak^n$,

$$\sigma_*^2 = 4\pi A \int_0^{k_*} \frac{k^{2+n}{\rm d}k}{(2\pi)^3} P(k) = \frac{4\pi A}{(2\pi)^3} \frac{k_*^{n+3}}{n+3} \stackrel{!}{=} 1, \tag{2.35}$$

$$\sigma^2 = \sigma_*^2 \left(\frac{k}{k_*}\right)^{n+3} = \left(\frac{k}{k_*}\right)^{n+3}. \tag{2.36}$$

- Masses and length scales are related by background density, $M = 4\pi\bar{\rho}R^3/3 \propto k^{-3}$. Hence we get

$$\sigma^2 = \left\langle \left(\frac{\delta M}{M}\right)^2 \right\rangle = \left(\frac{M}{M_*}\right)^{-1-n/3}. \tag{2.37}$$

The variance reads for the two asymptotic cases

$$\sigma^2 = \begin{cases} \left(\frac{M}{M_*}\right)^{-4/3} & \text{for } n = 1, \\ 1 & \text{for } n = -3. \end{cases} \tag{2.38}$$

- The previous considerations allow to infer how cosmological structures grow. In k space, (2.33) and (2.36) demonstrate that the variance is largest on small scales, i.e., the amplitude of small-scale fluctuations is largest. Hence these scales reach the non-linear mass first which causes them to collapse. As a result, structure forms "bottom-up" in CDM cosmologies. This hierarchical scheme of structure formation dictates that dwarf galaxies collapse and form before ellipticals, which in turn form earlier than galaxy clusters. Those sit atop the mass hierarchy as they have collapsed most recently in cosmic time. The reason for this can be easily understood by looking at the variance as a function of

collapsing mass (2.38). Gravity dictates that an overdensity continues to grow with time. The growth rate depends on the amount of matter: the more matter, the stronger the gravity, but the longer it takes to collapse. We can summarize, that the necessary and sufficient criterion for hierarchical structure formation is given by

$$\frac{\partial}{\partial M}\sigma(M,t) < 0. \tag{2.39}$$

- Another way of looking at this is that fluctuations on large scales are more subtle than fluctuations on small scales because the Universe is homogeneous on the largest scales according to the *cosmological principles* and as inferred from large-scale observations. Is there a deep reason why fluctuations a smaller on large scales? Let's look at the fluctuations in the gravitational potential,

$$\delta\Phi \sim \frac{GM}{R}\frac{\delta M}{M} \sim GM^{2/3}\bar{\rho}^{1/3}\frac{\delta M}{M} \tag{2.40}$$

since at any time $R \propto \bar{\rho}^{-1/3}$.

- Unless $\delta M/M \propto M^{-2/3}$, the potential fluctuations $\delta\Phi$ will diverge. Depending on the power-law index of $\delta M/M \propto M^{-\alpha}$, $\delta\Phi$ will diverge on large scales (for $\alpha < 2/3$) or on small scales (for $\alpha > 2/3$). Hence, the most natural fluctuation spectrum is $\delta M/M \propto M^{-2/3}$, which corresponds to the Harrison-Zel'dovich-Peebles spectrum with the characteristic spectral index of $n = 1$. This can be seen by considering $\delta\Phi \sim Gk\delta M$ and $M \propto R^3 \propto k^{-3}$ which yields

$$\frac{\delta M}{M} \propto M^{-(n+3)/6} \quad \Rightarrow \quad \delta M \propto M^{-(n-3)/6} \propto k^{(n-3)/2}, \tag{2.41}$$

or

$$\delta\Phi \propto k^{(n-1)/2}. \tag{2.42}$$

This shows that $n = 1$ is the characteristic power-law index that avoids any unphysical divergence.

2.2.3 Non-linear Evolution

- When the density contrast reaches unity, linear perturbation theory breaks down. For a correct treatment of the non-linear development, one has to resort to numerical simulations. They decompose the matter distribution into particles whose initial velocities are typically slightly perturbed according to some assumed power spectrum. The particles are then transported to redshifts high enough for linear evolution to hold on all scales considered. For later evolution, the equations of motion for all particles are solved. In the following, the most popular numerical techniques shall be presented:

1. Ideally, particles move under the influence of the gravity from all other particles, but direct summation of all the gravitational forces of $N-1$ particles on N particles becomes prohibitively time-consuming and the scheme attains numerical complexity of $O(N^2)$ for every timestep. Several approximation schemes are therefore being employed.
2. The particle-mesh (PM) algorithm computes the gravitational potential of the particle distribution on a grid (mesh) by solving Poisson's equation in Fourier space, making use of fast-Fourier techniques, thereby reducing the numerical complexity to $O(N \log N)$. The gravitational forces are then given by the gradients of the potential at the particle positions. This technique has a spatial resolution limited by the size of the mesh cells which makes it impractical for many modern applications.
3. The particle-particle particle-mesh (P^3M) algorithm improves the PM technique by adding corrections for nearby particles which are determined by direct summation. Here, the numerical complexity is also $O(N \log N)$ provided the number of particle-particle operations per timestep is kept constant. However, this is not the case for high-resolution "zoom" simulations of individually forming objects in cosmological environments.
4. Tree codes bundle distant particles into groups whose gravitational force on a particle is approximated as if they were point masses, or masses whose spatial distribution has a few low-order multipoles only, e.g. the monopole corresponding to a point mass, plus a dipole corresponding to a linear deformation, and so on. Depending on the solid angle that is subtended by the group on the sky seen by the particle, the "tree" is opened into its branches and leaves, i.e., higher-order multipoles of this group are considered. Alternatively, the monopole of that group, which is centered on its center-of-mass, is subdivided into the monopole moments of subgroups of the parent group, which subtend a smaller angle on the sky. It turns out that the numerical complexity of this technique is also $O(N \log N)$. The particle tree is updated as the evolution proceeds.

- Non-linear evolution causes density-perturbation modes to couple: while modes of different wave lengths evolve independently during linear evolution, mode coupling in the non-linear evolution moves power from large to small scales as structures collapse. The effect on the power spectrum is that the amplitude on small scales is increased at the expense of intermediate scales. Large scales continue to evolve linearly and independently.

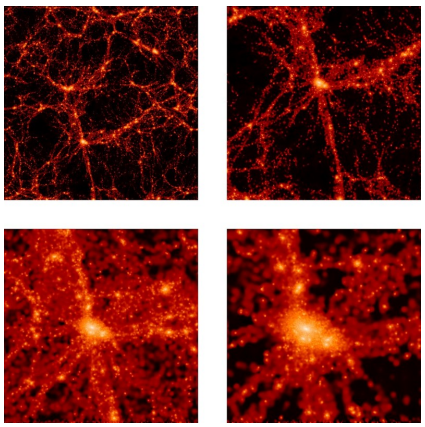

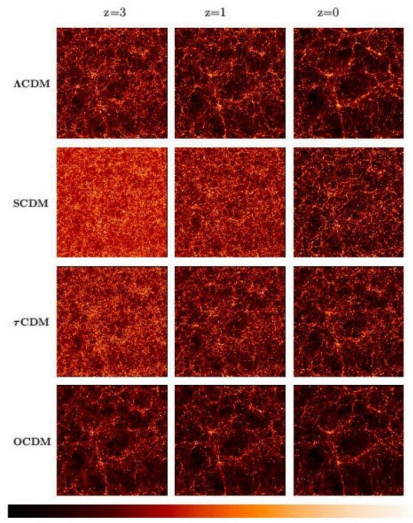

The VIRGO Collaboration 1996

nonlinear structure evolution, simulated in different cosmologies (Virgo collaboration)

- Even if the original density perturbation field δ is Gaussian, it must develop non-Gaussianities during non-linear evolution. This is evident because $\delta \geq -1$ by definition, but can become arbitrarily large. An originally Gaussian distribution of δ thus becomes increasingly skewed as it develops a tail towards infinite δ.

- Typical behavior seen in numerical simulations shows the formation of "pancakes" and filaments as predicted by the theory of Gaussian random fields. Gravitational fragmentation of filaments into individual lumps causes galaxy-sized dark matter overdensities to form, which are called halos. In the ΛCDM universe, those merge into galaxy groups which gradually stream towards the higher-density regions and larger mass concentrations at the intersections of filaments—galaxy clusters. Those form at the sites of constructive interference of long waves in the primordial fluctuations and are enhanced through gravitational collapse. Ongoing gravitational pull on the surrounding regions causes galaxy- and group-sized halos to continuously merge into clusters which sit atop the cosmic mass hierarchy of halos and thereby present the largest gravitationally collapsed objects to date. Giant voids form as matter accumulates in the walls of the cosmic network. Equivalently, the formation of voids can be considered to result from destructive interference of waves in the primordial fluctuations.

2.3 Spherical Collapse

2.3.1 Collapse of a Homogeneous Overdense Sphere

- The distribution of the dark matter in the universe can be considered as composed of individual so-called haloes, approximately spherical overdense clouds of dark matter which can reach highly non-linear densities in their centres.

- An approximate understanding of the parameters of such haloes and their relation to the dark-matter density contrast can be obtained by studying the dynamics of a spherical, homogeneous overdensity, leading to the so-called spherical collapse model. While realistic density perturbations are not spherical, considering an exact analytical solution that results from such an analysis nevertheless provides useful insights into non-linear collapse of more realistic situations. In particular the analysis (1) relates time (or redshift) at which the object collapses to its initial (linear) overdensity and (2) it maps the collapse time (redshift) to the final density of dark matter haloes that formed by collapse.

- The measured temperature anisotropies in the cosmic microwave background imply $\delta \ll 1$ at recombination. Thus, non-linear collapse happens at $a \gg a_{\rm rec}$, i.e., in the matter- or vacuum-dominated eras. We make the following assumptions in our analysis.

  - We consider a spherical perturbation that has initially a uniform overdensity.
  - The fluid is assumed to have zero pressure and is collisionless (i.e., the analysis applies to dark matter and not baryons). Later stages of baryonic collapse are different from that of dark matter since baryons additionally feel the pressure force, which causes the development of shocks in converging flows. However, since baryons only contribute $\sim 15\%$ of the total mass, they do not appreciably change the collapse of dark matter.
  - For simplicity, we set $\Omega = \Omega_{\rm m} = 1$, i.e., a flat matter-dominated universe. This can be generalized to cases with $\Omega_{\rm m0} \neq 1$ and $\Omega_\Lambda \neq 1$.

- We consider a sphere of mass M and proper radius R and assume that the universe outside the sphere remains spherically symmetric such that it exerts no gravitational force on the matter in the sphere. Since $M = \text{const.}$, we have

$$\frac{{\rm d}^2 R}{{\rm d}t^2} = -\frac{GM}{R^2} \,, \tag{2.43}$$

which can be integrated to yield

$$\frac{1}{2}\left(\frac{\mathrm{d}R}{\mathrm{d}t}\right)^2 - \frac{GM}{R} = \phi \ . \tag{2.44}$$

- We consider the gravitationally bound case, for which the energy per units mass is $\phi < 0$ and which leads to collapse. Adopting $R = 0$ at $t = 0$, we can integrate this equation and obtain

$$t = \int_0^R \frac{\mathrm{d}r}{\sqrt{2\,(GM/r + \phi)}} = \frac{A}{\sqrt{2|\phi|}} \int_{\theta(0)}^{\theta(R)} \frac{\sin\theta \mathrm{d}\theta}{\sqrt{2/(1-\cos\theta) - 1}} \ , \tag{2.45}$$

where we suitably changed the integration variable, using the transformation $r = A(1 - \cos\theta)$, where $A = GM/(2|\phi|)$. Employing trigonometric identities, we obtain

$$t = \frac{A}{\sqrt{2|\phi|}} \int_{\theta(0)}^{\theta(R)} (1 - \cos\theta)\mathrm{d}\theta = \frac{A}{\sqrt{2|\phi|}}(\theta - \sin\theta) \ . \tag{2.46}$$

Thus, the spherical collapse problem has the following parametric solution, which describes a cycloid,

$$R = A(1 - \cos\theta) \ , \quad A = \frac{GM}{2|\phi|} \ , \tag{2.47}$$

$$t = B(\theta - \sin\theta) \ , \quad B = \frac{GM}{(2|\phi|)^{3/2}} \ . \tag{2.48}$$

- The solution is characterised by an initial expansion phase from $R = 0$ at $\theta = 0$. It reaches a maximum radius $R_{\rm ta} = A$ at $\theta_{\rm ta} = \pi$ at which it turns around and collapses back to $R = 0$ at $\theta_{\rm c} = 2\pi$. In principle, it re-expands for $\theta > 2\pi$ but in practice, other physical effects become important and complicate things. The corresponding times are $t_{\rm ta} = \pi B$ for the maximum (turn-around) radius and $t_{\rm c} = 2\pi B = 2t_{\rm ta}$ for collapse at $R = 0$.

2.3.2 Connection to Linear Perturbation Theory

- The mean density inside the sphere is (2.47)

$$\rho = \frac{M}{4\pi/3\,R^3} = \frac{3M}{4\pi A^3}\frac{1}{(1-\cos\theta)^3} \ , \tag{2.49}$$

while the mean density of the background universe with $\Omega_{\rm m0} = 1$ is

$$\bar{\rho} = \frac{3H^2}{8\pi G} = \frac{1}{6\pi G t^2} = \frac{1}{6\pi G B^2}\frac{1}{(\theta - \sin\theta)^2} \ , \tag{2.50}$$

with $H = 2/(3t)$. The overdensity of the sphere (which is generally non-linear) can be obtained by combining these equations to yield

$$1 + \delta = \frac{\rho}{\bar{\rho}} = \frac{9}{2}\frac{(\theta - \sin\theta)^2}{(1-\cos\theta)^3} \ . \tag{2.51}$$

- To make the connection to linear perturbation theory, we consider the behaviour of the collapse at small t, which corresponds to small θ. Performing a Taylor series expansion of $\cos\theta$ and $\sin\theta$, we obtain

$$1 + \delta = 1 + \frac{3}{20}\theta^2 + O(\theta^4) , \tag{2.52}$$

$$t = \frac{B}{6}\theta^3 + O(\theta^5) . \tag{2.53}$$

  Solving for θ gives (using $t_{\rm ta} = \pi B$)

$$\theta = \left(\frac{6t}{B}\right)^{1/3} + \ldots = (6\pi)^{1/3}\left(\frac{t}{t_{\rm ta}}\right)^{1/3} + \ldots, \quad \text{for } t \ll t_{\rm ta}. \tag{2.54}$$

- Thus, $\theta \ll 1$ corresponds to $t \ll t_{\rm ta}$. Substituting (2.54) into (2.52) gives

$$\delta = \frac{3}{20}(6\pi)^{2/3}\left(\frac{t}{t_{\rm ta}}\right)^{2/3} \ll 1, \quad \text{for } t \ll t_{\rm ta}. \tag{2.55}$$

  This yields the scaling of the density contrast in the spherical collapse model, $\delta \propto t^{2/3} \propto a$ (since $t \propto a^{3/2}$ in the Einstein-de Sitter model), which is exactly the behaviour of the growing mode solution of linear perturbation theory. Note that the decaying mode solution is absent due to our choice of initial conditions at $t = 0$.

- A corollary emerges from (2.55) that if the sphere has a uniform initial overdensity ($\delta_{\rm i}$) at some early time ($t_{\rm i}$), then *all* interior spheres will have the same $t_{\rm ta}$ and hence the sphere remains uniform as it collapses!

- There is an important distinction between (1) the real overdensity and (2) the overdensity *extrapolated* according to linear theory,

$$\delta_{\rm lin} = \delta_{\rm i}\left(\frac{t}{t_{\rm i}}\right)^{2/3} = \frac{3}{20}(6\pi)^{2/3}\left(\frac{t}{t_{\rm ta}}\right)^{2/3} \quad \text{for all } t. \tag{2.56}$$

  The maximum expansion radius at turnaround ($t = t_{\rm ta}$) is

$$\delta_{\rm lin}(t_{\rm ta}) = \frac{3}{20}(6\pi)^{2/3} \approx 1.062 \tag{2.57}$$

  while the real (non-linear) overdensity is according to (2.51)

$$1 + \delta(t_{\rm ta}) = \frac{9\pi^2}{16} \approx 5.55. \tag{2.58}$$

- At collapse ($t = t_{\rm c} = 2t_{\rm ta}$), we have

$$\delta_{\rm c} \equiv \delta_{\rm lin}(t_{\rm c}) = \frac{3}{20}(12\pi)^{2/3} \approx 1.686. \tag{2.59}$$

In terms of the initial overdensity δ_i, collapse happens at time

$$t_\mathrm{c} = t_\mathrm{i}\left(\frac{\delta_\mathrm{c}}{\delta_\mathrm{i}}\right)^{3/2} \propto \delta_\mathrm{i}^{-3/2}, \tag{2.60}$$

$$1 + z_\mathrm{c} = (1 + z_\mathrm{i})\left(\frac{\delta_\mathrm{i}}{\delta_\mathrm{c}}\right) \propto \delta_\mathrm{i}\ , \tag{2.61}$$

since $t \propto a^{3/2} \propto (1 + z)^{-3/2}$. Thus, perturbations that are initially more overdense collapse earlier! Generally, $\delta_\mathrm{c} = \delta_\mathrm{c}(\Omega_\mathrm{m}, \Omega_\Lambda)$, but the dependence on Ω_m and Ω_Λ is weak so our result applies quite generally although it was derived for the Einstein-de Sitter model.

2.3.3 Final Density of a Collapsed Halo

- According to the spherical top hat collapse model, a uniform sphere collapses to a point of infinite density and then re-expands. In a realistic situation, the sphere contains inhomogeneities that generate tangential random velocities in the dark matter during collapse. This leads to an equilibrium configuration where the dark matter velocity dispersion balances its gravity. This relaxation process is called virialisation.

- We assume that the *final* dark matter halo is in dynamical equilibrium and obeys the virial theorem

$$2K_\mathrm{f} + V_\mathrm{f} = 0\ , \tag{2.62}$$

where K denotes the total kinetic energy in random motions, V is the total gravitational binding energy, and we neglected the surface pressure term due to further infalling material. We have

$$K_\mathrm{f} = \frac{M}{2}\sigma_\mathrm{f}^2\ , \quad \text{and} \tag{2.63}$$

$$V_\mathrm{f} = -G\int_0^{R_\mathrm{f}} \frac{4\pi r^3 \rho}{3r}\mathrm{d}m_\mathrm{shell} = -\frac{3}{5}\frac{GM^2}{R_\mathrm{f}}\ , \tag{2.64}$$

where σ is the three-dimensional velocity dispersion, $\mathrm{d}m_\mathrm{shell} = 4\pi r^2 \rho \mathrm{d}r$ and we assumed a uniform sphere of radius R_f. Hence

$$E_\mathrm{f} = K_\mathrm{f} + V_\mathrm{f} = \frac{1}{2}V_\mathrm{f} = -\frac{3}{10}\frac{GM^2}{R_\mathrm{f}}\ . \tag{2.65}$$

- At turn-around, the sphere is at rest, i.e., $K_\mathrm{ta} = 0$. The total energy at turn-around is

$$E_\mathrm{ta} = V_\mathrm{ta} = -\frac{3}{5}\frac{GM^2}{R_\mathrm{ta}}\ . \tag{2.66}$$

Since dark matter is collisionless, the conservation of total energy during the collapse yields $E_\mathrm{f} = E_\mathrm{ta}$ and hence, $R_\mathrm{f} = R_\mathrm{ta}/2$.

- The final density is thus $\rho_f = 8\rho(t_{ta})$. Assuming that virialisation happens at $t \approx t_c$ and since $\bar{\rho} \propto t^{-2}$ and $t_c = 2t_{ta}$, the overdensity of the final halo is

$$1 + \delta_v \equiv 1 + \delta_c = \frac{\rho_c}{\bar{\rho}\,(t_c/t_{ta})^{-2}} = 32\,[1 + \delta(t_{ta})] = 18\pi^2 = 178\ . \tag{2.67}$$

Hence, the final halo density is

$$\rho_f = (1 + \delta_v)\bar{\rho}(t_c) = 18\pi^2\bar{\rho}(t_c)\ . \tag{2.68}$$

δ_{lin} and $\delta_v \equiv \Delta_v$ are widely used in cosmology to characterise dark matter haloes. Other popular choices are $\Delta_v = 100, 200, 500$, where each definition has its merits and shortcomings.

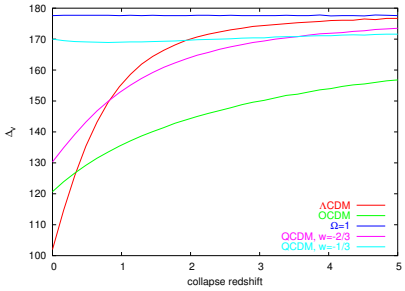

Virial overdensity in different cosmologies as a function of the halo collapse redshift.

- These two parameters derived from the spherical collapse model, δ_c and Δ_v, are very widely used in cosmology for characterising dark-matter haloes and their formation. Extending these calculations into more general cosmological models is surprisingly difficult and requires numerical solutions of the underlying differential equations. Approximations to the solutions for $\Omega_m < 1$ are

$$\delta_c = \frac{3}{5}\left(\frac{3\pi}{2}\right)^{2/3} \begin{cases} (1.0 + 0.0406\log_{10}\Omega_m) & (\Omega_{\Lambda 0} = 0) \\ (1.0 + 0.0123\log_{10}\Omega_m) & (\Omega_{\Lambda 0} = 1 - \Omega_{m0}) \end{cases} \tag{2.69}$$

and

$$\Delta_v = 9\pi^2 \begin{cases} \left[1 + 0.1210(\Omega_m - 1) + \Omega_m^{0.6756}\right] & (\Omega_{\Lambda 0} = 0) \\ \left[1 + 0.7076(\Omega_m - 1) + \Omega_m^{0.4403}\right] & (\Omega_{\Lambda 0} = 1 - \Omega_{m0}) \end{cases} \tag{2.70}$$

where Ω_m is the matter density parameter at the redshift of halo collapse.

2.4 The Halo Mass Function

2.4.1 The Press-Schechter Mass Function

- An important piece of information is the distribution of haloes over mass, the so-called mass function, which gives the number density of haloes at redshift z within the mass range between M and $M + \mathrm{d}M$.

- A characteristic length scale $R(M)$ can be assigned to a halo of mass M, which is defined as the radius of a homogeneous sphere filled with the mean cosmic matter density having mass M,

$$\frac{4\pi}{3}R^3\rho_{\rm cr}\Omega_{\rm m} = M \;\Rightarrow\; R(M) = \left(\frac{3M}{4\pi\rho_{\rm cr}\Omega_{\rm m}}\right)^{1/3} , \tag{2.71}$$

  where $\Omega_{\rm m}$ and $\rho_{\rm cr}$ have to be evaluated at the redshift required.

- Aiming at haloes of mass M, we consider the density contrast field filtered on the scale $R(M)$. We therefore use $\bar{\delta}$ as defined in (2.31), i.e. the density contrast convolved with a window function W_R which has a characteristic scale $R = R(M)$.

- It will be convenient to scale halo masses with the so-called non-linear mass, which is the mass M_* for whose characteristic length scale $R(M_*) \equiv R_*$ the variance (2.32) of the density contrast becomes $\delta_{\rm c}^2$,

$$\sigma_{R_*}^2 = 4\pi \int_0^\infty \frac{k^2\mathrm{d}k}{(2\pi)^3} P(k)\hat{W}_{R_*}^2(k) = \delta_{\rm c}^2 \; . \tag{2.72}$$

- For a Gaussian random field, the probability of finding at a given point $\boldsymbol{x}$ in space a filtered density contrast $\bar{\delta}(\boldsymbol{x})$ is

$$p(\bar{\delta}, a) = \frac{1}{\sqrt{2\pi\sigma_R^2(a)}} \exp\left[-\frac{\bar{\delta}^2(\boldsymbol{x})}{2\sigma_R^2(a)}\right] , \tag{2.73}$$

  where we have explicitly noted that the variance σ will depend on time or equivalently on the scale factor a through the linear growth factor, $\sigma_R(a) = \sigma_R D_+(a)$.

- Press & Schechter suggested that the probability of finding the filtered density contrast at or above the linear density contrast for spherical collapse, $\bar{\delta} > \delta_{\rm c}$, is equal to the fraction of the cosmic volume filled with haloes of mass M,

$$F(M, a) = \int_{\delta_{\rm c}}^\infty \mathrm{d}\bar{\delta} p(\bar{\delta}, a) = \frac{1}{2}\mathrm{erfc}\left(\frac{\delta_{\rm c}}{\sqrt{2}\sigma_R(a)}\right) , \tag{2.74}$$

where erfc(x) is the complementary error function. Obviously, this equation implies that the fraction of cosmic volume filled with haloes of fixed mass M is a highly sensitive function of the scale factor a.

- The distribution of haloes over masses M is simply $\partial F(M)/\partial M$, so we have to relate σ_R to M, which is accomplished by the characteristic radius $R(M)$,

$$\frac{\partial}{\partial M} = \frac{\mathrm{d}\sigma_R(a)}{\mathrm{d}M}\frac{\partial}{\partial \sigma_R(a)} = \frac{\mathrm{d}\sigma_R}{\mathrm{d}M}\frac{\partial}{\partial \sigma_R} \;, \tag{2.75}$$

where we have inserted the variance σ_R on the scale R at the present epoch. Using

$$\frac{\mathrm{d}}{\mathrm{d}x}\mathrm{erfc}(x) = -\frac{2}{\sqrt{\pi}}\mathrm{e}^{-x^2} \;, \tag{2.76}$$

we find

$$\left|\frac{\partial F(M)}{\partial M}\right| = \frac{1}{\sqrt{2\pi}}\frac{\delta_\mathrm{c}}{\sigma_R D_+(a)}\left|\frac{\mathrm{d}\ln\sigma_R}{\mathrm{d}M}\right|\exp\left(-\frac{\delta_\mathrm{c}^2}{2\sigma_R^2 D_+^2(a)}\right) \;, \tag{2.77}$$

where the absolute values have been added to ensure positiveness of the Press-Schechter mass function.

- The normalisation of the mass function is wrong, however. It is easy to see that

$$\int_0^\infty \left|\frac{\partial F(M)}{\partial M}\right|\mathrm{d}M = \frac{1}{2} \tag{2.78}$$

the reason for this problem is quite subtle. The solution can be obtained with an elegant argument interpreting the statistics of halo formation in terms of a random walk (see Sect. 2.4.2). For for now, we will arbitrarily multiply the mass function by a factor of two.

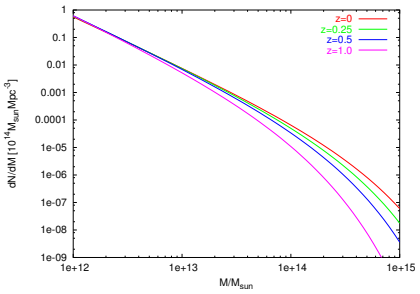

Press-Schechter mass function for the ΛCDM model at four different redshifts

- This fraction of the cosmic volume filled with haloes of masses within $[M, M+\mathrm{d}M]$ is converted to a (comoving) number density by dividing with the mean volume M/ρ_0 occupied by M

$$\begin{aligned} f(M,a)\mathrm{d}M &\equiv \frac{\partial n(M,a)}{\partial M}\mathrm{d}M \\ &= \sqrt{\frac{2}{\pi}}\frac{\rho_0\delta_\mathrm{c}}{\sigma_R D_+(a)}\left|\frac{\mathrm{d}\ln\sigma_R}{\mathrm{d}M}\right|\exp\left(-\frac{\delta_\mathrm{c}^2}{2\sigma_R^2 D_+^2(a)}\right)\frac{\mathrm{d}M}{M} \;. \end{aligned} \tag{2.79}$$

- The Press-Schechter mass function (2.79) has turned out to describe the mass distribution of dark-matter haloes in cosmological simulations remarkably well. Only recently have modifications been applied in order to improve its agreement with large, high-resolution simulations, or to take into account that halo collapse is not expected to proceed spherically, but elliptically.

2.4.2 Halo Formation as a Random Walk

- The normalisation problem, however, is embarrassing and needs to be resolved. The solution was given with an elegant argument interpreting the statistics of halo formation in terms of a random walk.

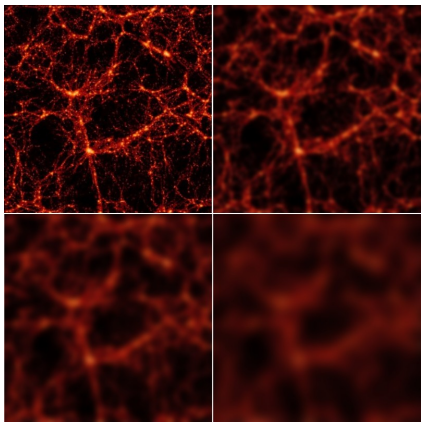

Progressive smoothing of the density field.

- Suppose the density-contrast field δ is given. A large sphere is centred on some point $\boldsymbol{x}$ and its radius gradually shrunk. For each radius R of the sphere, the density contrast $\bar{\delta}$ averaged within R is measured and monitored as a function of R. By choosing a window function W_R in the definition (2.31) of $\bar{\delta}$ whose Fourier transform has a sharp cut-off in k space, $\bar{\delta}$ will undergo a random walk because decreasing R corresponds to adding shells in k space which are independent of the modes which are already included.

- $\bar{\delta}(\boldsymbol{x})$ is thus following a random trajectory. A halo is expected to be formed at $\boldsymbol{x}$ if $\bar{\delta}(\boldsymbol{x})$ reaches δ_c for some radius R. If $\bar{\delta}(\boldsymbol{x}) < \delta_\mathrm{c}$ for some radius, it may well exceed δ_c for a smaller radius. Or, if $\bar{\delta}(\boldsymbol{x}) \geq \delta_\mathrm{c}$ for some radius, it may well drop below δ_c for a smaller radius.

- For determining halo numbers correctly, it is thus necessary to count all points in space which are part of haloes of any mass. As R is shrunk around a point $\boldsymbol{x}$, that point must be counted as being part of a halo if there is a radius R for which $\bar{\delta}(\boldsymbol{x}) \geq \delta_\mathrm{c}$.

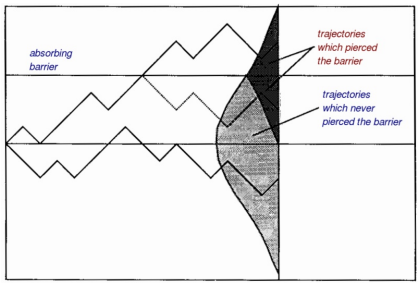

Random walk with an absorbing barrier.

- In the terminology of the random walk, we need to introduce an *absorbing barrier* at δ_c such that points $\boldsymbol{x}$ with trajectories $\bar{\delta}(\boldsymbol{x})$ vs. R which hit the barrier are removed from counting them as not being parts of haloes. To accomplish this, we follow the strategy of counting trajectories that do *not* make it into haloes such that the complement of that union represent trajectories of haloes.

- A trajectory meeting the boundary has equal probability for moving above or below. For any *forbidden* trajectory continuing above the boundary, there is an *allowed* mirror trajectory continuing below it, and conversely. For any trajectory reaching a point $\bar{\delta} < \delta_\mathrm{c}$ exclusively along *allowed* trajectories, there is a path reaching its mirror point on the line $\bar{\delta} = \delta_\mathrm{c}$ exclusively along *forbidden* trajectories, and conversely. Thus, the probability for reaching a point $\bar{\delta} < \delta_\mathrm{c}$ along *allowed* trajectories exclusively below the barrier is the probability for reaching it along *any* trajectory, minus the probability for reaching its mirror point $\delta_\mathrm{c} + (\delta_\mathrm{c} - \bar{\delta}) = 2\delta_\mathrm{c} - \bar{\delta}$ along *forbidden* trajectories,

$$p_\mathrm{s}(\bar{\delta})\mathrm{d}\bar{\delta} = \frac{1}{\sqrt{2\pi}\sigma_R}\left[\exp\left(-\frac{\bar{\delta}^2}{2\sigma_R^2}\right) - \exp\left(-\frac{(2\delta_\mathrm{c} - \bar{\delta})^2}{2\sigma_R^2}\right)\right] , \quad (2.80)$$

where σ_R is the variance of $\bar{\delta}$ on the scale R, as before.

- (2.80) is the probability distribution for the averaged density contrast to fall within $[\bar{\delta}, \bar{\delta} + \mathrm{d}\bar{\delta}]$ and *not* to exceed δ_c when averaged on *any* scale. The probability for $\bar{\delta}$ to *exceed* δ_c on some scale is thus

$$1 - P_\mathrm{s} = 1 - \int_{-\infty}^{\delta_\mathrm{c}} \mathrm{d}\bar{\delta} p_\mathrm{s}(\bar{\delta}) = \mathrm{erfc}\left(\frac{\delta_\mathrm{c}}{\sqrt{2}\sigma_R}\right) , \qquad (2.81)$$

without the factor $1/2$ in (2.74). The rest of the derivation of the Press-Schechter mass function proceeds as before.

2.4.3 Extended Press-Schechter Theory

- Considering the random walk of the density contrast field when averaged over increasing or decreasing scales allows the statistics of haloes to be greatly extended. In order to simplify notation, we abbreviate $S := \sigma_R^2$.

- First, we note that we can either consider the barrier height δ_c to be constant while σ_R is increasing with time, or σ_R to be constant, while δ_c is decreasing with time, because only the ratio $\delta_\mathrm{c}/\sigma_R$ enters the relevant expressions. Thus, the barrier can be considered moving towards zero as time progresses,

$$\omega := \frac{\delta_\mathrm{c}}{D_+(a)} , \qquad (2.82)$$

reflecting the fact that halo collapse becomes easier as structure formation proceeds. Since $\delta_\mathrm{c}(a)$ decreases monotonically with increasing time, it can uniquely be used instead of time. The evolution of a halo can now be expressed as a random walk in S as time proceeds, or ω decreases.

- Second, we note that

$$\begin{aligned} -\frac{\partial P_\mathrm{s}}{\partial S}\mathrm{d}S &= -\frac{\partial}{\partial S}\int_{-\infty}^{\delta_\mathrm{c}} \mathrm{d}\bar{\delta} p_\mathrm{s}(\bar{\delta}) \\ &=: p_S(S,\omega)\mathrm{d}S = \frac{\omega}{\sqrt{2\pi S^3}} \mathrm{e}^{-\omega^2/2S}\mathrm{d}S , \end{aligned} \qquad (2.83)$$

is the probability for $\bar{\delta}$ to hit the barrier δ_c for the first time when the variance is increased from S to $S + \mathrm{d}S$. It represents the fraction of mass in haloes of a mass M corresponding to the scale R.

- Consider now a trajectory passing through the barrier ω_2 for the first time at S_2, continuing to eventually pass through $\omega_1 > \omega_2$ at some $S_1 > S_2$. It represents a halo of mass M_1 corresponding to S_1 which, at a later time corresponding to ω_2, reaches mass

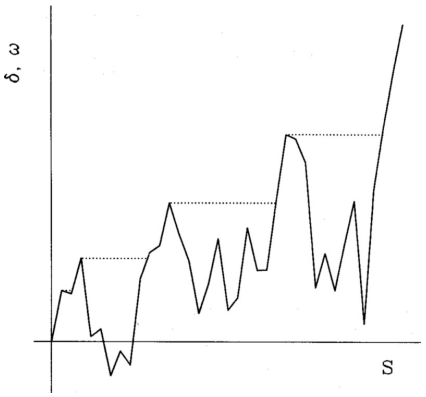

Trajectory of a halo in the S-ω plane. Increasing S means decreasing mass, and ω decreases with time.

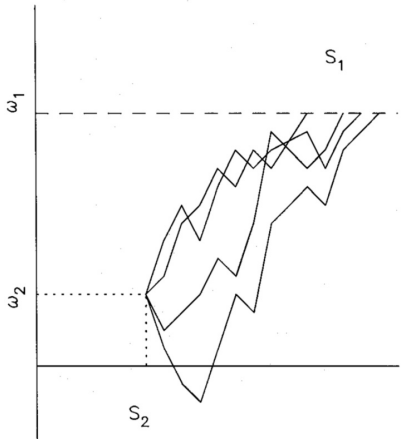

Trajectories of low-mass haloes at early time, forming a massive halo at a later time

$M_2 > M_1$ corresponding to S_2. The conditional probability for the halo to pass within $[S_1, S_1 + \mathrm{d}S_1]$ at ω_1, starting from S_2 at ω_2 is, according to (2.83),

$$p_{S_1}(S_1, \omega_1 | S_2, \omega_2)\mathrm{d}S_1 = \frac{\omega_1 - \omega_2}{\sqrt{2\pi}(S_1 - S_2)^{3/2}} \exp\left[-\frac{(\omega_1 - \omega_2)^2}{2(S_1 - S_2)}\right]\mathrm{d}S_1 \tag{2.84}$$

because the probability (2.83) only needs to be transformed shifting the origin of trajectories from $(S, \omega) = (0, 0)$ to $(S, \omega) = (S_2, \omega_2)$.

- From (2.84) and Bayes' theorem on conditional probabilities, we can straightforwardly derive the probability for a halo which for the first time reaches ω_1 at S_1 to reach ω_2 for the first time at S_2:

$$\begin{aligned}
& p_{S_2}(S_2, \omega_2 | S_1, \omega_1)\mathrm{d}S_2\, p_S(S_1, \omega_1)\mathrm{d}S_1 \\
= \;& p_{S_1}(S_1, \omega_1 | S_2, \omega_2)\mathrm{d}S_1\, p_S(S_2, \omega_2)\mathrm{d}S_2 \\
\Rightarrow \quad & p_{S_2}(S_2, \omega_2 | S_1, \omega_1)\mathrm{d}S_2 \\
= \;& \frac{p_{S_1}(S_1, \omega_1 | S_2, \omega_2)\mathrm{d}S_1\, p_S(S_2, \omega_2)\mathrm{d}S_2}{p_S(S_1, \omega_1)\mathrm{d}S_1} \\
= \;& \frac{1}{\sqrt{2\pi}}\left[\frac{S_1}{S_2(S_1 - S_2)}\right]^{3/2} \frac{\omega_2(\omega_1 - \omega_2)}{\omega_1} \\
\times \;& \exp\left[-\frac{(\omega_2 S_1 - \omega_1 S_2)^2}{2S_1 S_2(S_1 - S_2)}\right]\mathrm{d}S_2\,.
\end{aligned} \tag{2.85}$$

This provides the conditional probability for a halo of mass M_1 to have merged to form a halo of mass between M_2 and $M_2 + \mathrm{d}M_2$.

- The expected transition rate from S_1 to S_2 within the times t_1 and t_2 corresponding to ω_1 and ω_2 is determined by (2.85) taking the limit $\omega_2 \to \omega_1 =: \omega$,

$$\begin{aligned}
& \frac{\mathrm{d}^2 p_{S_2}}{\mathrm{d}S_2 \mathrm{d}\omega}(S_1 \to S_2 | \omega)\mathrm{d}S_2 \mathrm{d}\omega \\
= \;& \frac{1}{\sqrt{2\pi}}\left[\frac{S_1}{S_2(S_1 - S_2)}\right]^{3/2} \exp\left[-\frac{\omega^2(S_1 - S_2)}{2S_1 S_2}\right]\mathrm{d}S_2 \mathrm{d}\omega\,.
\end{aligned} \tag{2.86}$$

This gives the merger rate, i.e. the probability that, in the time interval corresponding to $\mathrm{d}\omega$, a halo of mass M_1 will merge with another halo of mass $M_2 - M_1$.

- We finally need to substitute the masses M_1 and M_2 for S_1 and S_2, and the time for ω. We wish to know the probability for a halo of mass M to accrete another halo of mass ΔM within the time interval $\mathrm{d}t$ at time t. The transformation is

$$\frac{\mathrm{d}^2 p_M}{\mathrm{d}\ln\Delta M \mathrm{d}t}(M_1 \to M_2 | t) = \frac{\mathrm{d}S_2}{\mathrm{d}\ln\Delta M}\left|\frac{\mathrm{d}\omega}{\mathrm{d}t}\right| \frac{\mathrm{d}^2 p_{S_2}}{\mathrm{d}S_2 \mathrm{d}\omega}\,. \tag{2.87}$$

- By the definition (2.82), the derivative of ω with respect to t is

$$\left|\frac{\mathrm{d}\omega}{\mathrm{d}t}\right| = \frac{\delta_\mathrm{c}}{D_+^2(a)} D'_+(a)\dot{a} = H\frac{\delta_\mathrm{c}}{D_+(a)}\frac{\mathrm{d}\ln D_+(a)}{\mathrm{d}\ln a}\ , \tag{2.88}$$

  where H is the Hubble parameter at scale factor a.

- Since $\Delta M = M_2 - M_1$, and S was introduced for σ_R^2, we have

$$\frac{\mathrm{d}S_2}{\mathrm{d}\ln\Delta M} = \Delta M\frac{\mathrm{d}\sigma_R^2(M_2)}{\mathrm{d}M_2}\ . \tag{2.89}$$

- With expressions (2.88) and (2.89), the merger probability (2.87) becomes

$$\begin{aligned}\frac{\mathrm{d}^2 p_M}{\mathrm{d}\ln\Delta M\mathrm{d}t} &= \sqrt{\frac{2}{\pi}}\frac{H\delta_\mathrm{c}}{\sigma_{R2}D_+}\frac{\mathrm{d}\ln D_+}{\mathrm{d}\ln a}\Delta M\frac{\mathrm{d}\ln\sigma_R}{\mathrm{d}M}(M+\Delta M)\\ &\times \left(1-\frac{\sigma_{R2}^2}{\sigma_R^2}\right)^{-3/2}\\ &\times \exp\left[-\frac{\delta_\mathrm{c}^2}{2\sigma_{R2}^2 D_+^2}\left(1-\frac{\sigma_{R2}^2}{\sigma_R^2}\right)\right]\ ,\end{aligned} \tag{2.90}$$

  where $\sigma_{R2} := \sigma_R(M_2) = \sigma_R(M+\Delta M)$.

- In much the same way, the random-walk interpretation of halo growth allows deducing halo-survival times and other interesting quantities related to halo growth.

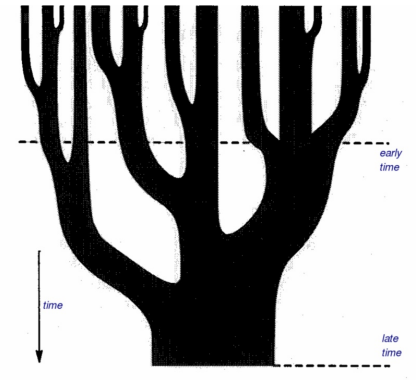

A "merger tree", i.e. a graphical representation of the accretion history of a halo

2.5 Halo Density Profiles

2.5.1 General Remarks

- Generally, a self-gravitating system of particles does not have an equilibrium state. The virial theorem demands that its total energy ($E = K + V$) is minus half its potential energy (V),

$$2K + V = E + K = 0 \quad \Rightarrow \quad K = -E = -\frac{V}{2}. \tag{2.91}$$

  Since $V < 0$ for self-gravitating systems, any inevitable energy loss, e.g., through the ejection of a body by means of three-body encounters, makes the potential energy become more negative. As a result, the halo becomes more tightly bound, which in turn increases its energy loss because the dynamical timescale is reduced by this contraction according to

$$t_{\rm dyn} \sim \left(\frac{R_{\rm g}^3}{GM}\right)^{1/2} \sim (G\rho)^{-1/2}\,, \tag{2.92}$$

  where $R_{\rm g} = GM/v^2$ is the gravitational radius. Thus, any halo density profile must reflect a potentially long-lived, but transient state.

- Knowing global halo properties like their mass, their distribution in mass and redshift, and their growth over time, their internal density profiles are an important characteristic. We will discuss two widely used models for the density profiles.

2.5.2 Isothermal Sphere

- A simple analytic model for the density profile is the isothermal sphere, which is a spherically-symmetric, self-gravitating system of non-interacting particles whose kinetic energy is characterised by a constant "temperature" $T = m/k\sigma^2$ where σ denotes the three-dimensional velocity dispersion.

- The equations describing the isothermal sphere are thus the Euler equation of hydrostatic equilibrium,

$$\frac{{\rm d}p}{{\rm d}r} = -\frac{GM(r)}{r^2}\rho\,, \tag{2.93}$$

  and the equation of state for the ideal gas

$$p = \frac{\rho}{m}kT\,, \tag{2.94}$$

  where m is the mean mass of the particles constituting the sphere.

- Inserting (2.94) into (2.93) yields

$$\frac{kT}{m}\frac{\mathrm{d}\ln\rho}{\mathrm{d}r} = -\frac{G}{r^2}\int_0^r 4\pi\rho(r')r'^2\mathrm{d}r' \ , \tag{2.95}$$

  where we have expressed the mass as an integral over the density. Differentiation with respect to r yields the second-order differential equation for ρ,

$$\frac{\mathrm{d}}{\mathrm{d}r}\left(r^2\frac{\mathrm{d}\ln\rho}{\mathrm{d}r}\right) = -\frac{4\pi Gm}{kT}r^2\rho \ . \tag{2.96}$$

- One solution of (2.96) is singular and can be obtained by means of a power-law ansatz in r to yield

$$\rho_1(r) = \frac{\sigma^2}{2\pi Gr^2} \qquad \sigma^2 \equiv \frac{kT}{m} \ , \tag{2.97}$$

  where σ is the (radially constant) velocity dispersion of the particles. The mass and circular velocity of the *singular isothermal sphere (SIS)* are given by

$$M(<r) = \frac{2\sigma^2}{G}r \quad \text{and} \quad v_\mathrm{c}^2 = \frac{GM(<r)}{r} = 2\sigma^2 \ . \tag{2.98}$$

- The solution to (2.96) depends on the boundary conditions. It turns out that there is a second solution, which has a finite central density ρ_0. To find this solution, we have to identify a characteristic length scale such that we can obtain a general solution in terms of dimensionless variables. The dimensional variables in (2.96) are G, ρ, and the combination $\sigma^2 = kT/m$. Those can be combined to yield a length scale, $\sigma/\sqrt{G\rho}$, which represents the typical distance a particle travels in the central dynamical time. We define the *King radius* at which the density profile cores out,

$$r_0 \equiv \left(\frac{9\sigma^2}{4\pi G\rho_0}\right)^{1/2} \ , \tag{2.99}$$

  and the dimensionless variables

$$\tilde{\rho} = \frac{\rho}{\rho_0} \ , \quad \text{and} \quad \tilde{r} = \frac{r}{r_0} \ . \tag{2.100}$$

- (2.96) cast into dimensionless form reads

$$\frac{\mathrm{d}}{\mathrm{d}\tilde{r}}\left(\tilde{r}^2\frac{\mathrm{d}\ln\tilde{\rho}}{\mathrm{d}\tilde{r}}\right) = -9\tilde{r}^2\tilde{\rho} \ . \tag{2.101}$$

  The (numerical) solution is obtained by integrating this differential equation outwards from $\tilde{r} = 0$ with the central boundary conditions $\tilde{\rho}(0) = 1$ and $\mathrm{d}\tilde{\rho}/\mathrm{d}\tilde{r} = 0$ (the second condition is necessary

since $M(\tilde{r})$ vanishes at $\tilde{r} = 0$). The resulting second solution can be approximated by

$$\tilde{\rho}_2(\tilde{r}) = \begin{cases} \left(1 + \tilde{r}^2\right)^{3/2} & \tilde{r} \lesssim 3, \\ \frac{2}{9}\tilde{r}^{-2} & \tilde{r} \gtrsim 3, \end{cases} \tag{2.102}$$

i.e., the SIS is the asymptotic solution at large $\tilde{r}$. Note that by defining dimensionless variables, we have reduced the *family* of solutions with different densities and temperatures to a single solution for appropriately scaled variables.

- Both solutions have the advantage that they reproduce the flat rotation curves observed in spiral galaxies. The rotational velocity $v_{\rm rot}$ of a particle orbiting at radius r is determined by

$$v_{\rm rot}^2 = \frac{GM}{r} , \tag{2.103}$$

which is constant at $r \gg r_0$ for both density profiles of the isothermal sphere. However, the temperature within a stable "gas" sphere cannot be constant because particles would evaporate from it. Besides, the mass of the isothermal sphere diverges linearly as $r \to \infty$. To get a halo of finite mass, we must truncate it at some large radius by confining it with an external "pressure" that is practise is provided by accretion of mass. The isothermal profile is thus at best an approximation for the inner parts of haloes.

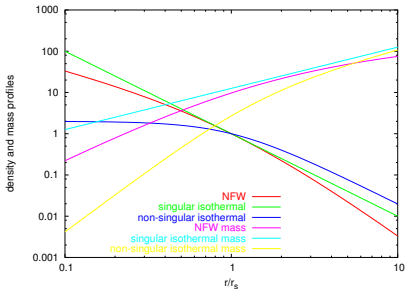

Singular and non-singular isothermal and NFW density and mass profiles.

2.5.3 Navarro-Frenk-White (NFW) Density Profile

- Numerical simulations of halo formation in the cold dark matter model consistently show density profiles like

$$\rho(r) = \frac{\rho_{\rm s}}{x(1+x)^2} , \quad x \equiv \frac{r}{r_{\rm s}} , \tag{2.104}$$

which have a characteristic scale radius $r_{\rm s}$ beyond which they fall off $\propto r^{-3}$, and within which the density profile flattens considerably.

- Using the identity $x/(1+x)^2 \equiv (1+x)^{-1} - (1+x)^{-2}$, the mass of such haloes within radius r can easily be derived,

$$M(r) = 4\pi\rho_{\rm s} r_{\rm s}^3 \int_0^x \frac{x'{\rm d}x'}{(1+x')^2} = 4\pi\rho_{\rm s} r_{\rm s}^3 \left[\ln(1+x) - \frac{x}{1+x}\right] . \tag{2.105}$$

It rises $\propto x^2$ for small x and diverges logarithmically for $x \to \infty$. The divergence is not a fundamental problem because the halo profile must become invalid at the latest where ρ drops to the cosmic background density. In practise, the assumption of spherical symmetry starts to break down earlier, and becomes invalid at scales beyond the virial radius.

- The virial radius $r_{\rm vir}$ of a halo is often defined as the radius r_{200} enclosing a mean overdensity of 200 times the *critical* cosmic density,

$$\rho_{\rm cr}(a) \equiv \frac{3H^2(a)}{8\pi G} \ , \text{ where} \tag{2.106}$$

$$H^2(a) \equiv H_0^2\left[\Omega_{\rm m0}a^{-3} + \Omega_{\Lambda 0} + \Omega_{\rm K}a^{-2}\right] \tag{2.107}$$

  is the Hubble function at late times, which are relevant for galaxies and clusters and which describes the expansion rate of the universe. This implies that the contribution of the cosmological constant Λ (and curvature K) to the critical density are included in the estimate of the reference density. Since Λ = const., this has the advantage that the mass of a halo that has decoupled from the cosmic expansion can only grow by accretion but remains constant otherwise (at least at lates times when the cosmological constant dominates the energy density of the universe, $a > a_{\rm eq,\Lambda}$). The factor 200 is a rough approximation to the density contrast of $18\pi^2 \approx 178$ expected at virialisation in the spherical collapse model. This implies

$$M_{200}\left(\frac{4\pi}{3}r_{200}^3\right)^{-1} = 200\rho_{\rm cr}(a) = 200\frac{3H^2(a)}{8\pi G} \ , \tag{2.108}$$

  where M_{200} is often identified with the total halo mass M. We obtain

$$r_{200} = \left(\frac{GM_{200}}{100H^2}\right)^{1/3} \ . \tag{2.109}$$

- Other frequent definitions use the radius enclosing a mean overdensity of 200 times the *mean* matter density (i.e., without the Λ contribution),

$$M_{200\rm m}\left(\frac{4\pi}{3}r_{200\rm m}^3\right)^{-1} = 200\rho_{\rm cr}(a)\Omega_{\rm m}(a) \ . \tag{2.110}$$

  This definition has the advantage that haloes of the same mass but at different redshifts show the same amount of kinetic pressure contribution or velocity anisotropy as a function of radius, i.e., this definition is close to a dynamical definition of the virial radius. However, it requires the knowledge of the ab initio unknown cosmological parameter $\Omega_{\rm m0}$ and has the property that the halo mass increases at late times because of the redshift dilution of the mean matter density as $\rho_{\rm m} = \rho_{\rm m0}a^{-3}$ even in the absence of mass accretion! Sometimes, people prefer a redshift dependent overdensity $\Delta(a)$ from the solution of a spherical top-hat perturbation *at* the time of collapse (2.70) rather than a constant overdensity threshold. While this property is easily calculable in simulations, the collapse time of a cluster is inaccessible in observations which jeopardises detailed comparisons of observations and theory.

- The ratio $c \equiv r_{200}/r_s$ is called *concentration* of the halo . It turns out to be a function of halo mass and redshift and to depend on cosmological parameters. Generally, c is the higher the earlier haloes form. This reflects the hierarchical growth of haloes and implies that smaller haloes form earlier when the mean background density was higher. As a result, these haloes have a higher density at small scales in comparison to larger halos when radii are scaled to R_{200}. Given the halo mass M, the (virial) radius is given by (2.109), the concentration parameter gives $r_s = r_{200}/c$, and the scale density ρ_s is then determined from (2.105) by the requirement that $M(r_{200}) = M_{200}$. Thus, the profile (2.104) is essentially determined by a single parameter, e.g. its mass.

- It is currently unclear how the density profile arises. Also, its slope near the core is being discussed.

Chapter 3

Evolution of the Baryonic Component

3.1 Non-radiative Physics

3.1.1 Adiabatic Processes and Entropy

- Before we enter a detailed discussion of the evolution of the baryonic component of a cluster, we review a few basic concepts. First, we start with the first law of thermodynamics (energy conservation):

$$\mathrm{d}q = T\mathrm{d}s = \mathrm{d}\epsilon + P\mathrm{d}\tilde{V}, \tag{3.1}$$

where $\tilde{V} \equiv \rho^{-1}$ is the specific volume, q is the heat per unit mass, s is the specific entropy, $\epsilon \equiv \varepsilon/\rho$ is the specific internal energy and ε is the internal energy density.

- The specific heat at constant volume

$$c_V \equiv \left(\frac{\partial q}{\partial T}\right)_V \tag{3.2}$$

is the amount of heat that must be added to raise the temperature of 1g of gas by 1K. At constant volume, the internal energy can only be changed by adding or releasing heat, $\mathrm{d}\epsilon = \mathrm{d}q$. If e depends only on temperature (and not density), $\epsilon(\tilde{V}, T) = \epsilon(T)$, then

$$c_V \equiv \left(\frac{\partial q}{\partial T}\right)_V = \left(\frac{\partial \epsilon}{\partial T}\right)_V = \frac{\partial \epsilon}{\partial T} \tag{3.3}$$

implying

$$\mathrm{d}q = c_V\mathrm{d}T + P\mathrm{d}\tilde{V}. \tag{3.4}$$

- The pressure of a gas of particles with mass m is given by

$$P\tilde{V} = \frac{k_\mathrm{B}T}{m} \implies P\mathrm{d}\tilde{V} = \frac{k_\mathrm{B}}{m}\mathrm{d}T. \tag{3.5}$$

Using $\mathrm{d}q = c_V\mathrm{d}T + P\mathrm{d}\tilde{V}$, the specific heat at constant pressure is

$$c_P \equiv \left(\frac{\partial q}{\partial T}\right)_P = c_V + P\frac{\mathrm{d}\tilde{V}}{\mathrm{d}T} = c_V + \frac{k_\mathrm{B}}{m}. \tag{3.6}$$

Changing the temperature at constant pressure requires more heat than at constant volume because some of the energy does into $P\mathrm{d}\tilde{V}$ work.

- For reasons that become soon clear, we define the adiabatic index $\gamma = c_P/c_V$. The ionized plasma of the intra-cluster medium (ICM) is to very good approximation a monoatomic gas and has therefore 3 translational degrees of freedom. In this case, the specific energy is

$$\epsilon = \frac{3}{2}\frac{k_\mathrm{B}T}{m} \implies c_V = \frac{3}{2}\frac{k_\mathrm{B}}{m} \implies c_P = \frac{5}{2}\frac{k_\mathrm{B}}{m} \implies \gamma = \frac{5}{3} \tag{3.7}$$

In general, the equation of state for an ideal gas is given by

$$\epsilon = \frac{1}{\gamma - 1}\frac{k_\mathrm{B}T}{m} = \frac{1}{\gamma - 1}\frac{P}{\rho}. \tag{3.8}$$

- The total differential of the equation of state of an ideal gas is

$$\mathrm{d}\epsilon = \frac{1}{\gamma - 1}\left(\frac{\mathrm{d}P}{\rho} - \frac{P}{\rho^2}\mathrm{d}\rho\right). \tag{3.9}$$

For adiabatic ($\mathrm{d}q = \mathrm{d}s = 0$) changes, we can combine this with the first law of thermodynamics

$$\mathrm{d}\epsilon = -P\mathrm{d}\tilde{V} = \frac{P}{\rho^2}\mathrm{d}\rho \tag{3.10}$$

and find (after multiplying with ρ/P)

$$\frac{1}{\gamma - 1}\left(\frac{\mathrm{d}P}{P} - \frac{\mathrm{d}\rho}{\rho}\right) = \frac{\mathrm{d}\rho}{\rho}, \tag{3.11}$$

implying

$$\frac{\mathrm{d}P}{P} = \gamma\frac{\mathrm{d}\rho}{\rho} \implies P = P_0\left(\frac{\rho}{\rho_0}\right)^\gamma \equiv K\rho^\gamma. \tag{3.12}$$

- Thus, a polytropic equation of state ($P \propto \rho^\gamma$) defines the quantities

$$K = \frac{P}{\rho^\gamma} = \frac{k_\mathrm{B}T}{m\rho^{\gamma-1}}, \text{ and} \tag{3.13}$$

$$K_\mathrm{e} = \frac{k_\mathrm{B}T_\mathrm{e}}{n_\mathrm{e}^{\gamma-1}} \propto K \tag{3.14}$$

which are constants upon adiabatic changes. In the context of galaxy clusters, they are often referred to as "entropy". This is especially the case for the observationally motivated K_e which can be conveniently computed with the X-ray observables $k_\mathrm{B}T_\mathrm{e}$ and n_e and has typical values of

$$K_\mathrm{e} \sim 100\left(\frac{k_\mathrm{B}T_\mathrm{e}}{1\ \mathrm{keV}}\right)\left(\frac{n_\mathrm{e}}{10^{-3}\ \mathrm{cm}^{-3}}\right)^{-2/3}\ \mathrm{keV\ cm}^2. \tag{3.15}$$

- To relate this cluster "entropy" to the proper thermodynamic entropy, we start with

$$\mathrm{d}\epsilon = -P\mathrm{d}\tilde{V} + T\mathrm{d}s \tag{3.16}$$

and consider adding or removing heat at constant ρ ($\mathrm{d}\tilde{V} = 0$),

$$T\mathrm{d}s = \mathrm{d}\epsilon = c_V\mathrm{d}T \tag{3.17}$$

implying

$$\mathrm{d}s = c_V\frac{\mathrm{d}T}{T} \implies s = c_V\ln T + \text{const.} \tag{3.18}$$

- Since $P \propto T$ at constant ρ, this implies that $s = c_V \ln P + \text{const.}$ We have just shown that adiabatic changes keep $P\rho^{-\gamma}$ constant, so these must be lines of constant entropy (in the P-ρ plane). Hence, for a single species gas, we have

$$s = c_V \ln(P\rho^{-\gamma}) + \text{const.} = \frac{k_\mathrm{B}}{(\gamma-1)m} \ln K + \text{const.} \tag{3.19}$$

or

$$s = c_V \ln\left(\frac{K}{K_0}\right) \quad \Longleftrightarrow \quad K = K_0 \exp\left(\frac{s}{c_V}\right). \tag{3.20}$$

3.1.2 Basic Conservation Equations

Preliminaries

- A physical system can be described at different levels: with quantum physics, at the classical particle level, or in the continuous fluid level. A fluid is a macroscopic description of a physical system that is characterized by its mass density ρ, temperature T, and velocity $\boldsymbol{u} = \boldsymbol{v} + \boldsymbol{w}$. Here $\boldsymbol{v} \equiv \langle \boldsymbol{u} \rangle$ is the mean velocity in the local fluid element and $\boldsymbol{w}$ is the random velocity component that defines the temperature. The equipartition theorem of classical mechanics states that each degree of freedom i that can be excited has energy $k_\mathrm{B}T/2$:

$$\left\langle \frac{1}{2} m w_i^2 \right\rangle = \frac{1}{2} k_\mathrm{B} T \implies \left\langle |\boldsymbol{w}|^2 \right\rangle = \frac{3 k_\mathrm{B} T}{m}. \tag{3.21}$$

  Fluid elements move and change their density and temperature, but particles random walk from one fluid element to another only slowly, through a diffusion process.

- A system can be well described as a fluid, if the particle mean free path is much shorter than the characteristic system size, $\lambda \ll L$. In an ionized plasma, the electron's effective interaction radius r_e is to order of magnitude give by an energy balance between the electrostatic potential of an ion of charge Ze and the thermal energy of an electron:

$$\frac{Ze^2}{r_\mathrm{e}} \sim m_\mathrm{e} w_\mathrm{e}^2 \sim k_\mathrm{B} T_\mathrm{e}, \tag{3.22}$$

  where e and m_e are the electron charge and mass, respectively. The electron mean free path is given by

$$\lambda = \frac{1}{n\sigma} \sim \frac{1}{n\pi r_\mathrm{e}^2} \sim \frac{1}{\pi n} \left(\frac{k_\mathrm{B} T_\mathrm{e}}{Ze^2}\right)^2 \tag{3.23}$$

$$\sim 1.5 \times 10^{22} \left(\frac{n}{10^{-3}\ \mathrm{cm}^{-3}}\right)^{-1} \left(\frac{k_\mathrm{B} T_\mathrm{e}}{1\ \mathrm{keV}}\right)^2 \ \mathrm{cm}, \tag{3.24}$$

  where we have assumed $Z = 1$.

- Careful calculations (which we will perform in Sect. 3.2.5) yield a result that is shorter by $\sim (\ln\Lambda)^{-1}$ because of the effects of distant interactions. Here, $\Lambda = b_{\max}/b_{\min}$ is the ratio of the largest-to-smallest impact parameter of such an interaction. The typical impact parameter in a large-angle deflection constitutes the minimum impact parameter, $b_{\min} \sim r_e$, and $b_{\max} \sim \lambda_D$ since the plasma becomes neutral on scales larger than the Debye length, $\lambda_D = \sqrt{k_B T/(4\pi n_e Z e^2)}$. Hence, we obtain to order of magnitude

$$\begin{aligned}\ln\Lambda &\sim \ln\frac{\lambda_D}{r_e} \sim \ln\sqrt{\frac{(k_B T)^3}{n_e 4\pi Z^3 e^6}} \\ &\sim 35 - \frac{1}{2}\ln\left(\frac{n_e}{10^{-2}\mathrm{cm}^{-3}}\right) + \frac{3}{2}\ln\left(\frac{k_B T}{\mathrm{keV}}\right). \end{aligned} \quad (3.25)$$

  Hence, $\lambda \ll L_{\mathrm{cluster}}$ and we can treat the bulk of the ICM as a fluid. However, on small scales or toward the cluster outskirts, this is not true and we have to consider plasma processes.

The Distribution Function and the Boltzmann Equation

- We define the distribution function $f(\boldsymbol{x}, \boldsymbol{u}, t)$ such that $f(\boldsymbol{x}, \boldsymbol{u}, t)\mathrm{d}^3x\mathrm{d}^3u$ is the probability of finding a particle in the phase space volume $\mathrm{d}^3x\mathrm{d}^3u$ centered on position $\boldsymbol{x}$, velocity $\boldsymbol{u}$ at time t. Integrating over all phase space yields the total number of particles

$$N = \int\int f(\boldsymbol{x}, \boldsymbol{u}, t)\mathrm{d}^3x\mathrm{d}^3u. \quad (3.26)$$

  Since particles are neither created nor destroyed, continuity implies

$$\frac{\mathrm{d}}{\mathrm{d}t}f(\boldsymbol{x}, \boldsymbol{u}, t) = \frac{\partial f}{\partial t} + \dot{\boldsymbol{x}}\cdot\boldsymbol{\nabla}f + \dot{\boldsymbol{u}}\cdot\boldsymbol{\nabla}_u f = \left.\frac{\mathrm{d}f}{\mathrm{d}t}\right|_c, \quad (3.27)$$

  where the term $\mathrm{d}f/\mathrm{d}t|_c$ represents discontinuous motions of particles through phase space as a result of collisions. While collisions happen at a fixed point in space, they can instantaneously change particle velocities and thus cause particles to jump in phase space. Substitution $\dot{\boldsymbol{x}} = \boldsymbol{v}$ and $\dot{\boldsymbol{u}} = \boldsymbol{g}$ leads to the Boltzmann equation

$$\frac{\mathrm{d}}{\mathrm{d}t}f(\boldsymbol{x}, \boldsymbol{u}, t) = \frac{\partial f}{\partial t} + \boldsymbol{u}\cdot\boldsymbol{\nabla}f + \boldsymbol{g}\cdot\boldsymbol{\nabla}_u f = \left.\frac{\mathrm{d}f}{\mathrm{d}t}\right|_c \quad (3.28)$$

  which describes the evolution of the phase space distribution function $f(\boldsymbol{x}, \boldsymbol{u}, t)$.

- In the fluid limit ($\lambda \ll L$), the collision term causes $f(\boldsymbol{u})$ to approach a Maxwellian velocity distribution while locally conserving mass, momentum, and energy. This property allows us to

coarse grain the information in phase space and distill the essential pieces of information, namely how density, mean velocity, and velocity dispersion change as a function of $\boldsymbol{x}$ and t. In practice, this is done by taking the appropriate moments of the Boltzmann equation and integrating over velocity space, d^3u. We identify the mass density

$$\rho = \rho(\boldsymbol{x}, t) = \int m f(\boldsymbol{x}, \boldsymbol{u}, t)\, \mathrm{d}^3u. \tag{3.29}$$

The mass-weighted average of some quantity q at position $\boldsymbol{x}$ is given by

$$\langle q \rangle = \frac{1}{\rho} \int q m f(\boldsymbol{x}, \boldsymbol{u}, t)\, \mathrm{d}^3u. \tag{3.30}$$

Mass Conservation – Continuity Equation

- We multiply (3.28) by m and integrate over d^3u to get

$$\frac{\partial}{\partial t} \int m f \mathrm{d}^3u + \sum_{i=1}^{3} \frac{\partial}{\partial x_i} \int m f u_i \mathrm{d}^3u + m \int \sum_{i=1}^{3} \frac{\partial}{\partial u_i} (g_i f) \mathrm{d}^3u = \int m \left.\frac{\partial f}{\partial t}\right|_{\mathrm{c}} \mathrm{d}^3u. \tag{3.31}$$

  Here we assume that the force $\boldsymbol{g}$ does not depend on velocity $\boldsymbol{u}$.

- Using the definitions (3.29) and (3.30) and applying Gauss' divergence theorem, this simplifies to

$$\frac{\partial}{\partial t} \rho(\boldsymbol{x}, t) + \sum_{i=1}^{3} \frac{\partial}{\partial x_i} (\rho \langle u_i \rangle) + m \int_{\partial\Omega} f(\boldsymbol{g} \cdot \boldsymbol{n}) \mathrm{d}^2A_u = 0, \tag{3.32}$$

  where $\boldsymbol{n}$ is the normal vector of the differential surface element d^2A_u. The right-hand side vanishes because of local mass conservation: collisions do not create or destroy particles at a fixed position, they can only discontinuously shift them in velocity space. Since the velocity can be split into a mean and a random component, $\boldsymbol{u} = \boldsymbol{v} + \boldsymbol{w}$, we have $\langle \boldsymbol{u} \rangle \equiv \boldsymbol{v}$ in the second term. Assuming that $f \to 0$ for $|\boldsymbol{u}| \to \infty$, the third term also vanishes on taking the limit of the integration boundary to infinity. We hence obtain

$$\frac{\partial \rho}{\partial t} + \boldsymbol{\nabla} \cdot (\rho \boldsymbol{v}) = 0. \tag{3.33}$$

- Taking the volume integral extending over the entire space and applying Gauss' divergence theorem, we can demonstrate that the

total mass of the system is conserved:

$$\begin{aligned} \frac{\partial}{\partial t}\int_\Omega \rho \mathrm{d}^3x + \int_\Omega \boldsymbol{\nabla}\cdot(\rho\boldsymbol{v})\mathrm{d}^3x &= 0, \\ \frac{\partial m}{\partial t} + \lim_{\partial\Omega\to\infty}\int_{\partial\Omega}\rho(\boldsymbol{v}\cdot\boldsymbol{n})\mathrm{d}^2A &= \frac{\mathrm{d}m}{\mathrm{d}t} = 0. \end{aligned} \tag{3.34}$$

In the last line, we exchanged the total for the partial time derivatives since m depends neither on position nor on velocity.

Momentum Conservation

- We multiply (3.28) by $m\boldsymbol{u}$ and integrate over d^3u to get

$$\frac{\partial}{\partial t}\int mu_j f\mathrm{d}^3u + \sum_{i=1}^{3}\frac{\partial}{\partial x_i}\int mfu_ju_i\mathrm{d}^3u + m\int\sum_{i=1}^{3}g_iu_j\frac{\partial f}{\partial u_i}\mathrm{d}^3u = \int mu_j\left.\frac{\partial f}{\partial t}\right|_{\mathrm{c}} d^3u. \tag{3.35}$$

- The first term is $\partial(\rho v_j)/\partial t$ and second term is

$$\sum_{i=1}^{3}\frac{\partial}{\partial x_i}(\rho\langle u_ju_i\rangle) = \sum_{i=1}^{3}\frac{\partial}{\partial x_i}(\rho v_jv_i + \rho\langle w_jw_i\rangle). \tag{3.36}$$

To simplify the third term, we use the identity

$$\frac{\partial}{\partial u_i}(u_jf) \equiv u_j\frac{\partial f}{\partial u_i} + \delta_{ij}f \tag{3.37}$$

and obtain

$$\sum_{i=1}^{3}mg_i\int\left[\frac{\partial}{\partial u_i}(u_jf) - \delta_{ij}f\right]d^3u = -\sum_{i=1}^{3}g_i\delta_{ij}\int mf\mathrm{d}^3u = -\rho g_j, \tag{3.38}$$

where $\delta_{ij} \equiv 1$ for $i = j$, 0 for $i \neq j$ and the first term in the bracket vanishes because of Gauss' divergence theorem. The right-hand side of (3.35) vanishes because collisions conserve momentum.

- We get the result

$$\frac{\partial}{\partial t}(\rho v_j) + \sum_{i=1}^{3}\frac{\partial}{\partial x_i}(\rho v_jv_i + \rho\langle w_jw_i\rangle) = \rho g_j. \tag{3.39}$$

The diagonal terms of $\langle w_iw_j\rangle$ are generally much larger than the off-diagonal terms since random velocities in different directions

are almost uncorrelated. It is useful to split the $\rho\langle w_i w_j\rangle$ term into an (isotropic) contribution from pressure, P, and a contribution from the anisotropic viscous stress tensor, $\bar{\mathbf{\Pi}}$,

$$P \equiv \frac{1}{3}\rho\langle|\boldsymbol{w}|^2\rangle, \tag{3.40}$$

$$\Pi_{ij} \equiv P\delta_{ij} - \rho\langle w_i w_j\rangle, \tag{3.41}$$

which is a symmetric and traceless tensor.

- The final result is the Navier-Stokes equation

$$\frac{\partial}{\partial t}(\rho v_j) + \sum_{i=1}^{3}\frac{\partial}{\partial x_i}\left(\rho v_i v_j + P\delta_{ij} - \Pi_{ij}\right) = \rho g_j, \text{ or} \tag{3.42}$$

$$\frac{\partial}{\partial t}(\rho\boldsymbol{v}) + \boldsymbol{\nabla}\cdot\left(\rho\boldsymbol{v}\boldsymbol{v}^{\mathrm{T}} + P\bar{\mathbf{1}} - \bar{\mathbf{\Pi}}\right) = \rho\boldsymbol{g}. \tag{3.43}$$

Taking the volume integral and applying Gauss' divergence theorem (as in 3.34), we can demonstrate that the total momentum, $\boldsymbol{p} = \int \rho\boldsymbol{v}\mathrm{d}^3x$ is conserved in the absence of an external force field that acts as a source of momentum.

- To simplify this equation, we rewrite the first two terms in (3.43),

$$\begin{aligned}
&\frac{\partial}{\partial t}(\rho\boldsymbol{v}) + \boldsymbol{\nabla}\cdot\left(\rho\boldsymbol{v}\boldsymbol{v}^{\mathrm{T}}\right)\\
&= \dot{\rho}\boldsymbol{v} + \rho\dot{\boldsymbol{v}} + \rho\boldsymbol{v}(\boldsymbol{\nabla}\cdot\boldsymbol{v}) + \rho(\boldsymbol{v}\cdot\nabla)\boldsymbol{v} + \boldsymbol{v}(\boldsymbol{v}\cdot\boldsymbol{\nabla}\rho) \qquad (3.44)\\
&= \boldsymbol{v}\left[\dot{\rho} + \boldsymbol{\nabla}\cdot(\rho\boldsymbol{v})\right] + \rho\left[\dot{\boldsymbol{v}} + (\boldsymbol{v}\cdot\boldsymbol{\nabla})\boldsymbol{v}\right] = \rho\left[\dot{\boldsymbol{v}} + (\boldsymbol{v}\cdot\boldsymbol{\nabla})\boldsymbol{v}\right].
\end{aligned}$$

In the last step, we have used the continuity equation (3.33).

- If we use this result in combination with the momentum equation (3.43), we get

$$\frac{\partial\boldsymbol{v}}{\partial t} + (\boldsymbol{v}\cdot\boldsymbol{\nabla})\boldsymbol{v} = \boldsymbol{g} - \frac{1}{\rho}\boldsymbol{\nabla}P + \frac{1}{\rho}\boldsymbol{\nabla}\cdot\bar{\mathbf{\Pi}}. \tag{3.45}$$

Viscosity acts to oppose shearing motion and interpenetration.

- To make progress, we adopt an ansatz for the viscous stress tensor and assume a "Newtonian fluid", i.e., we assume that Π_{ij} is linearly proportional to the velocity gradient, $\partial v_i/\partial x_j$. The most general symmetric tensor that is linear in $\partial v_i/\partial x_j$ is

$$\Pi_{ij} = \mu D_{ij} + \beta\delta_{ij}(\boldsymbol{\nabla}\cdot\boldsymbol{v}), \text{ where} \tag{3.46}$$

$$D_{ij} = \frac{\partial v_i}{\partial x_j} + \frac{\partial v_j}{\partial x_i} - \frac{2}{3}\delta_{ij}(\boldsymbol{\nabla}\cdot\boldsymbol{v}) \tag{3.47}$$

is the deformation tensor that vanishes for uniform expansion or contraction. μ and β are the coefficients of shear and bulk viscosity, respectively and have units of g cm^{-1} s^{-1}. The term μD_{ij} represents resistance to shearing motion and $\beta\delta_{ij}(\boldsymbol{\nabla}\cdot\boldsymbol{v})$ represents resistance to changes in volume.

Energy Conservation

- To obtain the internal energy equation, we multiply (3.28) by $m\boldsymbol{u}^2$ and integrate over d^3u. Making use of Gauss' divergence theorem and of the fact that collisions conserve energy (as well as mass and momentum) we get (after a similar procedure)

$$\rho\frac{\mathrm{d}\epsilon}{\mathrm{d}t} = \rho\left(\frac{\partial\epsilon}{\partial t} + \boldsymbol{v}\cdot\boldsymbol{\nabla}\epsilon\right)$$
$$= \frac{\partial}{\partial t}(\rho\epsilon) + \boldsymbol{\nabla}\cdot(\rho\epsilon\boldsymbol{v}) = -P\boldsymbol{\nabla}\cdot\boldsymbol{v} + \Psi - \boldsymbol{\nabla}\cdot\boldsymbol{Q}. \quad (3.48)$$

  In the second step, we have used the continuity equation (3.33). Here, ϵ is the specific internal energy (3.21), Ψ is the viscous dissipation rate, and $\boldsymbol{Q}$ is the conductive heat flux:

$$\epsilon \equiv \frac{1}{2}\left\langle|\boldsymbol{w}|^2\right\rangle, \quad (3.49)$$
$$\Psi \equiv \sum_{i,j=1}^{3}\Pi_{ij}\frac{\partial v_i}{\partial x_j}, \quad (3.50)$$
$$\boldsymbol{Q} \equiv \frac{1}{2}\rho\left\langle\boldsymbol{w}|\boldsymbol{w}|^2\right\rangle. \quad (3.51)$$

  Ψ represents conversion of bulk motion of the fluid into internal energy via viscous dissipation. It is the viscous analog of heating by $P\mathrm{d}V$ work.

- If the distribution of the random velocity component, $\boldsymbol{w}$, is symmetric about zero, then $\boldsymbol{Q}$ vanishes. If the distribution is skewed, then hot particles drift relative to cold particles and produce a heat flux in the direction of the drift. In most cases, a temperature gradient produces a conductive flux (see also Sect. 3.2.5),

$$\boldsymbol{Q} = -\chi\boldsymbol{\nabla}T, \quad \text{with } \chi \simeq 6\times10^{-7}\,T^{5/2}\,\mathrm{erg\ s^{-1}cm^{-1}K^{-1}}. \quad (3.52)$$

  We will also use $\kappa = \chi T/P$ instead of χ for convenience (κ has units of $\mathrm{cm^2\ s^{-1}}$, i.e., of a diffusion coefficient). However, if $\boldsymbol{Q}$ is uniform, heat flowing out is replaced by heat flowing in. Hence, the local thermal energy changes only if $\boldsymbol{\nabla}\cdot\boldsymbol{Q} \neq 0$.

- One can derive an equivalent equation for the entropy by considering the first law of thermodynamics,

$$\mathrm{d}\epsilon = -P\mathrm{d}\tilde{V} + T\mathrm{d}s = \frac{P}{\rho^2}\mathrm{d}\rho + T\mathrm{d}s. \quad (3.53)$$

  Combining this with the internal energy equation (3.48), we get

$$\frac{P}{\rho^2}\frac{\mathrm{d}\rho}{\mathrm{d}t} + T\frac{\mathrm{d}s}{\mathrm{d}t} = -\frac{P}{\rho}\boldsymbol{\nabla}\cdot\boldsymbol{v} - \frac{1}{\rho}\boldsymbol{\nabla}\cdot\boldsymbol{Q} + \frac{1}{\rho}\Psi. \quad (3.54)$$

Using the continuity equation, $\mathrm{d}\rho/\mathrm{d}t = -\rho\boldsymbol{\nabla}\cdot\boldsymbol{v}$, the first terms on both sides cancel each other and we obtain,

$$\rho T\frac{\mathrm{d}s}{\mathrm{d}t} = -\boldsymbol{\nabla}\cdot\boldsymbol{Q}+\Psi. \tag{3.55}$$

This shows explicitly, that heat conduction and viscous friction change the entropy. Equivalently, if these processes are absent, specific entropy is conserved.

3.1.3 Buoyancy Instabilities

- We are now interested in studying adiabatic hydrodynamic perturbations about an atmosphere in hydrostatic equilibrium. The starting point are conservation equations of mass, momentum, and internal energy (or equivalently entropy) in the absence of viscosity and magnetic fields:

$$\frac{\partial\rho}{\partial t}+\boldsymbol{\nabla}\cdot(\rho\boldsymbol{v}) = 0, \tag{3.56}$$

$$\frac{\partial\boldsymbol{v}}{\partial t}+(\boldsymbol{v}\cdot\boldsymbol{\nabla})\boldsymbol{v} = -\frac{\boldsymbol{\nabla}P}{\rho}+\boldsymbol{g}, \tag{3.57}$$

$$\rho T\frac{\mathrm{d}s}{\mathrm{d}t} = -\boldsymbol{\nabla}\cdot\boldsymbol{Q}, \tag{3.58}$$

where $\rho(t,\boldsymbol{x})$ and $\boldsymbol{v}(t,\boldsymbol{x})$ are the density and velocity of the cosmic fluid at position $\boldsymbol{x}$ and time t, $\boldsymbol{g}$ is a conservative force field per unit mass (such as the gravitational acceleration), P is the thermal pressure, T is the temperature, s is the entropy per unit mass and $\mathrm{d}/\mathrm{d}t = \partial/\partial t+\boldsymbol{v}\cdot\boldsymbol{\nabla}$ is a Lagrangian time derivative.

- In linear theory, there are two families of modes corresponding to whether pressure or gravity acts as the restoring force. This becomes clear from the right-hand side of the momentum equation (3.57). The pressure modes represent the familiar sound waves which propagate at the sound speed, $c_\mathrm{s} = \sqrt{\gamma P/\rho}$, where P is the thermal pressure, ρ is the mass density, and γ is the ratio of specific heat capacities. The pressure modes radiate out of any given region on the sound crossing time.

- Gravity modes have the important property that they can be trapped. They can induce vortical motions that feed into a turbulent cascade with important consequences for the thermal cluster state. To see this in detail, we will now derive the dispersion relation of a local g-mode. We will carry out a Wentzel-Kramers-Brillouin (WKB) perturbation analysis on a hydrostatic background. To this end, we assume that the background plasma is thermally stratified in the presence of a uniform gravitational

field in the vertical direction, $\boldsymbol{g} = -g\boldsymbol{e}_z$ ($\boldsymbol{e}_z$ is the unit vector in the z direction). Hence, the force balance implies $\mathrm{d}P_0/\mathrm{d}z = -\rho_0 g$ and $\boldsymbol{v}_0 = \boldsymbol{0}$ (the subscript 0 denotes background quantities). The background heat flux $\boldsymbol{Q}_0 = -\chi \mathrm{d}T_0/\mathrm{d}z$ requires us to demand $\boldsymbol{\nabla}\cdot\boldsymbol{Q}_0 = 0$ in order for the initial equilibrium to be in steady state which implies a temperature that varies at most linearly with height. Although this steady state assumption is formally required, we note that as long as the time scale for the evolution of the system is longer than the local dynamical time, the general features of the instability described here are unlikely to depend critically on this steady state assumption.

- We perturb the stratified plasma and split the dynamical quantities into background values and small perturbations: $\rho = \rho_0 + \delta\rho$, $\boldsymbol{v} = \delta\boldsymbol{v}$, $P = P_0 + \delta P$, and $s = s_0 + \delta s$. To first order, we obtain for the time derivative of the entropy

$$\begin{aligned}\frac{\partial s}{\partial t} &= \frac{1}{\gamma-1}\frac{k_\mathrm{B}}{m}\frac{\partial(\ln P\rho^{-\gamma})}{\partial t}\\ &= \frac{1}{\gamma-1}\frac{k_\mathrm{B}}{m}\left(\frac{1}{P_0}\frac{\partial\delta P}{\partial t}-\frac{\gamma}{\rho_0}\frac{\partial\delta\rho}{\partial t}\right).\end{aligned} \tag{3.59}$$

Using this, we obtain to first order for our conservation equations

$$\frac{\partial\delta\rho}{\partial t}+\boldsymbol{\nabla}\cdot(\rho_0\delta\boldsymbol{v})=0, \tag{3.60}$$

$$\frac{\partial\delta\boldsymbol{v}}{\partial t}-\frac{\delta\rho}{\rho_0^2}\boldsymbol{\nabla}P_0+\frac{\boldsymbol{\nabla}\delta P}{\rho_0}=0, \tag{3.61}$$

$$\frac{1}{\gamma-1}\left(\frac{\partial\delta P}{\partial t}-\frac{\gamma k_\mathrm{B}T_0}{m}\frac{\partial\delta\rho}{\partial t}\right)+\rho_0 T_0(\delta\boldsymbol{v}\cdot\boldsymbol{\nabla})s_0=-\boldsymbol{\nabla}\cdot\delta\boldsymbol{Q} \tag{3.62}$$

where we have used $\boldsymbol{g} = \boldsymbol{\nabla}P_0/\rho_0$ in (3.61).

- We can decompose all dynamical variables ($\delta\rho$, $\delta\boldsymbol{v}$, δs, δP, $\delta\boldsymbol{Q}$) into plane waves,

$$\delta\rho(\boldsymbol{x},t)=\int\frac{\mathrm{d}^3k}{(2\pi)^3}\,\delta\hat{\rho}(\boldsymbol{k},\omega)\,\mathrm{e}^{-\mathrm{i}\omega t+\mathrm{i}\boldsymbol{k}\cdot\boldsymbol{x}}, \tag{3.63}$$

introducing the Fourier amplitudes $\delta\hat{\rho}(\boldsymbol{k},\omega)$ which obey algebraic equations rather than partial differential equations. Formally, plane waves form an orthonormal system on a homogeneous background. As long as the perturbations of our stratified hydrostatic background are small, a decomposition into plane waves is complete. However, as we will see, the growth rate of the perturbations depends in general on position (i.e., height in the gravitational potential), which renders this approach inaccurate after some time because the wave vector will start to depend on position and different wave vectors are not any more linearly

independent. The wave vector is defined as $\boldsymbol{k} = k_x\boldsymbol{e}_x + k_y\boldsymbol{e}_y + k_z\boldsymbol{e}_z$ and the WKB assumption requires $kH \gg 1$, where H is the local scale height of the system and $k = |\boldsymbol{k}|$. We define $k_\perp^2 = k_x^2 + k_y^2$ to be the wave vector perpendicular to the local gravitational field.

- We get

$$-\mathrm{i}\omega\delta\hat{\rho} + (\delta\hat{\boldsymbol{v}}\cdot\boldsymbol{\nabla})\rho_0 + \mathrm{i}\rho_0\boldsymbol{k}\cdot\delta\hat{\boldsymbol{v}} = 0, \tag{3.64}$$

$$-\mathrm{i}\omega\delta\hat{\boldsymbol{v}} - \frac{\delta\hat{\rho}}{\rho_0^2}\boldsymbol{\nabla}P_0 + \mathrm{i}\boldsymbol{k}\frac{\delta\hat{P}}{\rho_0} = 0, \tag{3.65}$$

$$\mathrm{i}\omega\frac{\gamma}{\gamma-1}P_0\frac{\delta\hat{\rho}}{\rho_0} + \rho_0 T_0(\delta\hat{\boldsymbol{v}}\cdot\boldsymbol{\nabla})s_0 = -\mathrm{i}\boldsymbol{k}\cdot\delta\hat{\boldsymbol{Q}} \tag{3.66}$$

  To derive the third equation, we used the Boussinesq approximation which filters out time scales faster than the sound crossing time. Comparing the Fourier transform of the two terms in the parenthesis of (3.62) and using the dispersion relation of sound waves, the Boussinesq approximation requires

$$\delta\hat{P} = \frac{\omega^2}{k^2}\delta\hat{\rho} \overset{!}{\ll} c_\mathrm{s}^2\delta\hat{\rho} = \frac{\gamma k_\mathrm{B}T}{m}\delta\hat{\rho} \quad\Rightarrow\quad \omega \overset{!}{\ll} kc_\mathrm{s}. \tag{3.67}$$

  This implies that we effectively drop the δP term in the energy equation (but not in the momentum equation).

- We define a displacement vector $\boldsymbol{\xi} = \mathrm{i}\delta\hat{\boldsymbol{v}}/\omega$ (with $\xi = |\boldsymbol{\xi}|$) and use this to perform an order of magnitude analysis of the terms in (3.64):

$$\begin{array}{ccccccc} \dfrac{\delta\hat{\rho}}{\rho_0} & + & \dfrac{1}{\rho_0}(\boldsymbol{\xi}\cdot\boldsymbol{\nabla})\rho_0 & - & \dfrac{\boldsymbol{k}\cdot\delta\hat{\boldsymbol{v}}}{\omega} & = & 0 \\ \dfrac{\delta\hat{\rho}}{\rho_0} & \sim & \dfrac{\xi}{H} & \ll & k\xi & \text{since} & kH \gg 1 \end{array} \tag{3.68}$$

  which follows from the WKB approximation. Thus, the last term dominates over the first two terms and leaves us with the near incompressibility condition:

$$\boldsymbol{k}\cdot\delta\hat{\boldsymbol{v}} = 0 \quad\Rightarrow\quad k_\perp\delta\hat{v}_\perp + k_z\delta\hat{v}_z = 0 \tag{3.69}$$

- As we will now see, this conditions enables us to project the momentum equation (3.65) into a purely vertical and perpendicular equation, respectively:

$$-\mathrm{i}\omega\boldsymbol{k}\cdot\delta\hat{\boldsymbol{v}} = 0 = -\frac{\delta\hat{\rho}}{\rho_0}gk_z - \mathrm{i}k^2\frac{\delta\hat{P}}{\rho_0}, \tag{3.70}$$

$$\frac{\delta\hat{P}}{\rho_0} = \omega\frac{\delta\hat{v}_\perp}{k_\perp}. \tag{3.71}$$

- Combining (3.66), (3.70), (3.71) and neglecting heat flux perturbations for simplicity ($\boldsymbol{k} \cdot \delta\hat{\boldsymbol{Q}} = 0$), we obtain the dispersion relation for gravity waves,

$$\omega^2 = N^2 \frac{k_\perp^2}{k^2}, \quad N^2 = \frac{g}{\gamma} \frac{\partial \ln K}{\partial z}. \tag{3.72}$$

  Here, $K = P\rho^{-\gamma}$ and N denotes the Brunt-Väisälä frequency.

- This dispersion relation has two important consequences:

  1. For a stably stratified atmosphere where the entropy is increasing outward ($\partial s/\partial z > 0$ or $\partial K/\partial z > 0$), ω is positive and the displaced fluid parcel oscillates with the Brunt-Väisälä frequency around the equilibrium position. If the entropy is decreasing outward, we have an unstable situation: displacing high-entropy gas in such an atmosphere upwards causes it to rise further until the entropy profile is inverted and stably stratified, defining a new equilibrium.
  2. Since $k_\perp \leq |\boldsymbol{k}|$, g-modes have a maximum possible frequency of $\omega_{\max} = N$ at which point $k_\perp = |\boldsymbol{k}|$ and $k_z = 0$. If the Brunt-Väisälä frequency is a decreasing function of height z, g-modes of a given frequency ω will be confined/trapped below the height at which $N(z) = \omega$.

  The first result can also be obtained by thermodynamic considerations only and is known as the Schwarzschild criterion for convective instability. We show its derivation for completeness in Appendix A.2.

3.1.4 Vorticity

- Among other sources, g-modes can also generate vorticity that decays to smaller eddies and drives a turbulent cascade, as we will see. To lowest order in the (small) Mach number ($\mathcal{M} = v/c_s$) of the velocity perturbations, the flow is incompressible, $\boldsymbol{\nabla} \cdot \boldsymbol{v} = 0$. This implies that the velocity field in this approximation is a pure vortex field, $\boldsymbol{v} = \boldsymbol{\nabla} \times \boldsymbol{A}$ (where $\boldsymbol{A}$ is a vector potential). In other words, the excitation of g-modes leads to the generation of vorticity, $\boldsymbol{\omega} = \boldsymbol{\nabla} \times \boldsymbol{v}$. We will now derive an evolution equation for vorticity in the case of an ideal inviscid fluid, which has viscous forces that are much smaller than inertial forces. We only consider conservative external forces per unit mass, $\boldsymbol{g} = -\boldsymbol{\nabla}\Phi$.

- If we apply the curl operator to the momentum equation (3.57) and adopt the definition of vorticity, $\boldsymbol{\omega} = \boldsymbol{\nabla} \times \boldsymbol{v}$, we obtain

$$\frac{\partial \boldsymbol{\omega}}{\partial t} + \boldsymbol{\nabla} \times [(\boldsymbol{v} \cdot \boldsymbol{\nabla})\boldsymbol{v}] = \frac{1}{\rho^2}\boldsymbol{\nabla}\rho \times \boldsymbol{\nabla}P \tag{3.73}$$

  since $\boldsymbol{\nabla} \times \nabla\phi \equiv 0$ where ϕ is a scalar field. Using the identity

$$(\boldsymbol{v} \cdot \boldsymbol{\nabla})\boldsymbol{v} \equiv \frac{1}{2}\boldsymbol{\nabla}(\boldsymbol{v}^2) - \boldsymbol{v} \times \boldsymbol{\omega}, \tag{3.74}$$

  we can rewrite the second term in (3.73) as follows:

$$\begin{aligned} \boldsymbol{\nabla} \times [(\boldsymbol{v} \cdot \boldsymbol{\nabla})\boldsymbol{v}] &= -\boldsymbol{\nabla} \times (\boldsymbol{v} \times \boldsymbol{\omega}) \\ &= -(\boldsymbol{\omega} \cdot \boldsymbol{\nabla})\boldsymbol{v} + \boldsymbol{\omega}(\boldsymbol{\nabla} \cdot \boldsymbol{v}) + (\boldsymbol{v} \cdot \boldsymbol{\nabla})\boldsymbol{\omega} \end{aligned} \tag{3.75}$$

  since $\boldsymbol{\nabla} \cdot \boldsymbol{\omega} \equiv 0$.

- Hence the evolution equation for vorticity reads

$$\frac{\mathrm{d}\boldsymbol{\omega}}{\mathrm{d}t} = (\boldsymbol{\omega} \cdot \boldsymbol{\nabla})\boldsymbol{v} - \boldsymbol{\omega}(\boldsymbol{\nabla} \cdot \boldsymbol{v}) + \frac{1}{\rho^2}\boldsymbol{\nabla}\rho \times \boldsymbol{\nabla}P \tag{3.76}$$

  where $\mathrm{d}/\mathrm{d}t \equiv \partial/\partial t + \boldsymbol{v} \cdot \boldsymbol{\nabla}$ is the Lagrangian time derivative. In the limit of small velocities ($\mathcal{M} \ll 1$) this evolution equation reads to linear order

$$\frac{\partial \boldsymbol{\omega}}{\partial t} = \frac{1}{\rho^2}\boldsymbol{\nabla}\rho \times \boldsymbol{\nabla}P. \tag{3.77}$$

- Hence, vorticity production is associated with departures between surfaces of constant density and those of constant pressure. Given that the pressure gradient is essentially in the vertical direction (as defined by the local gravitational field), the term $\boldsymbol{\nabla}\rho \times \boldsymbol{\nabla}P$ and hence the generated vorticity will lie principally in the horizontal plane. This facilitates the identification of g-modes.

3.1.5 Turbulence

> "Big whirls have little whirls that feed on their velocity,
> and little whirls have lesser whirls and so on to viscosity."
> – *Lewis Fry Richardson*

- We start with the Navier-Stokes equation (3.44) for an incompressible fluid ($\boldsymbol{\nabla} \cdot \boldsymbol{v} = 0$) and obtain

$$\frac{\partial \boldsymbol{v}}{\partial t} + (\boldsymbol{v} \cdot \boldsymbol{\nabla})\boldsymbol{v} = \boldsymbol{g} - \frac{1}{\rho}\boldsymbol{\nabla} P + \nu \Delta \boldsymbol{v}, \tag{3.78}$$

  where we used (3.46) and (3.47) and defined the kinematic viscosity $\nu = \mu/\rho = \lambda_{\rm mfp} v_{\rm th}$ which is the product of particle mean free path and thermal velocity and has the units $\mathrm{cm}^2\ \mathrm{s}^{-1}$. From left to right, the terms have the following meaning: 1) rate of change of $\boldsymbol{v}$, 2) advective transport, 3) external force (e.g., gravity), 4) pressure force, 5) viscous dissipation term.

- We compare the time scales for advection, $t_{\rm adv}$, and for viscous dissipation, $t_{\rm diss}$:

$$t_{\rm adv} = \frac{L}{v} \quad \text{and} \quad t_{\rm diss} = \frac{L^2}{\nu}, \tag{3.79}$$

  where L and v are characteristic length and velocity scales of the (macroscopic) system. We define the Reynolds number to be the ratio of dissipative-to-advective time scale,

$$\mathrm{Re} = \frac{t_{\rm diss}}{t_{\rm adv}} = \frac{Lv}{\nu} = \frac{L}{\lambda_{\rm mfp}} \frac{v}{v_{\rm th}}. \tag{3.80}$$

  This shows that Re is the product of the ratios of macroscopic-to-microscopic length and velocity scales.

- Note that the assumption of an incompressible flow

$$\boldsymbol{v}(\boldsymbol{x}, t) = \int \hat{\boldsymbol{v}}(\boldsymbol{k}, \omega) \mathrm{e}^{\mathrm{i}(\boldsymbol{k}\cdot\boldsymbol{x} - \omega t)} \mathrm{d}^3 k \mathrm{d}\omega, \tag{3.81}$$

$$\boldsymbol{\nabla} \cdot \boldsymbol{v} = 0 \implies \boldsymbol{k} \cdot \hat{\boldsymbol{v}} = 0 \tag{3.82}$$

  does not allow for longitudinal disturbances (sound waves), but only for rotational flows, so-called "eddies" and implies subsonic velocities (since supersonic velocities would cause the formation of shocks, which necessarily have $\boldsymbol{\nabla} \cdot \boldsymbol{v} \neq 0$).

- If $\mathrm{Re} \gg 1$, advection is much faster than dissipation which cannot stabilize the dynamical growth. The vortical fluid motions interact non-linearly and turbulence sets in. In three dimensions, energy is being fed into the turbulent cascade on the macroscopic

"injection scale" L with a typical velocity v. Energy is being transported from large to small scales as large eddies break up into smaller eddies, thereby conserving vorticity in the absence of the baroclinic term. The energy transport to small scales continues until the energy is dissipated through the production of viscous heat on the microscopic "viscous" scale, $\lambda_{\rm visc}$, which is of order the particle mean free path. The scales in between, for $\lambda_{\rm visc} < \lambda < L$, are called the "inertial range". In two dimensions, however, small eddies merge to form larger eddies and energy flows from small to large scales along an "inverse cascade".

- Let λ be the size of an eddy and v_λ the typical rotational velocity across the eddy. The energy flow through that scale is the product of kinetic energy and the eddy turnover rate on that scale,

$$\dot{\epsilon} \approx \left(\frac{v_\lambda^2}{2}\right)\left(\frac{v_\lambda}{\lambda}\right) \approx \frac{v_\lambda^3}{\lambda}. \tag{3.83}$$

  In the inertial range, the energy flow must be independent on scale, $\dot{\epsilon} = $ const. because energy must not accumulate anywhere in steady state: the only channel for the energy to be transferred is through non-linear interactions with other eddies and hence, we obtain the velocity scaling from (3.83)

$$v_\lambda \approx v\left(\frac{\lambda}{L}\right)^{1/3}. \tag{3.84}$$

- The largest eddies assume the highest velocities (and thus the highest kinetic energies), but the smallest eddies have the highest vorticity

$$|\boldsymbol{\omega}| \approx \frac{v_\lambda}{\lambda} \approx \frac{v}{(\lambda^2 L)^{1/3}}. \tag{3.85}$$

  Since the overall vorticity is approximately conserved this implies that turbulence becomes more and more intermittent on smaller scales, i.e., less volume is filled with turbulent eddies.

- To compute the power spectrum of eddy velocity, $v_\lambda \approx (\dot{\epsilon}\lambda)^{1/3}$, we write down the correlation function which scales as

$$\xi_v \propto v_\lambda^2 \propto (\dot{\epsilon}\lambda)^{2/3}. \tag{3.86}$$

  Note that the kinetic energy on a scale λ scales exactly as the correlation function, $\epsilon \propto v_\lambda^2 \propto \lambda^{2/3}$. The Fourier transform of ξ_v is the velocity power spectrum which inherits the scaling

$$P_v \propto \lambda^3 \xi_v \propto k^{-3}\left(\dot{\epsilon}k^{-1}\right)^{2/3} \propto \dot{\epsilon}^{2/3}k^{-11/3}. \tag{3.87}$$

  The power per linear and logarithmic interval in k-space scale as

$$P_v k^2 \mathrm{d}k \propto \dot{\epsilon}^{2/3}k^{-5/3}\mathrm{d}k, \quad \text{and} \tag{3.88}$$

$$P_v k^3 \mathrm{d}\ln k \propto \dot{\epsilon}^{2/3}k^{-2/3}\mathrm{d}\ln k, \tag{3.89}$$

which is the Kolmogorov turbulence spectrum of driven turbulence.

- In contrast to driven subsonic turbulence, in clusters we encounter decaying turbulence: a merger injects kinetic energy on scales $L \sim r_c$, which will successively decay after a few eddy turnover time scales L/v. The possible implications of turbulence in clusters is mainly

  1. mixing of metals that have been injected by galactic winds,
  2. explaining the magnetization in clusters: driving a turbulent dynamo of either primordial magnetic fields or field that was injected by AGNs:
  3. shredding AGN bubbles and mixing relativistic components within the ICM
  4. heating cool cores and possible arresting the over-cooling in them, provided the coupling efficiency of $P\mathrm{d}V$ work to the turbulent cascade is high.

3.1.6 Shocks

General Considerations

- Imagine the propagation of a sound wave with finite amplitude. The sound speed is higher at higher temperature as $c_s^2 \propto k_B T$, so that the crest of the wave gradually overtakes the colder trough ($T \propto \rho^{\gamma-1}$). When faster moving gas overtakes slower moving gas, we would obtain a multivalued solution that is inconsistent with the hydrodynamic equations. Instead, we get a discontinuous change of density and velocity, a so-called "shock". This steepening happens even for $\gamma = 1$ because of the non-linearity of the equations. Shocks can also be produced by any supersonic compressible disturbance (or through non-linear interactions of subsonic compressible modes). This can result from a supernova explosion within a galaxy, by gas accreting super-sonically onto a cluster, or if two galaxy clusters merge to form a larger entity. In general, a shock wave is

  1. propagating faster than the "signal speed" for compressible waves, c_s,
  2. producing an irreversible change of the fluid state, i.e., an increase in entropy, and
  3. can either be caused by a pressure-driven compressive disturbance, results from non-linear wave interactions, or is caused by supersonic collisions of two streams of fluids (e.g., as a result of their mutual gravitational interactions).

- In most cases, a shock involves a "discontinuous" change of the fluid properties over a scale proportional to the effective mean free path $\lambda_{\rm eff}$. In "collisional" shocks, λ is set by Coulomb-force mediated particle-particle collisions. In a "collisionless" plasma (which is of relevance for galaxy clusters) electromagnetic viscosities mediate interactions between charged particles and thus reduce $\lambda_{\rm eff}$ by many orders of magnitude, $\lambda_{\rm eff} \ll \lambda_{\rm Coulomb}$, so that we are dealing here with "collisionless" shocks.

- In order to understand general properties at fluid discontinuities, we are now considering the conservation laws of mass, momentum, and internal energy in the absence of external gravitational forces and conductive heat flux (which act on time scale that are much longer in comparison to the transition times at shocks or contact discontinuities),

$$\frac{\partial \rho}{\partial t} + \boldsymbol{\nabla} \cdot (\rho \boldsymbol{v}) = 0, \tag{3.90}$$

$$\frac{\partial \boldsymbol{v}}{\partial t} + (\boldsymbol{v} \cdot \boldsymbol{\nabla})\boldsymbol{v} = -\frac{\boldsymbol{\nabla} P}{\rho} + \frac{1}{\rho}\boldsymbol{\nabla} \cdot \bar{\boldsymbol{\Pi}} \tag{3.91}$$

$$\frac{\partial}{\partial t}(\rho\epsilon) + \boldsymbol{\nabla} \cdot (\rho\epsilon \boldsymbol{v}) = -P\boldsymbol{\nabla} \cdot \boldsymbol{v} + \Psi. \tag{3.92}$$

- Since we are interested how the total energy density changes in a given volume, $\rho \boldsymbol{v}^2/2 + \rho\epsilon$, we are supplementing the internal energy equation (3.92) with a conservation law of $\rho \boldsymbol{v}^2/2$. To this end, we consider

$$\frac{\partial}{\partial t}\left(\frac{\rho \boldsymbol{v}^2}{2}\right) = \frac{\boldsymbol{v}^2}{2}\frac{\partial \rho}{\partial t} + \rho \boldsymbol{v} \cdot \frac{\partial \boldsymbol{v}}{\partial t} \tag{3.93}$$

  and substitute (3.90) and (3.91) to get

$$\frac{\partial}{\partial t}\left(\frac{\rho \boldsymbol{v}^2}{2}\right) = -\frac{\boldsymbol{v}^2}{2}\boldsymbol{\nabla}(\rho \boldsymbol{v}) - \rho \boldsymbol{v}(\boldsymbol{v} \cdot \boldsymbol{\nabla})\boldsymbol{v} - \boldsymbol{v} \cdot \boldsymbol{\nabla} P + \boldsymbol{v} \cdot (\boldsymbol{\nabla} \cdot \bar{\boldsymbol{\Pi}}). \tag{3.94}$$

  Using the identity $(\boldsymbol{v} \cdot \boldsymbol{\nabla})\boldsymbol{v} \equiv \boldsymbol{\nabla}\boldsymbol{v}^2/2$, we obtain an equation for the conservation of kinetic energy density

$$\frac{\partial}{\partial t}\left(\frac{\rho \boldsymbol{v}^2}{2}\right) + \boldsymbol{\nabla}\left(\frac{1}{2}\rho \boldsymbol{v}^2 \boldsymbol{v}\right) = -\boldsymbol{v} \cdot \boldsymbol{\nabla} P + \boldsymbol{v} \cdot (\boldsymbol{\nabla} \cdot \bar{\boldsymbol{\Pi}}). \tag{3.95}$$

Jump Conditions

- Consider a propagating fluid discontinuity in the rest frame of the discontinuity. Fluid moves from upstream to downstream. We denote the *upstream conditions* by ρ_1, v_1, T_1 and *downstream conditions* by ρ_2, v_2, T_2.

- We would like to derive the relations (also known as "jump conditions") between ρ_1, v_1, T_1 and ρ_2, v_2, T_2 for a steady-state, plane-parallel geometry of a fluid discontinuity such as a shock. First, we assume that the velocity is perpendicular to the surface of the discontinuity. While this may seem to be a substantial loss of generality, it captures the main effect of discontinuities as we will see by generalizing this simplification in the last part of this section. As we will also see, there are two types of discontinuities:

  1. shocks that are characterized by a mass flux through their interface, and
  2. contact discontinuities which have *no* mass flux through their interface.

- Within the shock front or "transition layer" on a scale of $\lambda_{\rm eff}$, viscous effects are important and cause the shock in the first place, i.e., dissipate kinetic energy and thus generate heat and entropy. However, outside the layer, viscous effects are small on scales $L \gg \lambda_{\rm eff}$. We will derive conservation equations of the form

$$\frac{\mathrm{d}}{\mathrm{d}x} Q(\rho, v, P) = 0 \implies Q(\rho, v, P) = \text{const.} \tag{3.96}$$

  and although Q involves viscous terms, we can ignore these outside the shock zone and can derive jump conditions from equations without viscosity terms.

- We assume steady state ($\partial/\partial t = 0$) and plane-parallel geometry ($\partial/\partial y = \partial/\partial z = 0$, $\partial/\partial x = \mathrm{d}/\mathrm{d}x$). The conservation laws (3.90), (3.91), (3.92), and (3.95) simplify to yield

$$\frac{\mathrm{d}}{\mathrm{d}x}(\rho v) = 0, \tag{3.97}$$

$$v\frac{\mathrm{d}v}{\mathrm{d}x} = -\frac{1}{\rho}\frac{\mathrm{d}P}{\mathrm{d}x} + \frac{1}{\rho}\frac{\mathrm{d}}{\mathrm{d}x}\left[\left(\frac{4}{3}\mu + \beta\right)\frac{\mathrm{d}v}{\mathrm{d}x}\right], \tag{3.98}$$

$$\frac{\mathrm{d}}{\mathrm{d}x}(\rho\epsilon v) = -P\frac{\mathrm{d}u}{\mathrm{d}x} + \left(\frac{4}{3}\mu + \beta\right)\left(\frac{\mathrm{d}v}{\mathrm{d}x}\right)^2, \tag{3.99}$$

$$\frac{\mathrm{d}}{\mathrm{d}x}\left(\frac{1}{2}\rho v^2 v\right) = -v\frac{\mathrm{d}P}{\mathrm{d}x} + v\frac{\mathrm{d}}{\mathrm{d}x}\left[\left(\frac{4}{3}\mu + \beta\right)\frac{\mathrm{d}v}{\mathrm{d}x}\right]. \tag{3.100}$$

- The equation for mass conservation (3.97) gives

$$\rho v = \text{const.} \implies \rho_1 v_1 = \rho_2 v_2 = j \implies [\rho v] = 0, \tag{3.101}$$

  where j is the current density and the brackets, $[\ldots]$, indicate differences between the up- and downstream quantities. Note, that the up- and downstream velocities, v_1 and v_2, are measured in the frame of the discontinuity!

- Using

$$\frac{\mathrm{d}}{\mathrm{d}x}\left(\rho v^2\right) = \rho v\frac{\mathrm{d}v}{\mathrm{d}x} + v\frac{\mathrm{d}}{\mathrm{d}x}(\rho v) \overset{(3.101)}{=} \rho v\frac{\mathrm{d}v}{\mathrm{d}x} \tag{3.102}$$

allows (3.98) to be rewritten as

$$\rho v\frac{\mathrm{d}v}{\mathrm{d}x} + \frac{\mathrm{d}P}{\mathrm{d}x} - \frac{\mathrm{d}}{\mathrm{d}x}\left[\left(\frac{4}{3}\mu + \beta\right)\frac{\mathrm{d}v}{\mathrm{d}x}\right]$$

$$= \frac{\mathrm{d}}{\mathrm{d}x}\left[\rho v^2 + P - \left(\frac{4}{3}\mu + \beta\right)\frac{\mathrm{d}v}{\mathrm{d}x}\right] = 0 \tag{3.103}$$

$$\Longrightarrow \left[\rho v^2 + P - \left(\frac{4}{3}\mu + \beta\right)\frac{\mathrm{d}v}{\mathrm{d}x}\right] = 0 \tag{3.104}$$

This demonstrates that within the transition zone (where μ, β, and $\mathrm{d}v/\mathrm{d}x$ are non-zero) $\rho v^2 + P \neq$ const. However, in the pre- and post-shock zones, μ, β, and $\mathrm{d}v/\mathrm{d}x$ are negligible, implying

$$\left[\rho v^2 + P\right] = 0. \tag{3.105}$$

- In principle, we could use (3.104) to follow the behavior in the transition zone, i.e., to understand how entropy is generated. But on scales $L < \lambda$ the fluid description breaks down and we have to reside to kinetic theory (or use plasma particle-in-cell codes to understand the nonlinear behavior of the heating process). From now on, we neglect viscosity effects in the bulk.

- Adding (3.99) and (3.100) yields (for the region outside the transition zone)

$$0 = \frac{\mathrm{d}}{\mathrm{d}x}\left[v\left(\frac{1}{2}\rho v^2 + \rho\epsilon\right) + Pv\right] = \frac{\mathrm{d}}{\mathrm{d}x}\left[\rho v\left(\frac{1}{2}v^2 + \epsilon + \frac{P}{\rho}\right)\right]$$

$$= \left(\frac{1}{2}v^2 + \epsilon + \frac{P}{\rho}\right)\frac{\mathrm{d}}{\mathrm{d}x}(\rho v) + \rho v\frac{\mathrm{d}}{\mathrm{d}x}\left(\frac{1}{2}v^2 + \epsilon + \frac{P}{\rho}\right). \tag{3.106}$$

Since $\mathrm{d}(\rho v)/\mathrm{d}x = 0$ and $\rho v \neq 0$, we obtain

$$\frac{\mathrm{d}}{\mathrm{d}x}\left(\frac{1}{2}v^2 + \epsilon + \frac{P}{\rho}\right) \Longrightarrow \left[\frac{1}{2}v^2 + \epsilon + \frac{P}{\rho}\right] = 0. \tag{3.107}$$

- Summarizing, we have the Rankine-Hugoniot jump conditions for a plane-parallel shock in the shock rest frame:

$$[\rho v] = 0, \tag{3.108}$$

$$\left[\rho v^2 + P\right] = 0, \tag{3.109}$$

$$\left[\frac{1}{2}v^2 + \epsilon + \frac{P}{\rho}\right] = 0. \tag{3.110}$$

Independent of the complicated physics within the transition layer, these conditions simply follow from the conservation laws. The first follows from mass conservation, the second from mass and momentum conservation, and the third from mass and total energy conservation.

- Using $\epsilon_i = P_i/[\rho_i(\gamma_i - 1)]$, we can rewrite the energy jump condition to get

$$\frac{1}{2}v_1^2 + \frac{\gamma_1}{\gamma_1 - 1}\frac{P_1}{\rho_1} = \frac{1}{2}v_2^2 + \frac{\gamma_2}{\gamma_2 - 1}\frac{P_2}{\rho_2} \tag{3.111}$$

  for a single-species gas that is described by a polytropic equation of state. In principle, $\gamma_1 \neq \gamma_2$, since a shock can e.g., dissociate molecules, or raise T so that previously inaccessible degrees of freedom become accessible.

Tangential Discontinuities

- $[\rho v] = 0$ allows for two types of solutions. The first type is clearly $\rho_1 v_1 = \rho_2 v_2 = 0$ and since ρ_1 and ρ_2 are non-zero, we have

$$v_1 = v_2 = 0, \tag{3.112}$$
$$P_1 = P_2 \implies [P] = 0 \tag{3.113}$$

  which follows from (3.109). The constancy of the normal component of the velocity across such an interface implies that there is no mass flux through a tangential discontinuity. If additionally the tangential velocity is also continuous, a special discontinuity is present which is called a contact discontinuity.

- At a tangential discontinuity, there can be an arbitrary jump of density, that however needs to be compensated by the same jump of T, but in the opposite direction!

Shock Mach Number

- The other type of solution requires $\rho_1 v_1 \neq 0$ so that we have a mass flux through this type of discontinuity that we call a "shock".

- We define a dimensionless number that characterizes the shock strength, the Mac number as the ratio of shock speed to upstream sound speed $c_1^2 = \gamma P/\rho$,

$$\mathcal{M}_1 \equiv \frac{v_1}{c_1} = \sqrt{\frac{\rho_1 v_1^2}{\gamma P_1}} = \sqrt{\frac{m v_1^2}{\gamma k_B T_1}}, \tag{3.114}$$

  which can be interpreted as a ratio of ram pressure $(\rho_1 v_1^2)$-to-thermal pressure in the pre-shock gas or equivalently a ratio of kinetic-to-thermal energy density.

- We can rewrite the Rankine-Hugoniot jump conditions in terms of $\mathcal{M}_1$ ($\gamma_1 = \gamma_2$)

$$\frac{\rho_2}{\rho_1} = \frac{v_1}{v_2} = \frac{(\gamma+1)\mathcal{M}_1^2}{(\gamma-1)\mathcal{M}_1^2+2} \xrightarrow{\gamma=1} \mathcal{M}_1^2 \tag{3.115}$$

$$\frac{P_2}{P_1} = \frac{\rho_2 k_\mathrm{B} T_2}{\rho_1 k_\mathrm{B} T_1} = \frac{2\gamma\mathcal{M}_1^2-(\gamma-1)}{\gamma+1} \xrightarrow{\gamma=1} \mathcal{M}_1^2 \tag{3.116}$$

$$\frac{T_2}{T_1} = \frac{\left[(\gamma-1)\mathcal{M}_1^2+2\right]\left[2\gamma\mathcal{M}_1^2-(\gamma-1)\right]}{(\gamma+1)^2\mathcal{M}_1^2} \xrightarrow{\gamma=1} 1 \tag{3.117}$$

- Those relations simplify for strong shocks ($\mathcal{M} \gg 1$), yielding

$$\frac{\rho_2}{\rho_1} = \frac{v_1}{v_2} \approx \frac{\gamma+1}{\gamma-1} = 4, \tag{3.118}$$

$$P_2 \approx \frac{2\gamma}{\gamma+1}\mathcal{M}_1^2 P_1 = \frac{2}{\gamma+1}\rho_1 v_1^2 = \frac{3}{4}\rho_1 v_1^2, \tag{3.119}$$

$$k_\mathrm{B} T_2 \approx \frac{2\gamma(\gamma-1)}{(\gamma+1)^2} k_\mathrm{B} T_1 \mathcal{M}_1^2 = \frac{2(\gamma-1)}{(\gamma+1)^2} m v_1^2 = \frac{3}{16} m v_1^2, \tag{3.120}$$

  where we used a non-relativistic ideal gas ($\gamma = 5/3$) in the last equalities.

- In the shock rest frame, the post-shock kinetic and thermal specific energies are ($\gamma = 5/3$, $\mathcal{M} \gg 1$)

$$\frac{1}{2}v_2^2 \approx \frac{1}{32}v_1^2, \tag{3.121}$$

$$\frac{3}{2}\frac{k_\mathrm{B} T_2}{m} \approx \frac{9}{32}v_1^2 = \frac{9}{16}\left(\frac{1}{2}v_1^2\right). \tag{3.122}$$

  So roughly half of the pre-shock kinetic energy is converted to thermal energy (in the shock rest frame). The total specific energy ϵ_tot of the post-shock gas,

$$\epsilon_{\mathrm{tot},2} = \frac{1}{2}v_2^2 + \frac{3}{2}\frac{k_\mathrm{B} T_2}{m} \approx \frac{10}{16}\left(\frac{1}{2}v_1^2\right) = \frac{5}{8}\epsilon_{\mathrm{kin},1} = \epsilon_1 \tag{3.123}$$

  is lower (in the shock rest frame) because of the $P\mathrm{d}V$ work done by pressure and viscosity on the post-shock gas in compressing its volume. Note that this $P\mathrm{d}V$ term is absent in the rest frame of the post-shock gas.

- The post-shock Mach number is

$$\mathcal{M}_2 \equiv \frac{v_2}{c_2} = \frac{v_1}{c_1}\frac{v_2}{v_1}\frac{c_1}{c_2} = \mathcal{M}_1 \frac{v_2}{v_1}\left(\frac{T_1}{T_2}\right)^{1/2}. \tag{3.124}$$

This simplifies in the strong-shock limit, yielding

$$\mathcal{M}_2 \approx \mathcal{M}_1 \frac{\gamma-1}{\gamma+1}\left[\frac{(\gamma+1)^2}{2\gamma(\gamma-1)\mathcal{M}_1^2}\right]^{1/2} = \left(\frac{\gamma-1}{2\gamma}\right)^{1/2} \approx 0.45. \tag{3.125}$$

A shock converts supersonic gas into denser, slower moving, higher pressure, subsonic gas.

Shock Adiabatic Curve

- The shock increases the specific entropy of the gas by an amount

$$\begin{aligned} s_2 - s_1 &= c_V \ln\left(\frac{P_2}{\rho_2^\gamma}\right) - c_V \ln\left(\frac{P_1}{\rho_1^\gamma}\right) \\ &= c_V \ln\left(\frac{P_2}{P_1}\right) - c_V\gamma \ln\left(\frac{\rho_2}{\rho_1}\right) = c_V \ln\left(\frac{K_2}{K_1}\right). \end{aligned} \tag{3.126}$$

  Hence, the shock shifts the gas to a higher adiabatic curve that is uniquely labeled by $K = P\rho^{-\gamma}$: gas can move adiabatically along an adiabatic curve while changes in entropy move it from one adiabatic curve to another.

- With the definition of the current density $j = \rho_1 v_1 = \rho_2 v_2 = \text{const.}$, we obtain for (3.109)

$$[\rho v^2 + P] = \left[\frac{j^2}{m}V + P\right] = 0 \implies \frac{j^2}{m}V_1 + P_1 = \frac{j^2}{m}V_2 + P_2. \tag{3.127}$$

- Hence, the slope of the shock adiabatic curve in the P-V diagram is

$$\frac{j^2}{m} = \frac{P_2 - P_1}{V_1 - V_2}. \tag{3.128}$$

Oblique Shocks

- So far, our specific discussion about shocks has been constrained to plane-parallel shock geometries, i.e., we only considered a fluid velocity that was aligned with the shock normal. In general, the fluid can impact the shock at some oblique angle. We define a velocity component parallel to the shock normal, $v_\parallel \equiv \boldsymbol{v}\cdot\boldsymbol{n}$, as well as a perpendicular component, $v_\perp$.

- The momentum conservation equation (3.43) defines a momentum current through a unit surface area with normal vector $\boldsymbol{n}$,

$$\rho\boldsymbol{v}(\boldsymbol{v}\cdot\boldsymbol{n}) + P\boldsymbol{n}. \tag{3.129}$$

The momentum current has to be continuous across the shock in order for the forces that are acting on both sides of the shock on the gas, are identical. In our case, $\boldsymbol{n}$ coincides with the shock normal and points along $\boldsymbol{e}_x$. Continuity of the x, y, and z components of the momentum current yields

$$[\rho v_x^2 + P] = 0, \tag{3.130}$$
$$[\rho v_x v_y] = 0, \tag{3.131}$$
$$[\rho v_x v_z] = 0. \tag{3.132}$$

- At a shock $j = \rho v_x \neq 0$ and $\rho \neq 0$ so that we get

$$[v_y] = 0 \quad \text{and} \quad [v_z] = 0, \tag{3.133}$$

i.e., the tangential velocities are continuous across the shock. Thus, only the parallel velocity component is modified at a shock according to $v_{\parallel,2} = v_{\parallel,1}\rho_1/\rho_2$ while the perpendicular component remains invariant, $v_{\perp,1} = v_{\perp,2} = v_\perp$. This implies a refraction of the (oblique) flow toward the shock surface.

3.1.7 Entropy Generation by Accretion

Philosophical Detour

- The Uncertainty Principle is $\Delta p_x \Delta x = h$, and statistical mechanics counts the number of states with $h^{-3}\mathrm{d}^3\mathrm{d}^3 p$. Hence the phase space density of cluster gas is

$$f \sim \frac{h^3 \mathrm{d}^6 N}{\mathrm{d}^3 x \mathrm{d}^3 p} \sim n \left(\frac{h}{m_\mathrm{p} v}\right)^3$$
$$\sim 6 \times 10^{-35} \left(\frac{n}{10^{-3}\ \mathrm{cm}^{-3}}\right)\left(\frac{v}{10^3\ \mathrm{km\ s}^{-1}}\right)^{-3} \propto K^{-3/2}. \tag{3.134}$$

If this was unity, we would deal with a degenerate gas. Instead, this is extremely small, making it the least degenerate (nonrelativistic) gas in the Universe or equivalently, the highest entropy gas (of equilibrium systems)!

Smooth Accretion

- One way to approach the problem of gravitationally driven generation is through spherically symmetric models of smooth accretion in which gas passes through an accretion shock as it enters the cluster. If the incoming gas is cold, then the cluster accretion shock is the sole source of cluster entropy. If instead, the incoming gas has been heated before passing through the accretion

shock, the Mach number is smaller and the cluster entropy level reflects both, the amount of pre-heating and entropy production at the accretion shock.

- We first consider the case of cold accretion (P and K of the incoming gas are negligible) which implies the strong-shock regime. Conveniently, we transform our Rankine-Hugoniot jump conditions to the rest frame of the post-shock gas, i.e., the cluster rest frame.

  shock frame: $$v_2 = \frac{v_1}{4} \tag{3.135}$$

  post-shock rest frame: $$v_{\rm acc} = v_1 - v_2 = v_1\left(1 - \frac{1}{4}\right) = \frac{3}{4}v_1$$

  $$kT_2 = \frac{3}{16}mv_1^2 = \frac{1}{3}mv_{\rm acc}^2 \tag{3.136}$$

- Note that the location of the accretion shock does *not* move outward with $v_{\rm acc}/4$ because the gravitational attraction of the cluster potential causes causes it to fall onto the cluster. Depending on that infall rate, the accretion shock can either be stationary or move slowly outward.

- Suppose that mass accretes in a series of concentric shells, each with a baryon fraction $f_{\rm b}$, that initially comove with the Hubble flow as in the spherical collapse model of Sect. 2.3. In this simple model, a shell that initially encloses total mass M reaches zero velocity at the turnaround radius $r_{\rm ta}$ and falls back through an accretion shock at radius $r_{\rm acc}$ in the neighborhood of the virial radius $r_{\rm ta}/2$. The system of governing equations are

$$\dot{M}_{\rm g} = 4\pi r_{\rm acc}^2\rho_1 v_{\rm acc} = f_{\rm g}\dot{M}, \tag{3.137}$$

$$v_{\rm acc}^2 = \frac{2GM}{r_{\rm ta}}, \quad \text{(assuming } \Omega_\Lambda = 0\text{)}, \tag{3.138}$$

$$k_{\rm B}T_2 = \frac{1}{3}mv_{\rm acc}^2, \quad m = \mu m_{\rm p}, \tag{3.139}$$

$$\rho_2 = 4\rho_1. \tag{3.140}$$

  Here, ρ_1 is the pre-shock density, ρ_2 and T_2 are the post-shock density and temperature, $r_{\rm acc} = r_{\rm ta}/2$ is the accretion radius. In the post-shock frame, the post-shock thermal energy equals the pre-shock ram pressure (+ initial thermal energy that we neglect here) and (3.139) implies

$$\frac{3}{2}\frac{k_{\rm B}T_2}{m} = \frac{3}{2}\frac{1}{3}v_{\rm acc}^2 = \frac{v_{\rm acc}}{2}. \tag{3.141}$$

- Using (3.139) and (3.140), we can compute the post-shock entropy that is produced by smooth accretion

$$K_{2,\rm sm} \equiv \frac{k_{\rm B}T_2}{m\rho_2^{2/3}} = \frac{v_{\rm acc}^2}{3(4\rho_1)^{2/3}}. \tag{3.142}$$

Combining (3.137) and (3.138) yields

$$\dot{M}_{\rm g} = 4\pi r_{\rm acc}^2 \rho_1 \left(\frac{GM}{r_{\rm acc}}\right)^{1/2} \quad \Longrightarrow \quad \rho_1 = \frac{\dot{M} f_{\rm g}}{4\pi r_{\rm acc}^{3/2}\sqrt{GM}}. \quad (3.143)$$

- Inserting this into (3.142) yields

$$\begin{aligned} K_{2,\rm sm} &= \frac{v_{\rm acc}^2}{3(4\rho_1)^{2/3}} = \frac{1}{3}\left[\frac{\pi (GM)^2}{f_{\rm g}\dot{M}}\right]^{2/3} \\ &= \frac{1}{3}\left(\frac{\pi G^2}{f_{\rm g}}\right)^{2/3}\left(\frac{{\rm d}\ln M}{{\rm d}\ln t}\right)^{-2/3}(Mt)^{2/3}. \end{aligned} \quad (3.144)$$

Because the entropy generated at the shock front increases monotonically with time, such an ideal, smoothly accreting cluster never convects but rather accretes shells of baryons as if they were onion skins. It is useful to cast (3.144) into dimensionless form using a characteristic cluster entropy K_{200},

$$K_{200} \equiv \frac{k_{\rm B}T_{200}}{m(200 f_{\rm b}\rho_{\rm cr})^{2/3}} = \frac{1}{2}\left[\frac{2\pi}{15}\frac{G^2 M_{200}}{f_{\rm b}H(z)}\right]^{2/3}. \quad (3.145)$$

Note that we have adopted here the critical density of the Universe, $\rho_{\rm cr}$, and the characteristic temperature of a singular isothermal sphere, $k_{\rm B}T_{200}$,

$$\rho_{\rm cr} \equiv \frac{3H^2(z)}{8\pi G}, \quad (3.146)$$

$$k_{\rm B}T_{200} = \frac{GM_{200}m}{2r_{200}} = \frac{m}{2}\left[10GM_{200}H(z)\right]^{2/3}. \quad (3.147)$$

- We effectively define a radial coordinate corresponding to the amount of gas accreted at t divided by that at the present time, t_0:

$$\eta \equiv \frac{M_{\rm g}(t)}{f_{\rm b}M_{200}(t_0)} \quad (3.148)$$

and cast (3.145) into dimensionless form

$$\begin{aligned} \frac{K_{2,\rm sm}}{K_{200}} &= \frac{2}{3}\left(\frac{15}{2}\frac{H_0}{M_{200}}\right)^{2/3}\left(\frac{{\rm d}\ln M}{{\rm d}\ln t}\right)^{-2/3}(Mt)^{2/3} \\ &= \frac{2}{3}\left(\frac{15}{2}H_0 t_0\right)^{2/3}\left(\frac{{\rm d}\ln \eta}{{\rm d}\ln t}\right)^{-2/3}\left(\frac{\eta t(\eta)}{t_0}\right)^{2/3}. \end{aligned} \quad (3.149)$$

Thus, the entropy profile due to smooth accretion of cold gas depends entirely on the mass accretion history $M(t)$, and the entropy profiles of objects with similar $M(t)$ should be self-similar with respect to K_{200}.

- Extended Press-Schechter theory or numerical simulations show that for clusters in the mass range 10^{14}-$10^{15}\,M_\odot$ grow roughly as $M(t) \propto t$ to $M(t) \propto t^2$ i the concordance model. Inserting these growth times $t \propto M^{0.5...1}$ into (3.149) yields

$$K_{2,\mathrm{sm}} \propto M_\mathrm{g}^{1...4/3}. \tag{3.150}$$

- Throughout a cluster, M_g encompassed by a given radius is approximately $M \propto r$ (which is exact for the singular isothermal sphere, 4.38). We obtain the following radial entropy profile

$$K_{2,\mathrm{sm}} \propto r^{1...4/3} \tag{3.151}$$

  which compares well with numerical simulations $K_{2,\mathrm{sm}} \propto r^{1.1}$.

Hierarchical Merging

- In real clusters the accreting gas is lumpy and not smooth which transforms the nature of entropy generation. Incoming gas that is bound to accreting sublumps of matter enters the cluster with a wide range of densities. There is no well-defined accretion shock but rather a complex network of shocks as different lumps of infalling gas mix with the intracluster medium of the main cluster.

- Numerical codes employing different numerical techniques (Eulerian grid codes or Lagrangian "particle" codes) all agree on the baseline profile in non-radiative gas simulations for $r > 0.1r_{200}$,

$$K_\mathrm{sim} = 1.32K_{200}\left(\frac{r}{r_{200}}\right)^{1.1}. \tag{3.152}$$

  For $r < 0.1r_{200}$, there is more dispersion among the simulated clusters and the answer depends somewhat on the numerical technique, with grid codes showing an elevated entropy core due to efficient "entropy mixing".

- Despite the complexity of shock structure in hierarchical accretion, the simulated entropy profiles resemble that from smooth accretion models, but with an important distinction: the normalization of the smooth models is higher. The likely reason is that smooth accretion maximizes the entropy production as smoothing does not change the accretion velocity but reduces the mean density of accreting gas lumps. Since the post-shock entropy scales as $K_2 \propto v_\mathrm{acc}^2 \rho_1^{-2/3}$, a smaller (smoothed) density implies larger entropy everywhere.

- This may be of physical relevance: consider the case of preheating gas before it falls into clusters. Heating causes the gas to adiabatically expand and smoothes the density field of the preshock gas. This could then explain elevated entropy profiles of low-temperature clusters relative to the baseline profile.

3.1.8 Cluster Scaling Relations

- In order to use clusters as cosmological probes, we need to relate the different observables to a functional that is sensitive to cosmology. Traditionally this is obtained by using the mass function.

- The main assumption underlying this approach is the choice of an average density of the matter so that this implicitly defines a cluster "radius" by

$$M_\Delta = \frac{4}{3}\pi r_\Delta^3 \Delta \rho_{\rm cr}(z), \quad \Delta = 100 \ldots 500, \tag{3.153}$$

  which also relates the temperature to this definition, $T \sim T_\Delta$.

- Cautionary remarks: when considering X-ray emission, we encounter $\rho_{\rm X}$, $T_{\rm X}$ which is not necessarily identical to $\bar{\rho} = \Delta\rho_{\rm cr}$ and T_Δ as it is degenerate with observational biases. Not accounting for these would break self-similarity as e.g., the presence of a clumped multiphase medium may bias $T_{\rm X}$ towards the dense, colder phase with a higher X-ray emissivity. On the other hand, we encounter similar problems when defining a three-dimensional "radius" from a projected, non-isotropic density distribution (or X-ray emissivity $j_{\rm X} \propto \rho^2$). Careful mock observations of simulated clusters are necessary in either case.

Cosmologist's Ideal Cluster

- We assume hydrostatic equilibrium and obtain the scaling

$$\frac{k_{\rm B}T}{m} \sim v^2 \sim \frac{GM_\Delta}{r_\Delta} \propto M_\Delta^{2/3}\rho_{\rm cr}^{1/3} \tag{3.154}$$

  which immediately yield the temperature-mass scaling

$$T_\Delta \propto M_\Delta^{2/3}\rho_{\rm cr}^{1/3}(z) \propto [M_\Delta E(z)]^{2/3}. \tag{3.155}$$

- We assume that the gas fraction, $f_{\rm gas}(< r_\Delta) = M_{\rm gas}/M_{\rm tot}$, and stellar mass fraction, $f_*(< r_\Delta) = M_*/M_{\rm tot}$, do not scale with cluster mass. Here, $M_{\rm tot} = M_{\rm tot}(< r_\Delta) = M_{\rm dm} + M_{\rm gas} + M_*$ is the gravitational mass. We get the gas and stellar mass scaling,

$$M_{\rm gas} = \int_0^{r_\Delta} \rho_{\rm gas} {\rm d}V \approx M_\Delta f_{\rm gas} \propto M_\Delta, \tag{3.156}$$

$$M_* \approx M_\Delta f_* \propto M_\Delta \implies N_{\rm gals} \propto M_\Delta. \tag{3.157}$$

  Especially $N_{\rm gals} \propto M_\Delta$ assumes a fair sampling of the luminosity function which is not anymore the case on group scales with $\mathcal{O}(10)$ galaxies.

- To obtain the Sunyaev-Zel'dovich scaling relation, we integrate the Compton-y parameter over the solid angle Ω subtended by the cluster,

$$Y = \int_\Omega y \mathrm{d}A = \frac{\sigma_T}{m_\mathrm{e} c^2} \int_\Omega n_\mathrm{e} k_\mathrm{B} T_\mathrm{e} \mathrm{d}A, \tag{3.158}$$

$$Y \propto M_\mathrm{gas} T_\Delta \propto M_\Delta^{5/3} E(z)^{2/3}. \tag{3.159}$$

- Finally, the X-ray scaling relation is obtained by assuming that free-free emission (a two-body process) is the dominating radiative process. In this case, the emissivity per unit volume is $j_\mathrm{X} \propto n_\mathrm{e} n_\mathrm{ion} T^{1/2}$ and we obtain the following scaling of X-ray luminosity with cluster mass,

$$L_\mathrm{X} \propto \int_\Omega n_\mathrm{e} n_\mathrm{ion} \sqrt{k_\mathrm{B} T_\mathrm{e}} \mathrm{d}A \propto M_\mathrm{gas} \rho_\mathrm{cr} T_\Delta^{1/2}, \tag{3.160}$$

$$L_\mathrm{X} \propto M_\Delta^{4/3} E(z)^{1/3} \propto T_\Delta^2 E(z)^{-1}. \tag{3.161}$$

Real Clusters

- Observational scaling relations do not follow the self-similar prediction above. One finds

$$L_\mathrm{X} \propto T_\mathrm{X}^3, \tag{3.162}$$

$$\frac{\mathrm{d}}{\mathrm{d}M}\left(\frac{M_\mathrm{gas}}{M}\right) > 0, \tag{3.163}$$

$$\frac{\mathrm{d}}{\mathrm{d}M}\left(\frac{M_*}{M}\right) < 0 \tag{3.164}$$

  where M is some observational proxy for M_Δ. $Y(M)$ and $T_\mathrm{X}(M)$ are roughly in agreement with the self-similar prediction. It appears that gas physics modifies these simple scale-invariant models and imposes new scales to the otherwise scale-free gravity!

- Consider a simple cored model for the gas distribution of the ICM:

$$\rho(r) = \begin{cases} \text{const.} & \text{for } r < r_\mathrm{c}, \\ \rho_\Delta \left(\dfrac{r}{r_\Delta}\right)^{-2} & \text{for } r > r_\mathrm{c}. \end{cases} \tag{3.165}$$

  We define the cluster concentration parameter $c = r_\Delta / r_\mathrm{c}$, implying $\rho(r_\mathrm{c}) \equiv \rho_\mathrm{c} = c^2 \rho_\Delta$.

- If bremsstrahlung (free-free emission) is the dominating emission process, we obtain an X-ray luminosity in this model,

$$L_\mathrm{X} \propto \int_0^R \rho^2 T^{1/2} r^2 \mathrm{d}r, \tag{3.166}$$

$$\frac{\mathrm{d}L_\mathrm{X}}{\mathrm{d}\ln r} \propto r^3 \rho^2 T^{1/2} \sim \begin{cases} r^3 & \text{for } r < r_\mathrm{c}, \\ r^{-1} T^{1/2} & \text{for } r > r_\mathrm{c}. \end{cases} \tag{3.167}$$

Thus, the contribution to the X-ray luminosity per logarithmic bin in radius increases steeply toward r_c (because of the larger available volume) and then drops beyond r_c (after realizing that $T \sim r^{-1/2}$ in the peripheral cluster parts). The radii around r_c dominate L_X and thus, we expect

$$L_X \propto \rho_c^2 T^{1/2} r_c^3 \approx \rho_\Delta^2 c r_\Delta^3 T^{1/2}. \tag{3.168}$$

Using (3.155) and (3.156), we obtain

$$L_X \propto c M_\Delta^{4/3} E(z)^{1/3} \propto c T_\Delta^2 E(z)^{-1} \tag{3.169}$$

- If c is independent of mass, we recover (3.161). However, gas physics modifies c so that it assumes a mass dependence. There have been three classes of models suggested to explain the deviation from scale invariance:

  1. "Pre-heating" the gas by supernova winds or some other feedback mechanism *before* falling into clusters imprints an "entropy floor" in the gas distribution – a minimum entropy level $K_{\rm min}$ below which it cannot fall. The clusters' central entropy is $K_0 \propto T\rho_0^{-2/3} \propto Tc^{-4/3}$. If all clusters have $K_0 = K_{\rm min} = \text{const.}$, then

  $$c \propto T^{3/4} K_{\rm min}^{-3/4} \implies L_X \propto T^{2.75}. \tag{3.170}$$

  Thus, an entropy floor leads to larger core (relative to r_Δ), $r_c = r_\Delta/c \propto (K_{\rm min}/T)^{3/4} r_\Delta$, which is larger for smaller clusters (lower T) and thus to a steeper L_X-T relation close to the observations.

  2. An alternative possibility is that the gas gets heated after falling into the cluster, potentially through feedback by active galactic nuclei (AGN). This is however energetically much more expensive: to reach the same entropy as in the pre-heating case, one needs more energy if it is injected at the center by a factor

  $$\frac{k_B T_{\rm center}}{k_B T_{\rm pre-heat}} \sim \frac{K_{\rm center}}{K_{\rm pre-heat}} \left[\frac{n_{\rm center}}{n_{\rm pre-heat}}\right]^{2/3} \sim 10^2. \tag{3.171}$$

  Here, we adopted typical values for $n_{\rm center} \sim 2 \times 10^{-3}\,{\rm cm}^{-3}$ and $n_{\rm pre-heat} \sim 10\bar{n} \sim 2 \times 10^{-6}\,{\rm cm}^{-3}$. However, AGNs can provide this energy (see Sect. 3.2.2) if the energy can be effectively coupled into the ICM.

  3. Cooling out the low-entropy gas at the cluster center and fueling central star formation selectively removes the low-entropy gas. The gas at larger radii (and on higher adiabatic curves) flows in adiabatically and replaces the condensed

gas which leads to the formation of an entropy floor. This process is observed to happen, but the star formation rate is only 10% of what would be needed to explain the steeper L_X-T slope.

3.2 Radiative Physics

- Observed cluster scaling relations do not obey self-similar predictions. Hence we have to take more realistic physics such as radiative cooling and star formation into consideration. The nonlinearity of the problem requires numerical simulations that represent a formidable computational challenge. This requires numerical codes that simulate three-dimensional hydrodynamics in simulations that span an enormous range in scales and track a plethora of physical processes. Typically, we simulate a periodic box of side length L that contains a representative volume of the universe and is large enough to host enough objects of interest to provide a sufficiently large statistical sample.

  - $L \gtrsim 300\,\mathrm{Mpc} \sim 10^{27}\,\mathrm{cm}$. This large volume is necessary in order to get a few sites of constructive interference of long wavelength modes which evolve into a few massive ($M \sim 10^{15}\,\mathrm{M}_\odot$) galaxy clusters.
  - $l \sim 30\,\mathrm{kpc} \sim 10^{23}\,\mathrm{cm}$. The simulation needs to resolve the diameter l of the stellar content of galaxies by at least 10 resolution elements. Such a Eulerian mesh would then have $[L/(0.1l)]^3 \sim 10^{15}$ individual cells—too many elements even for current state-of-the-art simulations. A solution to this problem consists by either introducing adaptive grid-refinement capabilities in Eulerian codes (which increase the numerical resolution where needed, i.e., inside collapsing objects) or Lagrangian simulation frameworks that discretize the simulated mass rather than simulation space.
  - $l_* \sim 3\,\mathrm{pc} \sim 10^{19}\,\mathrm{cm}$. The star forming regions have typical sizes of 3 pc. The resulting dynamical range of the simulation volume, $(L/l_*)^3 \sim 10^{24}$, is prohibitively large to be reliably included in first-principle, ab initio simulations. Instead, this requires a subgrid prescription of star formation physics to include the necessary dynamical back-reaction effects on the resolved larger scales.

- First, we will turn to the physics of cooling and condensation of baryons into stars (that will happen inevitably once the gas gets sufficiently dense). Numerical simulations show that this transforms a fraction of $f_*/f_{\mathrm{gas}} \sim 25\% \ldots 50\%$ into stars without accounting for energy feedback. Since this is 5 to 10 times as much as observed in a cluster, we will then look at various "feedback processes" that were suggested to solve the "overcooling problem" of galaxy formation or equivalently the "cooling flow problem" in galaxy cluster evolution.

3.2.1 Radiative Cooling

- At high temperatures ($k_{\rm B}T \gtrsim 2$ keV) the light- and intermediate-mass elements of the ICM are fully ionized so that the only cooling process for them is free-free emission (thermal bremsstrahlung). Below $k_{\rm B}T \sim 2$ keV recombination-line cooling of heavy elements (Fe, ...) starts to dominate the cooling process (and the associated X-ray emission, assuming typical heavy element abundances relative to hydrogen, which are ~ 0.3 times those found in the Sun).

- The physics of bremsstrahlung emission is simple: electrons scatter off ions and are deflected in the Coulomb field of the ions. They radiate because of their acceleration and thus lose energy, i.e., they "cool".

- The spectral X-ray emissivity j_ν is defined as as the amount of energy emitted in photons of frequency ν per unit frequency interval dν, per unit time and per unit plasma volume, $j_\nu = {\rm d}^3E/({\rm d}\nu{\rm d}t{\rm d}V)$. It must scale with the product of electron and ion number density (because it is a two-body interaction), with the time available for the scattering process, $t \sim l/\Delta v \sim l/\sqrt{k_{\rm B}T/m}$, where Δv is the relative velocity of electron and ion, and with the Boltzmann factor for the distribution of energy at a given temperature. Hence we get

$$j_\nu = \frac{{\rm d}^3E}{{\rm d}\nu{\rm d}t{\rm d}V} = \tilde{C}\frac{n^2}{\sqrt{k_{\rm B}T}}{\rm e}^{-h\nu/k_{\rm B}T}, \quad \tilde{C} = {\rm const.} \tag{3.172}$$

- The volume emissivity is the integral of j_ν over frequency,

$$j \equiv \frac{{\rm d}^2E}{{\rm d}t{\rm d}V} = \int_0^\infty \frac{{\rm d}^3E}{{\rm d}\nu{\rm d}t{\rm d}V}{\rm d}\nu = \tilde{C}\frac{n^2}{\sqrt{k_{\rm B}T}}\frac{k_{\rm B}T}{h}\int_0^\infty {\rm e}^{-x}{\rm d}x \tag{3.173}$$

$$= Cn^2\sqrt{k_{\rm B}T} = 2.5\times10^{-23}\left(\frac{n_{\rm H}}{1\,{\rm cm}^{-3}}\right)^2\left(\frac{T}{10^8\,{\rm K}}\right)^{1/2}\frac{\rm erg}{{\rm cm}^3\,{\rm s}}, \tag{3.174}$$

  for 0.3 times solar metallicity $Z_\odot$.

- Comparing the thermal energy content to the total (frequency-integrated) X-ray emissivity defines the cooling time

$$t_{\rm cool} = \frac{\varepsilon_{\rm th}}{\dot{\varepsilon}_{\rm brems}} = \frac{3nk_{\rm B}T}{2j} \tag{3.175}$$

$$\approx 2\left(\frac{k_{\rm B}T}{\rm keV}\right)^{1/2}\left(\frac{n_{\rm e}}{10^{-2}\,{\rm cm}^{-3}}\right)^{-1}\,{\rm Gyr}, \tag{3.176}$$

  where $n = \rho/(\mu m_{\rm p})$, $n_{\rm H} = X_{\rm H}\,,\rho/m_{\rm p}$, the mean molecular weight of a fully ionized primordial gas is $\mu = 0.588$, with the primordial hydrogen mass fraction $X_{\rm H} = 0.76$ (see App. A.1).

- Hence in the centers of galaxy clusters, $t_{\rm cool}$ is smaller than the Hubble time: if gas in pressure equilibrium cools, it becomes denser and cools even faster. This is a run-away process that should lead to a large amount of cold gas and star formation—in conflict with observations. This is the famous "cooling flow problem".

- We can gain further insight if we rewrite $t_{\rm cool}$ in terms of the cluster entropy $K_{\rm e} \equiv k_{\rm B} T n_{\rm e}^{-2/3}$. We define $t_0 = 2$ Gyr, $k_{\rm B} T_0 = $ keV, and $n_0 = 10^{-2}\,{\rm cm}^{-3}$, to obtain

$$t_{\rm cool} = t_0 \left(\frac{k_{\rm B} T}{k_{\rm B} T_0}\right)^{1/2} \frac{n_0}{n_{\rm e}} = t_0 \left(\frac{K_{\rm e}}{K_0}\right)^{3/2} \frac{k_{\rm B} T_0}{k_{\rm B} T}, \tag{3.177}$$

  where $K_0 = 21.5\,{\rm keV\,cm}^2$ is a typical value for the central entropy in cool core clusters. Because $t_0 \ll t_{\rm Hubble} \approx 14\,{\rm Gyr}$ the cooling ICM needs additional (non-gravitational) energy injection that stabilizes it against the cooling catastrophe.

- This demonstrates that clusters with similar temperatures (or potential depths) have longer cooling times if the central entropy is larger. We can derive a critical entropy

$$K_{\rm c}(T) \approx 80 \left(\frac{t_{\rm cool}}{14\,{\rm Gyr}}\right)^{2/3} \left(\frac{k_{\rm B} T}{\rm keV}\right)^{2/3} {\rm keV\,cm}^2, \tag{3.178}$$

  that is large enough to avoid the cooling catastrophe in galaxy groups with $k_{\rm B} T \sim$ keV.

3.2.2 Cooling versus Heating

- We have seen that the cooling time in the core region of cool core clusters is smaller than the Hubble time which would imply a cooling catastrophe if not countered by energy feedback. To see how much feedback is needed, we first compute the cooling rate and redefine the X-ray emissivity as an energy cooling rate $\Lambda(T)$ according to

$$j = C n_{\rm H}^2 \sqrt{k_{\rm B} T} = \Lambda_0(t) n_{\rm H}^2, \quad \text{where} \tag{3.179}$$

$$\Lambda_0 = 2.5 \times 10^{-23} \left(\frac{T}{10^8\,{\rm K}}\right)^{1/2} \frac{{\rm erg\,cm}^3}{\rm s}, \quad (Z = 0.3 Z_\odot). \tag{3.180}$$

- We adopt a typical gas density profile as found in X-ray observations, the so-called beta profile which is simply a King profile with the outer slope parametrized by $\beta \approx 2/3 \ldots 1$:

$$n(r) = n_0 \left[1 + \left(\frac{r}{r_{\rm c}}\right)^2\right]^{-3\beta/2}. \tag{3.181}$$

- We consider the X-ray luminosity as a proxy for the cooling luminosity. It is given by

$$L_{\rm X} = \int_0^\infty j{\rm d}V = \Lambda_0 \sqrt{\frac{k_{\rm B}T}{k_{\rm B}T_0}}\, 4\pi \int_0^\infty n^2(r) r^2 {\rm d}r \tag{3.182}$$

$$= \frac{4\pi}{3} r_{\rm c}^3 n_0^2 \Lambda_0 \sqrt{\frac{k_{\rm B}T}{k_{\rm B}T_0}} \times 3 \int_0^\infty \frac{x^2 {\rm d}x}{(1+x^2)^{3\beta}} \tag{3.183}$$

$$= \frac{4\pi}{3} r_{\rm c}^3 n_0^2 \Lambda_0 \sqrt{\frac{k_{\rm B}T}{k_{\rm B}T_0}} \times \begin{cases} \frac{3\pi}{16} & \text{for } \beta = 1 \\ \frac{3\pi}{4} & \text{for } \beta = 2/3 \end{cases} \tag{3.184}$$

$$\sim 10^{44} \left(\frac{r_{\rm c}}{100\,{\rm kpc}}\right)^3 \left(\frac{n_0}{10^{-2}\,{\rm cm}^{-3}}\right)^2 \left(\frac{k_{\rm B}T}{3\,{\rm keV}}\right)^{1/2} {\rm erg\ s}^{-1}, \tag{3.185}$$

  where we adopted $\beta = 1$ in the last step. Note that to order of magnitude, it suffices to assume a homogeneous sphere with radius $r_{\rm c}$ and a density that is equal to that of the core region to calculate $L_{\rm X}$. This corresponds to our finding ${\rm d}L_{\rm X}/{\rm d}\ln r \propto r^3 n^2 \sqrt{T}$ (3.166) that radii around $r_{\rm c}$ dominate $L_{\rm X}$.

- Hence, a successful feedback process has to heat the ICM at an average rate of 10^{44} erg s^{-1} to balance the cooling losses.

3.2.3 Feedback by Supernovae

The first obvious candidate for energy feedback are supernovae (SNe), i.e., exploding stars at the end of their lifetimes. There are two types of SNe: 1. core-collapse SNe (of type Ib,c or II) and 2. thermonuclear SNe (SNe of type Ia).

- **Core-collapse SNe.**
  - At the end of the lifetime of a massive star ($M \gtrsim 10\,{\rm M}_\odot$) it has used up its "fuel" (H, He, ...), i.e., the energy generated by nuclear burning and it cannot anymore balance the gravitational attraction. As a result, the core collapses and forms a black hole or a neutron star (pulsar). The envelope also collapses to nuclear densities which triggers an outward traveling shock that unbinds the envelope and ejects it. This enriches the surrounding medium with intermediate-mass elements, so-called "α elements" which can be built from α-particle nuclei (^{4}He) such as ^{16}O, ^{20}Ne, ^{24}Mg, ^{28}Si, ^{32}S, ^{36}Ar, ^{40}Ca, ^{48}Ti.
  - To estimate the effect of SNe heating on the ICM, we make three simplifications. We assume that 1. metals are fully mixed within the ICM, 2. neglect radiative losses, and 3. assume solar abundances. Since the metallicity Z of clusters is

typically $0.3Z_\odot$ and radiative losses cause a large fraction of this SNe energy to be radiated away, these numbers represent the absolute upper limit that SNe can contribute to the heating which is plausibly no reachable in the ICM.

– The mass fraction of α elements for a gas of solar abundance is

$$\frac{M_\alpha}{M_{\rm gas}} \approx 0.02. \tag{3.186}$$

Hence the supernova energy per α element that is created by the SN is given by

$$\frac{E_{\rm SN} m_{\rm p}}{M_\alpha} \sim \frac{10^{51}\,{\rm erg}\, m_{\rm p}}{10\,{\rm M}_\odot} \sim \frac{10^{51-24-34}}{2}\frac{\rm erg}{\rm nucleon} \sim 50\,\frac{\rm keV}{\rm nucleon}. \tag{3.187}$$

Mixing this energy into to ICM (and neglecting radiative losses), we get

$$\frac{E_{\rm SN} m_{\rm p}}{M_{\rm gas}} \sim 1\,\frac{\rm keV}{\rm nucleon}. \tag{3.188}$$

- **Thermonuclear SNe.** The progenitor system of a type Ia supernova consists of a binary with at least one massive ($\approx 1\ {\rm M}_\odot$) carbon-oxygen white dwarf:

  – The *single-degenerate scenario* assumes that the companion of the white dwarf is an evolved star. When the companion star becomes a red giant, it grows over its Roche volume and transfers mass to the white dwarf. White dwarfs are stabilized by the Fermi pressure of a degenerate electrons gas. This can only stabilize masses up to $1.4\,{\rm M}_\odot$ against gravity. When the companion star feeds the white dwarf beyond this limit, a thermonuclear runaway burning is eventually triggered, which explodes the white dwarf. This scenario appears to be ruled out for explaining the majority of type Ia supernovae.

  – Alternatively, the *double-degenerate scenario* assumes the existence of a binary consisting of two carbon-oxygen white dwarfs. At the end of their evolution, they merge and cause a thermonuclear runaway burning of carbon and oxygen in the more massive progenitor. The resulting type Ia supernovae explosion generates $\approx 1\ {\rm M}_\odot$ ^{56}Ni, which decays radioactively into ^{56}Ni and eventually to ^{56}Fe. This decay is responsible for the extraordinary brightness of type Ia supernovae ($\sim 10^{11}$ times more luminous in comparison to a star on the main sequence).

– Using the same assumptions as above, we obtain

$$\frac{M_{\rm Fe}}{M_{\rm gas}} \approx 0.001 \quad \text{(solar abundance)}, \tag{3.189}$$

$$\frac{E_{\rm SN} m_{\rm p}}{M_{\rm Fe}} \sim \frac{10^{51}\,{\rm erg}\, m_{\rm p}}{1\,{\rm M}_\odot} \sim 500\,\frac{\rm keV}{\rm nucleon}, \tag{3.190}$$

$$\frac{E_{\rm SN} m_{\rm p}}{M_{\rm gas}} \sim 0.5\,\frac{\rm keV}{\rm nucleon}. \tag{3.191}$$

- **Problems.** As we will now show, there are two problems with this hypothetical picture in which SNe provide the feedback energy: 1. the energetics is not sufficient and 2. the radiative losses are too strong to solve the "cooling flow problem".

  1. For comparison we estimate the gravitational energy of a Milky Way-type galaxy and a massive galaxy cluster

$$E_{\rm gal} \approx \frac{m_{\rm p}}{2} v_{\rm gal}^2 \approx 0.25 \left(\frac{v_{\rm gal}}{220\,{\rm km\ s^{-1}}}\right)^2 {\rm keV}, \tag{3.192}$$

$$E_{\rm gal} \approx \frac{m_{\rm p}}{2} \sigma_{\rm cluster}^2 \approx 8 \left(\frac{\sigma_{\rm cluster}}{1200\,{\rm km\ s^{-1}}}\right)^2 {\rm keV}. \tag{3.193}$$

     While SNe feedback can energetically modulate the star formation within galaxies, it is (by about an order of magnitude even for the unrealistically optimistic case) too weak in clusters to have any thermodynamic impact.

  2. In order to avoid radiative losses, SNe heating has to raise the entropy of the gas it heats to at least $\sim 100\,{\rm keV\,cm^2}$ (3.178). An evenly distributed thermal energy input of order 1 keV would thus have to go into gas significantly less dense than $10^{-3}\,{\rm cm^{-3}}$ to avoid such losses. But gas near the centers of present-day cluster (not to mention the densities of the interstellar medium within galaxies where SNe occur) is denser than that with average densities $\bar{n}_{\rm ISM} \sim 1\,{\rm cm^{-3}}$, particularly at earlier times when most of the star formation happened. Simulations that spread SNe feedback evenly thus produce too many stars in clusters!

3.2.4 Feedback by Active Galactic Nuclei

- There is a compact region at the center of every galaxy that dominates the luminosity of its electromagnetic spectrum, the "active galactic nucleus" (AGN). Observationally, it is known that the AGN emission is caused by mass accretion onto a supermassive black hole (SMBH) which can launch relativistic outflows (so called "jets"). Particle acceleration in jets causes non-thermal radio synchrotron and γ-ray emission.

- The masses of SMBH at the centers of galaxies fall typically in the range of $10^6 \lesssim M_{\rm SMBH}/{\rm M}_\odot \lesssim 10^{10}$. Those SMBH masses are tightly correlated with the stellar mass in galactic bulges. Bulges are defined as the central spheroidal stellar component of a disk galaxy ("late types") or the entire elliptical stellar distribution of ellipticals ("early types"), including the population of bright central galaxies (BCGs) in clusters.

- The mass of the stellar bulge and the SMBH obey the correlation

$$M_{\rm SMBH} \sim 0.005 M_{\rm bulge}, \tag{3.194}$$

  so that we obtain typical masses for SMBHs at the centers of clusters according to

$$M_{*,\rm BCG} \sim 10^{12}\,{\rm M}_\odot \quad \Rightarrow \quad M_{\rm SMBH} \sim 5\times 10^9 {\rm M}_\odot, \tag{3.195}$$

  upon identifying $M_{*,\rm BCG}$ with the bulge mass. This compares well with the latest mass measurement of the SMBH in M87 of $6 \times 10^9\,{\rm M}_\odot$ (M87 is the BCG in Virgo, our closest galaxy cluster with $D_{\rm Virgo} \sim 17$ Mpc).

- The accretion power onto the SMBH can be estimated by the release of gravitational energy with a radiative efficiency of $\eta \sim 0.1$,

$$E_{\rm AGN} \sim \eta M_{\rm SMBH} c^2 \sim 10^{63} \left(\frac{M_{\rm SMBH}}{5\times 10^9\,{\rm M}_\odot}\right) {\rm erg} \tag{3.196}$$

$$\frac{E_{\rm AGN} m_{\rm p}}{M_{\rm gas}} \sim \frac{10^{63}\,{\rm erg}\, m_{\rm p}}{10^{14}\,{\rm M}_\odot} \sim \frac{10^{63-14-24-33}}{2}\,\frac{\rm erg}{\rm nucleon} \sim 5\,\frac{\rm keV}{\rm nucleon}. \tag{3.197}$$

  From the energetic viewpoint, this is a much more promising heating source in comparison to supernova feedback.

- The centers of many (if not all) cool core clusters with low-entropy gas whose cooling time is less than the age of the universe also contain AGNs. Relativistic jets from these AGNs inflate radio-emitting lobes of typical radii $r_{\rm lobe} \sim (10 \ldots 50)$ kpc and distances to the central AGN of $R \sim (20 \ldots 100)$ kpc. The location of these radio-emitting lobes coincide with cavities in X-ray maps. This suggests that the momentum of the relativistic outflow has been slowed down by the inertia of the ICM ($n_{\rm ICM} \sim 10^{-2}\,{\rm cm}^{-3}$, $k_{\rm B}T \sim 3\,{\rm keV}$) which got pushed away by the jet fluid in the process of inflating the lobes.

- **Emerging picture.** As the central gas is cooling, it can eventually form stars and feed the accretion disk of the AGN. The accreting gas has to lose its angular momentum which can be used to trigger a relativistic jet that is composed of cosmic rays (relativistic

particle populations) and magnetic fields. Eventually, the jet momentum slows down due to the ram pressure of the ambient ICM and inflates lobes of relativistic plasma. As the jets terminate, the lobes detach from the ceasing outflows. Because of the relativistic filling, the lobes or bubbles are lighter than the heavier ambient ICM. Since these bubbles got injected at the bottom of the gravitational cluster potential, we have a convectively unstable situation and the bubbles start to rise buoyantly and subsonically in the stratified cluster atmosphere.

- The relativistic jets displace the ICM at the location of the cavities, i.e., they do $P\mathrm{d}V$ work against the ICM, as well as supply internal energy, U, to the cavities. Hence the total energy required to create the cavity is equal to its enthalpy,

$$H = U + PV = \frac{1}{\gamma_\mathrm{b} - 1} PV + PV = \frac{\gamma_\mathrm{b}}{\gamma_\mathrm{b} - 1} PV = 4PV, \quad (3.198)$$

  where we used $\gamma_\mathrm{b} = 4/3$ (assuming a relativistic filling of the radio emitting bubbles). Of this $4PV$, only $1PV$ is directly available for mechanical work on the surroundings while $3PV$ are stored as internal energy.

- Hence, the work done by the two bubbles in one outburst (as supposed to the many accompanying SMBH growth, as implied in (3.196)) on the ambient ICM is

$$W = PV = 2 \times \frac{4}{3} \pi r_\mathrm{b}^3 n_\mathrm{a} k_\mathrm{B} T \sim 10^{59}\,\mathrm{erg}, \quad (3.199)$$

  where we used $r_\mathrm{b} = 20\,\mathrm{kpc}$, $n_\mathrm{a} = 10^{-2}\,\mathrm{cm}^{-3}$, $k_\mathrm{B}T = 3\,\mathrm{keV}$.

- There are (at least) three different ways to estimate the bubble's rise time, using 1. the sound crossing time, 2. the buoyant rise time, and 3. the time required for the ambient medium to refill the displaced volume as the bubble rises upward.

  1. The sound crossing time of the distance from the cavity center to the SMBH (using $\gamma_\mathrm{a} = 5/3$ for the ambient ICM) is given by

$$t_\mathrm{s} = R \sqrt{\frac{\mu m_\mathrm{p}}{\gamma_\mathrm{a} k_\mathrm{B} T}} \approx 4 \times 10^7 \left(\frac{R}{40\,\mathrm{kpc}}\right) \left(\frac{k_\mathrm{B}T}{3\,\mathrm{keV}}\right)^{-1/2}. \quad (3.200)$$

  2. To estimate the buoyancy time, we compute the buoyancy force acting upon the bubble

$$\boldsymbol{F}_\mathrm{buoy} = -\boldsymbol{g} V (\rho_\mathrm{a} - \rho_\mathrm{b}), \quad (3.201)$$

     where $\boldsymbol{g}$ is the gravitational acceleration (assuming hydrostatic equilibrium of the ambient gas), V is the bubble volume, ρ_a and ρ_b denote the mass density of the ambient gas

and the bubble, respectively. The ram pressure exerts a drag force on the bubble, oppositely directed to the rise velocity,

$$\boldsymbol{F}_{\rm drag} = -\frac{C}{2}\sigma\rho_{\rm a}v^2\frac{\boldsymbol{v}}{v}, \tag{3.202}$$

where σ is the cross section of the bubble, C is the drag coefficient that depends on bubble geometry and Reynolds number (i.e., whether the flow is turbulent or laminar): $C \approx 0.6$ for a Mach number $\mathcal{M} \approx 0.7$. In equilibrium, the terminal velocity is obtained by balancing $|\boldsymbol{F}_{\rm buoy}|$ and $|\boldsymbol{F}_{\rm drag}|$, yielding

$$v = \sqrt{\frac{2gV}{\sigma C}\frac{\rho_{\rm a}-\rho_{\rm b}}{\rho_{\rm a}}} \approx \sqrt{\frac{2gV}{\sigma C}}, \tag{3.203}$$

where we assumed $\rho_{\rm b} \ll \rho_{\rm a}$ in the last step. For a singular isothermal sphere (SIS), we can write down $g \approx v_{\rm c}^2/R = 2\sigma^2/R = 2k_{\rm B}T/(\mu m_{\rm p}R)$. With $\sigma = \pi r^2$ and $V = 4\pi r^3/3$, we obtain

$$t_{\rm buoy} \approx R\sqrt{\frac{2gV}{\sigma C}} \approx t_{\rm s}\sqrt{\frac{3C\gamma_{\rm a}}{16}\frac{R}{r}} \approx 0.6t_{\rm s}\left(\frac{R}{2r}\right)^{1/2}. \tag{3.204}$$

3. The time required to refill the volume as the bubble rises upward is

$$t_{\rm rise} \approx 2R\sqrt{\frac{r}{GM(R)}} \approx t_{\rm s}\sqrt{\frac{2\gamma_{\rm a}r}{R}} \approx 1.3t_{\rm s}\left(\frac{2r}{R}\right)^{1/2}. \tag{3.205}$$

In the second step, we used the potential of the SIS, $\Phi_{\rm SIS} = GM/R = 2k_{\rm B}T/(\mu m_{\rm p})$.

- This demonstrates that all three estimates provide similar results (albeit with a different scaling in the ratio r/R.) We finally obtain the AGN heating rate by combining (3.199) and (3.204),

$$L_{\rm AGN} \approx \frac{PV}{t_{\rm buoy}} \approx \frac{10^{59}\,{\rm erg}}{10^{15}\,{\rm s}} \approx 10^{44}\,{\rm erg\,s^{-1}} \approx L_{\rm X}, \tag{3.206}$$

i.e., it is comparable to the X-ray "cooling" luminosity (3.182).

- There are a number of open questions in this scenario which are currently being actively researched.

1. How is the accretion output *thermalized*? Suggestions include dissipation of non-linear waves, turbulence of streaming cosmic rays (that can excite Alfvén waves in the magnetized ICM which get damped).

2. Is the heating-cooling balance *stable* to local thermal perturbations? While turbulent heating is not stable, cosmic-ray Alfvén wave heating is stabilized around 1 keV, which coincides with the lower temperature floors observed at the centers of cool core clusters.
3. How is the accretion rate *tuned*? The Schwarzschild radius of a SMBH is

$$r_{\rm SMBH} = \frac{2GM_{\rm SMBH}}{c^2} \approx 1.3 \times 10^{15}\,{\rm cm} \approx 1\,{\rm light\ day}. \quad (3.207)$$

On the contrary, cooling occurs on scales of about 30 kpc $\approx 10^{23}$ cm $\approx 10^8\, r_{\rm SMBH}$.

- At least Nature finds a way to solve all of these problems because observationally, SMBH activity accompanies transition to complexity when $t_{\rm cool} \lesssim 1$ Gyr.

3.2.5 Heat Conduction and Thermal Stability

Derivation

- A system can be in hydrostatic equilibrium, but out of thermal equilibrium. The entropy equation reads

$$\rho T \frac{{\rm d}s}{{\rm d}t} = \boldsymbol{\nabla} \cdot (\kappa \boldsymbol{\nabla} T)\,. \quad (3.208)$$

Using ${\rm d}q = T{\rm d}s$ and $c_P \equiv ({\rm d}q/{\rm d}T)_P$, we get

$$c_P {\rm d}T = T{\rm d}s \quad \Rightarrow \quad {\rm d}s = c_P {\rm d}\ln T. \quad (3.209)$$

- Hence, we can rewrite (3.208),

$$\rho c_P \frac{{\rm d}T}{{\rm d}t} = \kappa \boldsymbol{\nabla}^2 T \quad \text{or} \quad \frac{{\rm d}T}{{\rm d}t} = \chi \boldsymbol{\nabla}^2 T, \quad (3.210)$$

where $\chi \equiv \kappa/\rho c_P$. This shows that the temperature can only change as a result of thermal conduction if $\boldsymbol{\nabla} T \neq \mathbf{0}$ since the temperature gradient is the source of free energy.

- We now want to estimate the heat conductivity κ. To this end, we consider a system in thermal equilibrium with a temperature T and with particles moving randomly in all directions. ΔA denotes the area of a screen perpendicular to the x axis. The number of particles that fly per unit time through the screen from one side to the other is given by

$$\frac{\Delta N}{\Delta t} = \frac{nv\Delta A}{6}, \quad (3.211)$$

where the factor of 6 arises because on average, 1/3 of all particles fly along the x axis and of those, only 1/2 in either direction.

- The particle mean free path is $\lambda = 1/(n\sigma)$ with σ as the collisional cross section. Particles at $x - \lambda$ transport gas properties to x and vice versa. This is particularly important for gradients in gas properties that will be smoothed out as a result of such a transport.

- Hence, in the presence of a density gradient, $\partial n/\partial x \neq 0$, the net number of particles flying from the denser to the more dilute region is

$$\frac{\Delta N}{\Delta t} = \frac{n(x+\lambda)v\Delta A}{6} - \frac{n(x-\lambda)v\Delta A}{6} \approx \frac{v\Delta A}{6}\frac{\partial n}{\partial x}2\lambda, \qquad (3.212)$$

  where we have expanded the density field to first order and have assumed that the typical length of a gradient Δx is much larger than the mean free path, $\lambda \ll \Delta x$.

- The diffusion coefficient that relates the particle current $j = \Delta N/(\Delta t \Delta A)$ to the number density gradient is given by

$$\frac{\Delta N}{\Delta t \Delta A} \stackrel{!}{=} D\frac{\partial n}{\partial x} \quad \text{with} \quad D \equiv \frac{v\lambda}{3} = \frac{v}{3n\sigma}. \qquad (3.213)$$

  If the temperature changes along x (i.e., $\partial T/\partial x \neq 0$), the particles transport energy,

$$\frac{\Delta E}{\Delta t} = \frac{nv\Delta A}{6}[E(x+\lambda) - E(x-\lambda)] \qquad (3.214)$$

$$= \frac{nv\lambda}{3}\left(\frac{\partial E}{\partial T}\frac{\partial T}{\partial x}\right) = \frac{nvc_V\lambda}{3}\frac{\partial T}{\partial x}, \qquad (3.215)$$

  where c_V is the heat capacity at constant volume (3.7). Hence, we find

$$\frac{\Delta E}{\Delta t \Delta A} \stackrel{!}{=} \kappa\frac{\partial T}{\partial x} \quad \text{with} \quad \kappa = \frac{nvc_V\lambda}{3} = \frac{vc_V}{3\sigma} = \frac{vk_\mathrm{B}}{2\sigma}, \qquad (3.216)$$

  where we used the heat capacity at constant volume $c_V = 3k_\mathrm{B}/2$ (3.7) in the last step (assuming an ideal, monoatomic gas) and the heat conductivity κ has units of erg cm^{-1} s^{-1} K^{-1}.

- Heat is conducted by electrons since they move faster than ions by $v_\mathrm{e}/v_\mathrm{i} = \sqrt{m_\mathrm{i}/m_\mathrm{e}} \approx 43\sqrt{Z}$ (assuming $T_\mathrm{e} = T_\mathrm{i}$ which applies to the ICM except for immediate post-shock regions). The electron mean free path is determined by the ion number density and the scattering cross section, implying $\lambda = 1/(n_\mathrm{i}\sigma)$.

Coulomb Logarithm

- Let's first consider an electron scattering in the Coulomb field of an ion:

  1. If the deflection angle is small, $\theta_{\rm D} \ll 1$, we can approximate its value by computing the perpendicular impulse exerted by the ion's Coulomb field, integrating along the electron's unperturbed straight line trajectory (the "Born approximation")

$$\begin{aligned} m_{\rm e} v_{\rm e} \theta_{\rm D} &= \int_{-\infty}^{\infty} \boldsymbol{\nabla}_{\perp} \phi_i {\rm d}t = \int_{-\infty}^{\infty} \frac{\partial}{\partial b} \left(\frac{Ze^2}{\sqrt{b^2 + v_{\rm e}^2 t^2}} \right) {\rm d}t \\ &= \int_{-\infty}^{\infty} \frac{Ze^2 b {\rm d}t}{(b^2 + v_{\rm e}^2 t^2)^{3/2}} = \frac{Ze^2}{v_{\rm e}} \int_{-\infty}^{\infty} \frac{b^2 {\rm d}x}{b^3 (1+x^2)^{3/2}} \\ &= \frac{Ze^2}{v_{\rm e} b} \left. \frac{x}{\sqrt{1+x^2}} \right|_{-\infty}^{\infty} = \frac{2Ze^2}{b v_{\rm e}}, \end{aligned} \tag{3.217}$$

     where b is the impact parameter of the electron's trajectory. Hence we obtain

$$\theta_{\rm D} = \frac{b_0}{b} \quad \text{for} \quad b \gg b_0 \equiv \frac{2Ze^2}{m_{\rm e} v_{\rm e}^2}. \tag{3.218}$$

  2. If the dominant source of this electron deflection were a single large-angle scattering event in the Coulomb field of an ion, then the relevant cross section would be $\sigma = \pi b_0^2$ (since all impact parameters $\lesssim b_0$ produce large-angle scatterings) and the mean deflection frequency $\nu_{\rm D}$ and time $t_{\rm D}$ would be

$$\nu_{\rm D} = \frac{1}{t_{\rm D}} = n_{\rm i} \sigma v_{\rm e} = n_{\rm i} \pi b_0^2 v_{\rm e} \ \text{(for large-angle scattering)}. \tag{3.219}$$

- The cumulative, random-walk effects of many small-angle scatterings off ions produce a net deflection of order a radian in a shorter time. As the directions of the individual scatterings are random, the mean defection angle after many scatterings vanish, $\langle \theta \rangle = 0$. However, $\langle \theta^2 \rangle$ will not vanish and we have

$$\langle \theta^2 \rangle = \sum_{\text{all encounters}} \theta_{\rm D}^2 = \sum_{\text{all encounters}} \left(\frac{b_0}{b} \right)^2. \tag{3.220}$$

- The number of encounters that occur with impact parameters between b and $b + {\rm d}b$ during time t is ${\rm d}N = n_{\rm i} v_{\rm e} t 2\pi b {\rm d}b$. Hence the mean square deflection angle accumulates up to

$$\langle \theta^2 \rangle = \int_{b_{\rm min}}^{b_{\rm max}} \left(\frac{b_0}{b} \right)^2 {\rm d}N = n_{\rm i} 2\pi b_0^2 v_{\rm e} t \ln \left(\frac{b_{\rm max}}{b_{\rm min}} \right). \tag{3.221}$$

- While the integral diverges logarithmically, physics regularizes it quite naturally. The minimum impact parameter,

$$b_{\min} = \frac{Ze^2}{k_B T}, \tag{3.222}$$

equals the radius where the Coulomb energy of the electron in the field of the ion vanishes, $U = mv^2/2 - Ze^2/b_{\min} \stackrel{!}{=} 0$. The maximum impact parameter is given by the maximum distance over which electric fields of individual particles can reach without being screened by the oppositely charged particles in a plasma. This is known as the Debye length,

$$b_{\max} = \lambda_D = \sqrt{\frac{k_B T}{4\pi n_e Z e^2}}. \tag{3.223}$$

- Hence, we can define the Coulomb logarithm

$$\ln\Lambda = \ln\left(\frac{b_{\max}}{b_{\min}}\right) = \ln\sqrt{\frac{(k_B T)^3}{4\pi n_e Z^3 e^6}} \tag{3.224}$$

$$= 35 - \frac{1}{2}\ln\left(\frac{n_e}{10^{-2}\mathrm{cm}^{-3}}\right) + \frac{3}{2}\ln\left(\frac{k_B T}{\mathrm{keV}}\right). \tag{3.225}$$

- The value of t that implies $\langle\theta^2\rangle \approx 1$ is the deflection time t_D,

$$\nu_D^{ei} = \frac{1}{t_D^{ei}} = n_i 2\pi b_0^2 v_e \ln\Lambda = \frac{8\pi n_i Z^2 e^4}{m_e^2 v_e^3}\ln\Lambda \tag{3.226}$$

and $\ln\Lambda \approx 35\ldots40$ in the ICM. This deflection frequency is larger by a factor of $2\ln\Lambda$ than the frequency of (3.219), which is valid for a single large-angle scattering event.

- Back to our heat conductivity of electrons,

$$\kappa = \frac{n_e v_e c_V \lambda}{3} = \frac{n_e v_e c_V}{3\sigma n_i}. \tag{3.227}$$

From (3.226), we can read off σ by remembering $\nu_D = n_i \sigma v_e$:

$$\sigma = 2\pi b_0^2 \ln\Lambda = \frac{8\pi Z^2 e^4 \ln\Lambda}{m_e^2 v_e^4}. \tag{3.228}$$

This yields the heat conductivity of electrons that are scattered by ions in a thermal gas,

$$\kappa = \frac{n_e v_e}{3} c_V \frac{m_e^2 v_e^4}{8\pi n_i Z^2 e^4 \ln\Lambda} = \frac{1}{3}\left(\frac{m_e^2}{8\pi Z^2 e^4}\right)\left(\frac{n_e}{n_i}\right)\frac{c_V v_e^5}{\ln\Lambda}. \tag{3.229}$$

- The heat capacity at constant volume is $c_V = 3k_B/2$ and the thermal electron velocity is $v_e = \sqrt{3k_B T_e/m_e}$. Inserting these expressions into (3.229) yields a value for the heat conductivity

$$\begin{aligned}\kappa &= \frac{k_B}{2}\left(\frac{m_e^2}{8\pi Z^2 e^4}\right)\left(\frac{n_e}{n_i}\right)\left(\frac{3k_B T_e}{m_e}\right)^{5/2}\frac{1}{\ln\Lambda} \\ &= 1.7\times 10^{-7}\left(\frac{T}{1\,\mathrm{K}}\right)^{5/2}\left(\frac{\ln\Lambda}{35}\right)^{-1}\frac{\mathrm{erg}}{\mathrm{s\,K\,cm}} \\ &= 1.7\times 10^{13}\left(\frac{T}{10^8\,\mathrm{K}}\right)^{5/2}\left(\frac{\ln\Lambda}{35}\right)^{-1}\frac{\mathrm{erg}}{\mathrm{s\,K\,cm}}, \qquad (3.230)\end{aligned}$$

  where we have used appropriate values for the Coulomb logarithm in cool core regions in clusters.

Thermal Stability: Fields Length

- Cool star forming clouds should only appear in systems whose size is *greater* than a critical length scale, known as the *Fields length* below which thermal conduction smoothes out temperature inhomogeneities. Formally we would have to a Lagrangian perturbation analysis to derive this length scale. Instead, we will derive the Field length heuristically by considering thermal balance for a cool cloud of radius r embedded in a medium of temperature T.

- Electron thermal conduction sends energy into the cloud at a rate

$$\mathcal{H}_{\mathrm{cond}} \sim r^2\kappa(T)\frac{T}{r} \sim \kappa_0 f_e r\left(\frac{T}{T_8}\right)^{7/2}. \qquad (3.231)$$

  Here, $T_8 = 10^8$ K, f_e is a magnetic suppression factor that depends on the topology of magnetic field lines connecting our cloud of consideration, and we used the *Spitzer conductivity* (which assumes a value for the Coulomb logarithm of $\ln\Lambda = 10$),

$$\kappa = 6\times 10^{13}\left(\frac{T}{10^8\,\mathrm{K}}\right)^{5/2} f_e\frac{\mathrm{erg}}{\mathrm{s\,K\,cm}}. \qquad (3.232)$$

- Radiative cooling can radiate away energy at a rate

$$C_{\mathrm{rad}} \sim r^3 n_H^2\Lambda_0(T) \sim r^3 n_H^2\Lambda_0\left(\frac{T}{T_8}\right)^{1/2}, \text{ with} \qquad (3.233)$$

$$\Lambda_0(T) \approx 2.5\times 10^{-29}\left(\frac{T}{T_8}\right)^{1/2}\frac{\mathrm{erg\,cm^3}}{\mathrm{s}}, \qquad (3.234)$$

  where we have used (3.180).

- Cooling and conduction are thus in approximate balance, $\mathcal{H}_{\rm cond} \sim C_{\rm rad}$, for systems with a radius of order the Fields length

$$\lambda_{\rm F} \equiv \left[\frac{T\kappa(T)}{n_{\rm H}^2\Lambda_0(T)}\right]^{1/2} = \left(\frac{\kappa_0 f_{\rm e} x_{\rm e}^2}{k_{\rm B}\Lambda_0 k_{\rm B}^2 T_8^2}\right)^{1/2} K_{\rm e}^{3/2} \tag{3.235}$$

$$\approx 4\,{\rm kpc}\left(\frac{K_{\rm e}}{10\,{\rm keV\ cm^2}}\right)^{3/2} f_{\rm e}^{1/2}, \tag{3.236}$$

  where we have used $K_{\rm e} = k_{\rm B}T/n_{\rm e}^{2/3}$ and the square of the hydrogen number density is given by $n_{\rm H}^2 = X_{\rm H}^2\rho^2/m_{\rm p}^2 = n_{\rm e}^2/x_{\rm e}^2$. Through a coincidence of scaling, the Field length is a function of entropy alone when free-free emission is the dominant cooling mechanism.

- We can translate this criterion in the entropy-radius plane by adopting $\lambda_{\rm F}(K) = r$. This yields a thermal stability threshold that obeys a scaling with radius of $K \propto r^{2/3} f_{\rm e}^{-1/3} = \lambda_{\rm F}^{2/3} f_{\rm e}^{-1/3}$. Gas that is below that threshold and resides within radius r constitutes a subsystem with $r > \lambda_{\rm F}$ (at constant K), i.e., the amount of entropy in the larger cloud is too small to support fast enough conduction that is necessary to prevent a cooling run-away, allowing multiphase gas to persist and star formation to proceed. Gas above the threshold resides in the region of thermal stability in which conduction is fast enough and leads to evaporation of a cool cloud and eventually homogeneity.

- In Sect. 3.1.7, we found that the entropy profile of the ICM at larger scales shows the behavior $K \propto r^{1.1}$. This leaves us with two possibilities of cluster states in reality (which appear to be dynamical attractor solutions of thermal stability considerations):

  1. Clusters can have an entropy profile that is elevated enough so that it stays always above the thermal stability threshold. As a consequence, the steeper entropy profile on larger scale necessarily needs to break at sufficiently large radii to join an elevated level of central entropy. This defines the class of *non-cool core clusters*.
  2. Clusters can have an entropy profile that continues to decrease toward smaller radii until it drops below the thermal stability threshold. There the gas is subject to thermal instability, and multiphase gas can form, potentially seeding star formation. This constitutes the class of *cool core clusters*.

Thermal Stability with Magnetic Fields

3.3 Non-thermal Processes

3.3.1 Magnetic Fields

Generating Magnetic Fields: Biermann Battery

Evolution: Magneto-hydrodynamics

Magneto-hydrodynamic Waves and Turbulence

3.3.2 Cosmic Rays

Diffusive Shock Acceleration (First-order Fermi Acceleration)

Second-order Fermi Acceleration

Cosmic Ray Transport

- Consider a spatial random coordinate $x(t)$ of a CR particle diffusing in a fluid of bulk velocity v. For simplicity, we restrict ourselves to the one-dimensional case. During a time interval which is much shorter compared to the diffusion time, the particle's position varies by $\Delta x = v\Delta t + \delta x$. The first contribution is due to the bulk motion of the scattering medium and the second term is due to the random walk diffusion with vanishing mean and the variance $\langle \delta x^2 \rangle = 2D(x, p)\Delta t$, where $D(x, p)$ denotes the diffusion coefficient.

- The distribution of galactic CRs is governed by a competition between injection, escape, energy gain (acceleration), and energy loss (catastrophic and continuous) processes. The transport equation which describes the balance of these processes is a Fokker-Planck type equation that includes the description of fluid motions, radiative losses, and phase space diffusion. It can be obtained by considering the collisionless Boltzmann equation and working out the magneto-hydrodynamic forces acting on a CR particle including the Lorentz force as well as pitch angle scattering on hydro-magnetic waves (details can be found in my *High Energy Astrophysics* lectures; in the following I only sketch the picture).

- The transport equation governs the evolution of the isotropic part $f(x, p)$ of the CR distribution function in phase space, assuming

weak anisotropy of the CR momentum distribution function:

$$\frac{\partial}{\partial t}f + \frac{\partial}{\partial x}v(x,p)f = -\frac{1}{p^2}\frac{\partial}{\partial p}p^2A(x,p)f + \frac{1}{p^2}\frac{\partial}{\partial p}p^2\Gamma(x,p)\frac{\partial}{\partial p}f + \frac{\partial}{\partial x}D(x,p)\frac{\partial}{\partial x}f + s(x,p). \quad (3.237)$$

The distribution is normalized such that the number density of CRs $n_{\rm CR} = 4\pi\int fp^2{\rm d}p$. The 'friction' term A describes not only various kinds of energy losses but also the energy gain by first order processes in $\beta \equiv v/c$ (adopting relativistic particles), the second contribution on the right-hand side describes the energy gain through the second order Fermi process, the third term on the right-hand side describes spatial diffusion, and the last term accounts for sources such as freshly injected CR particles at shocks whose origin can be understood by means of plasma physical calculations. The physical meaning of these processes will be sketched in the following:

– **Synchrotron and inverse Compton losses.** A relativistic charged particle of a Lorentz factor $\gamma = (1-\beta^2)^{-1/2}$ experiences Compton scattering with either real or virtual photons (which represent the magnetic field in the case of synchrotron radiation). This causes the particle to emit photons in the forward direction into a narrow cone of half-angle γ^{-1} with respect to its momentum leading to an energy loss which can effectively be described by a friction force in opposite direction to its momentum:

$$A_{\rm rad} \equiv \left.\frac{\langle\Delta p\rangle}{\Delta t}\right|_{\rm rad} = -\frac{4}{3}\sigma_{\rm T}\left(\frac{m_{\rm e}}{m}\right)^2(\varepsilon_B + \varepsilon_{\rm ph})\gamma^2, \quad (3.238)$$

where $\sigma_{\rm T}$ denotes the Thompson cross section, $\varepsilon_B = B^2/(8\pi)$ and $\varepsilon_{\rm ph}$ are the energy densities of the magnetic field (responsible for synchrotron losses) and the low energy photon field (causing the Compton effect in the Thompson regime). The radiative losses of baryons are suppressed by $(m_{\rm e}/m)^2$ such that they can be neglected unless they are ultra-high energetic CRs with energies $\gtrsim 10^{18}$ eV.

– **First order Fermi process.** The contribution of the first order Fermi process can be described by a non inertial entrainment due to the deceleration of the scattering medium: a compressed flow ($\boldsymbol{\nabla}\cdot\boldsymbol{v} < 0$) produces first order acceleration of charged particles. In this situation, the inertial force is $F_j = -p_i(\partial v_j/\partial x_i)$ that gives rise to an accelerating power

$$P_{\rm acc} = -\langle v_j p_i\rangle\frac{\partial v_j}{\partial x_i} = -\frac{pv}{3}\boldsymbol{\nabla}\cdot\boldsymbol{v} \quad \rightarrow \quad A_{\rm acc} = -\frac{p}{3}\frac{\partial v}{\partial x}. \quad (3.239)$$

– **Second order Fermi process.** Charged particles gyrate around, and travel slowly along magnetic field lines. Occasionally, they get scattered on magnetic irregularities and plasma waves (mostly Alfvén waves). This scattering process can be described by a random walk of the particle's pitch angle with the magnetic field direction, θ, yielding the characteristic variance $\langle \delta\mu^2 \rangle \propto \nu_s \Delta t$ where ν_s denotes the average scattering frequency and $\mu = \cos\theta$. Because the particle scatters off moving targets, the particle systematically gains energy through random variations of the CR momentum $\delta p = \pm\beta_A p \delta\mu$ where $\beta_A = v_A/c$ is the dimensionless Alfvén velocity in the case of scattering Alfvén waves. The second order Fermi process is thus described by a diffusion process in momentum space with the momentum diffusion coefficient

$$\Gamma \equiv \frac{\langle \delta p^2 \rangle}{2\Delta t} \sim \beta_A^2 \nu_s p^2. \tag{3.240}$$

– **Diffusive losses from the disk.** CRs experience momentum dependent diffusion in a turbulent magnetic field with a Kolmogorov-type spectrum on small scales. This process leads to a loss time scale which is proportional to $p^{-1/3}$. In an equilibrium situation, this results in a steepening of the observed spectrum within the disc by $p^{-1/3}$ relative to the injected spectrum.

– **Radioactive decay.** The observed isotope ratios resulting from radioactive decay provide a clock for cosmic ray transport and yields the time scale of diffusive losses from the disk. For any given isotope, radioactive decay can be a loss or a gain process in the equation of balance.

– **Coulomb and ionization losses** are strongest for protons or heavier nuclei, but also relevant for electrons. The ionization process limits the lower energy of the proton spectrum to approximately 50 MeV after traversing a path length through most of the interstellar medium. Energetic CRs experience energy losses even within an ionized medium through Coulomb interactions. Coulomb losses efficiently remove the low-energetic part of the injected CR spectrum on a short timescale and redistribute these particles and their energy into the thermal pool.

– **Catastrophic losses.** Another loss process is the inelastic reaction of CR nuclei with atoms and molecules of the interstellar medium. The CR protons interact hadronically with the ambient thermal gas and produce mainly neutral and charged pions, provided their momentum exceeds the kinematic threshold of 0.78 GeV for the reaction. The neutral pions successively decay into γ-rays while the charged

pions decay into secondary electrons and neutrinos.

– **Spallation.** Spallation describes the destruction of atomic nuclei in a collision with a CR particle that is in most cases a proton or an alpha particle. In this destruction process, many pieces of debris are formed where commonly a single nucleon gets stripped and a distribution of lighter nuclei is obtained. Since the abundances of the elements Lithium, Beryllium, and Boron are much larger in CRs than in the interstellar medium, spallation processes are assumed to account for the origin of these elements. For any specific isotope, spallation can again occur as a loss or a gain process in the equation of balance.

Chapter 4

Cluster Physics across Wavelengths

4.1 Optical: Galaxy Properties and Virial Theorem

4.1.1 Observational Facts

4.1.2 Galaxy Interactions and Transformations

Tidal Stripping and Shocks

Dynamical Friction

Ram Pressure Stripping

4.1.3 Virial Theorem

Derivation

Weighting a Cluster with Galaxies

4.2 Gravitational Lensing

The theory presented in this section is based on two main assumptions: (i) the Newtonian limit of a slowly varying gravitational field is taken from Einstein's field equations, namely $|\Phi| \ll c^2$ and $|v_{\rm lens}| \ll c$, in order to characterize the properties of lenses, and (ii) the lensing objects are considered to be thin, i.e. the deflecting mass is isolated and concentrated within a region L much smaller than the distances between source and deflector and deflector and observer, $L \ll cH_0^{-1}$. This approximation holds remarkably well in the astrophysical cases of galaxies or clusters of galaxies.

4.2.1 Deflection Angle

Linearizing the gravitational field equations and taking non–relativistic sources results in the "post–Minkowskian" metric to first order, neglecting the gravitational vector potential,

$$\mathrm{d}s^2 = \left(1 + \frac{2\Phi}{c^2}\right) c^2 \mathrm{d}t^2 - \left(1 - \frac{2\Phi}{c^2}\right) \mathrm{d}\boldsymbol{r}^{\,2}\,, \tag{4.1}$$

where Φ represents the Newtonian potential and $\mathrm{d}\boldsymbol{r}$ characterizes the spatial part of the Minkowski metric. Using the fact that light propagates on null geodesics, namely $\mathrm{d}s^2 = 0$, yields an effective velocity of light c' in the presence of a weak gravitational field,

$$c' = \frac{|\mathrm{d}\boldsymbol{r}|}{\mathrm{d}t} \simeq c\left(1 + \frac{2\Phi}{c^2}\right) \equiv \frac{c}{n}\,, \tag{4.2}$$

$$n = \left(1 - \frac{2\Phi}{c^2}\right) \geq 1\,, \tag{4.3}$$

which defines an *effective index of refraction n* of the gravitational field in analogy to geometrical optics in dense media. Note that the gravitational potential Φ is by definition negative as it represents an attractive gravitational force. Applying Fermat's principle leads to an equation for the spatial light paths by using the Euler–Lagrange equations for carrying out the variation

$$\delta \int_A^B n\,\mathrm{d}l = \delta \int_A^B n(\boldsymbol{r})\,\sqrt{|\dot{\boldsymbol{r}}|^2}\,\mathrm{d}\lambda \stackrel{!}{=} 0 \tag{4.4}$$

$$\text{or} \qquad \dot{\boldsymbol{r}} = -\frac{2}{c^2}\nabla_\perp \Phi(\boldsymbol{r}), \tag{4.5}$$

where the different curves are parametrized by the affine curve parameter λ, the dot denotes a derivative with respect to λ and $\nabla_\perp \Phi(\boldsymbol{r})$ is the gradient of the potential perpendicular to the perturbed light ray. The

total deflection is therefore the integral along the light path of the differential displacements,

$$\hat{\boldsymbol{\alpha}}(\boldsymbol{r}) = -\int \nabla_\perp n(\boldsymbol{r})\,\mathrm{d}l = \frac{2}{c^2}\int \nabla_\perp \Phi(\boldsymbol{r})\,\mathrm{d}l\,. \tag{4.6}$$

Because in nearly all cases of astrophysical interest the deflection angle is small, $\hat{\boldsymbol{\alpha}} \ll 1$, one usually applies the "Born approximation" and evaluates the integral along the unperturbed ray, i.e. along a straight line. Since the non–relativistic matter is characterized by its density perturbations only, the gravitational potential which gives rise to light deflections (4.6) neither depends on the actual nature of matter nor its composition or physical state. Therefore gravitational light deflection probes the total matter density of gravitationally interacting particles irrespective of baryonic and dark matter.

4.2.2 Lens Equation

The lensing equation relates the intrinsic angular source position of an astrophysical object to its observable image position on the sky which was possibly changed in the presence of gravitational light deflection along the line of sight. In order to derive this equation in the thin screen approximation, it is useful first to consider lensing by a point mass. The Newtonian potential as well as its perpendicular gradient can be written as

$$\Phi(\boldsymbol{\xi}, z) = -\frac{GM}{\sqrt{\xi^2 + z^2}} \tag{4.7}$$

$$\text{and} \qquad \nabla_\perp \Phi(\boldsymbol{\xi}, z) = \frac{GM\boldsymbol{\xi}}{(\xi^2 + z^2)^{3/2}}\,, \tag{4.8}$$

where the tree dimensional vector $\boldsymbol{r}$ is decomposed into the z–coordinate along the unperturbed ray and the two dimensional impact parameter $\boldsymbol{\xi}$ orthogonal to the unperturbed ray pointing towards the point mass. Equation (4.6) leads to the deflection angle

$$\hat{\alpha}(\boldsymbol{\xi}) = \frac{2}{c^2}\int_{-\infty}^{\infty} \frac{GM\boldsymbol{\xi}}{(\xi^2 + z^2)^{3/2}}\,\mathrm{d}z = \frac{4GM}{c^2\xi}\frac{\boldsymbol{\xi}}{|\boldsymbol{\xi}|} = \frac{2R_S}{\xi}\frac{\boldsymbol{\xi}}{|\boldsymbol{\xi}|}\,, \tag{4.9}$$

with R_S being the Schwarzschild radius of the point mass. The Born approximation in this context makes sure that the integral is evaluated along the straight coordinate line z.

If we now consider extended objects acting as lenses, but still located within a small region compared to the total distance between lens and observer, the mass distribution of the lensing object can be projected along the line of sight. The smooth three–dimensional distribution can then be replaced by a mass layer perpendicular to the line of sight, which

is called *lens plane*. The surface mass density on the lens plane is given by

$$\Sigma(\boldsymbol{\xi}) = \int \rho(\boldsymbol{\xi}, z)\, \mathrm{d}z\,, \tag{4.10}$$

and the deflection angle at position $\boldsymbol{\xi}$ is the overall deflection effect due to a superposition of "point–mass" elements in the plane because of linearity of the system:

$$\hat{\boldsymbol{\alpha}}(\boldsymbol{\xi}) = \frac{4G}{c^2} \int \frac{\Sigma(\boldsymbol{\xi}')(\boldsymbol{\xi} - \boldsymbol{\xi}')}{|\boldsymbol{\xi} - \boldsymbol{\xi}'|^2}\, \mathrm{d}^2\xi'\,. \tag{4.11}$$

This equation holds in the lens plane with the impact parameter measured in physical units. Assuming the small angle approximation, the *lens equation* relates the position of the source to the observable image position on the sky. The geometry of a typical gravitational lens system is shown in figure (4.1).

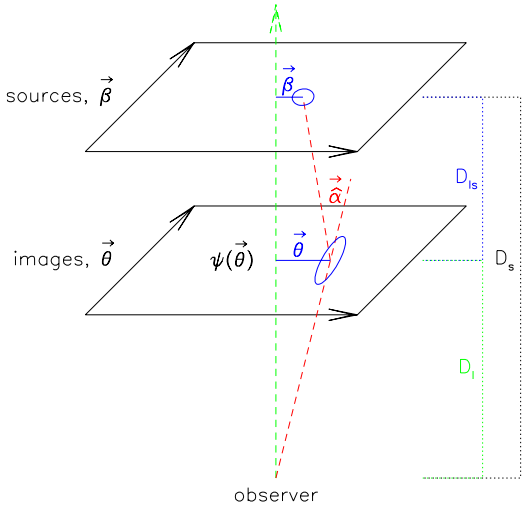

Figure 4.1: Illustration of a typical gravitational lens system. The angles are exaggerated for visualization purposes.

The true position of the source with respect to some arbitrarily chosen optical axis is denoted by $\boldsymbol{\beta}$ and the angular image position on the sky as viewed by an observer is given by $\boldsymbol{\theta}$. All distances along the line of sight are angular diameter distances, where D_{ls} denotes the distance between lens and source, D_l the distance between lens and observer and D_s the distance between source and observer. Using the relation $\boldsymbol{\xi} \simeq D_l\boldsymbol{\theta}$ and introducing the reduced deflection angle,

$$\boldsymbol{\alpha}(\boldsymbol{\theta}) = \frac{D_{ls}}{D_s}\hat{\boldsymbol{\alpha}}(\boldsymbol{\theta}), \tag{4.12}$$

equation (4.11) can be written as

$$\boldsymbol{\alpha}(\boldsymbol{\theta}) = \frac{4G}{c^2}\frac{D_l D_{ls}}{D_s} \int \frac{\Sigma(\boldsymbol{\theta}')(\boldsymbol{\theta} - \boldsymbol{\theta}')}{|\boldsymbol{\theta} - \boldsymbol{\theta}'|^2}\, \mathrm{d}^2\theta'\,. \tag{4.13}$$

The critical surface mass density $\Sigma_{\rm cr}$ and the convergence κ are defined by

$$\Sigma_{\rm cr} \equiv \left(\frac{4\pi G}{c^2}\frac{D_l D_{ls}}{D_s}\right)^{-1} \qquad \text{and} \qquad \kappa \equiv \frac{\Sigma}{\Sigma_{\rm cr}}\,. \tag{4.14}$$

It is important to note that the distance combination appearing in equation (4.13), $\frac{D_l D_{ls}}{D_s}$, acts as a lensing efficiency function. It approaches zero at both the source and the observer and has a maximum in between. Using definitions (4.14), the deflection angle as a function of the image position $\boldsymbol{\theta}$ reduces to

$$\boldsymbol{\alpha}(\boldsymbol{\theta}) = \frac{1}{\pi}\int \kappa(\boldsymbol{\theta}')\frac{\boldsymbol{\theta}-\boldsymbol{\theta}'}{|\boldsymbol{\theta}-\boldsymbol{\theta}'|^2}\,\mathrm{d}^2\theta'\,. \tag{4.15}$$

This equation shows that only the ration of Σ and $\Sigma_{\rm cr}$ is measurable, or in other words, using gravitational lensing on its own, one is not able to determine both the mass of a lensing object and the involved distances independently. From figure (4.1) we can read off $\boldsymbol{\theta} D_s - \hat{\boldsymbol{\alpha}} D_{ls} = \boldsymbol{\beta} D_s$, assuming the small angle approximation and using the theorem on intersecting lines. Using the expression for the reduced deflection angle, this establishes the *lens equation* in its simplest form

$$\boldsymbol{\beta} = \boldsymbol{\theta} - \boldsymbol{\alpha}(\boldsymbol{\theta})\,. \tag{4.16}$$

In general, this equation is nonlinear and can thus yield multiple images on the sky for a single source position $\boldsymbol{\beta}$. Moreover, the shape and the size of the images will differ from the original source because light bundles are deflected differentially.

4.2.3 Circular Symmetric Lenses – Einstein Radius

Consider a circularly symmetric lens with an arbitrary mass profile. Due to the high degree of symmetry, we can place the coordinate origin at the center of symmetry and reduce light deflection to a one-dimensional problem. The deflection angle always points toward the center of symmetry with a modulus

$$\hat{\alpha}(\xi) = \frac{4GM(\xi)}{c^2\xi}, \tag{4.17}$$

where $\xi = D_l\theta$ is the distance from the lens center and $M(\xi)$ is the enclosed mass within ξ,

$$M(\xi) = 2\pi\int_0^{\xi}\Sigma(\xi')\xi'\mathrm{d}\xi'. \tag{4.18}$$

Combining equations (4.12) and (4.17) enables us to rewrite the lensing equation (4.19), yielding

$$\beta(\theta) = \theta - \frac{D_{ls}}{D_l D_s}\,\frac{4GM(\theta)}{c^2\theta} \tag{4.19}$$

Owing to the rotational symmetry of the lens, a source, which lies exactly on the optical axis ($\beta = 0$) is imaged as a ring if the lens is supercritical ($\Sigma > \Sigma_{\rm cr}$). Setting $\beta = 0$ in equation (4.19) gives the radius of the ring, the so-called *Einstein radius*,

$$\theta_{\rm E} = \sqrt{\frac{4GM(\theta)}{c^2}\,\frac{D_{ls}}{D_l D_s}}. \tag{4.20}$$

It is not only a property of the lens, but also depends on the distance efficiency function. It provides the natural angular scale to describe the lensing geometry for the following reasons: (i) in the case of multiple imaging, the angular separation of images is of order $2\theta_{\rm E}$, (ii) sources that lie closer than approximately $\theta_{\rm E}$ to the optical axis experience strong lensing yielding to strong magnification and sheared images whereas sources at much larger distances are only very little magnified, and (iii) in many lens models the Einstein radius roughly represents the boundary of source positions that are either multiply-imaged if they lie inside $\theta_{\rm E}$ or singly-imaged. Comparing equations (4.14) and (4.20) reveals that the surface mass density inside $\theta_{\rm E}$ is exactly the critical surface density $\Sigma_{\rm cr}$. For a point mass, we can obtain the Einstein radius

$$\theta_{\rm E} = \sqrt{\frac{4GM}{c^2}\,\frac{D_{ls}}{D_l D_s}} \approx 30'' \left(\frac{M}{10^{14} M_\odot}\right)^{1/2} \left(\frac{D}{\rm Gpc}\right)^{-1/2}, \tag{4.21}$$

where we defined the lensing efficiency distance $D = D_l D_s / D_{ls}$ and inserted typical values for clusters to highlight the relevant angular scales for giant (tangential) arcs in clusters. In the case of clusters, detailed mass modeling is necessary since only a fraction of the cluster mass resides within the Einstein radius.

For a point mass lens, we can use the Einstein radius of equation (4.20) to rewrite the lens equation in the form

$$\beta = \theta - \frac{\theta_{\rm E}^2}{\theta}. \tag{4.22}$$

This equation has two solutions

$$\theta_\pm = \frac{1}{2}\left(\beta \pm \sqrt{\beta^2 + 4\theta_{\rm E}^2}\right). \tag{4.23}$$

Any source inside $\theta_{\rm E}$ is imaged twice by a point mass lens. The two images are on either side of the source with one image inside the Einstein ring and the other one outside. As the source moves away from the center of the lens (i.e., with increasing β), one of the images approaches the lens and becomes very faint, while the other image approaches the true position of the source and tends toward a magnification of order unity.

4.2.4 The Lensing Potential and Local Lens Properties

It is convenient to define the lensing potential $\Psi(\boldsymbol{\theta})$ which is the scaled and projected Newtonian potential of the lens,

$$\Psi(\boldsymbol{\theta}) = \frac{D_{ls}}{D_l D_s}\frac{2}{c^2}\int \Phi(D_l\boldsymbol{\theta}, z)\mathrm{d}z\,. \tag{4.24}$$

The lensing potential has the nice property that its gradient with respect to $\boldsymbol{\theta}$ is the deflection angle

$$\nabla_\theta\Psi(\boldsymbol{\theta}) = \frac{D_{ls}}{D_s}\frac{2}{c^2}\int \nabla_\perp\Phi(\boldsymbol{\xi}, z)\mathrm{d}z = \boldsymbol{\alpha}(\boldsymbol{\theta}), \tag{4.25}$$

where the perpendicular gradient is now acting on the physical impact parameter having used the small angle approximation $\boldsymbol{\xi} \simeq D_l\boldsymbol{\theta}$. Assuming further that the changes of the Newtonian potential along the line of sight average out, which is true for instance, as long as the lensing object is only slowly varying and does not undergo a rapid collapse. More precisely, the time–scale on which light travels across the lensing object, has to be much smaller than the collapse time–scale of the light deflecting object. Then the two–dimensional Laplacian can be replaced by its three–dimensional analogue,

$$\Delta^{(2)}\Phi(\boldsymbol{r}) = \sum_{i=1}^{2}\frac{\partial^2\Phi(\boldsymbol{r})}{\partial\xi_i^2} \simeq \sum_{i=1}^{3}\frac{\partial^2\Phi(\boldsymbol{r})}{\partial r_i^2} = \Delta^{(3)}\Phi(\boldsymbol{r})\,. \tag{4.26}$$

Therefore, the Laplacian of the lensing potential acting on its angular coordinate $\boldsymbol{\theta}$ equals twice the surface mass density scaled with its critical value, i.e. the convergence κ,

$$\Delta_\theta^{(2)}\Psi(\boldsymbol{\theta}) = \frac{2}{c^2}\frac{D_l D_{ls}}{D_s}\int \Delta^{(3)}\Phi(\boldsymbol{\xi}, z)\mathrm{d}z = 2\frac{4\pi G}{c^2}\frac{D_l D_{ls}}{D_s}\int \rho(\boldsymbol{\xi}, z)\mathrm{d}z = 2\kappa(\boldsymbol{\theta})\,, \tag{4.27}$$

where Poisson's equation has been used in the second step. Since Ψ satisfies the two–dimensional Poisson's equation, its Green's function has to be considered, namely

$$\Delta^{(2)}G(\boldsymbol{\theta}, \boldsymbol{\theta}') = 2\pi\delta_D(\boldsymbol{\theta}, \boldsymbol{\theta}') \qquad \Longrightarrow \qquad G(\boldsymbol{\theta}, \boldsymbol{\theta}') = \ln|\boldsymbol{\theta} - \boldsymbol{\theta}'|\,. \tag{4.28}$$

Therefore the lensing potential $\Psi(\boldsymbol{\theta})$ is given by the convolution integral of the source function $\kappa(\boldsymbol{\theta})$ and the Green's function in two dimensions,

$$\Psi(\boldsymbol{\theta}) = \frac{1}{\pi}\int \kappa(\boldsymbol{\theta}')\ln|\boldsymbol{\theta} - \boldsymbol{\theta}'|\mathrm{d}^2\theta'\,. \tag{4.29}$$

Liouville's theorem and the conservation of the physical number density of photons during the process of gravitational light bending imply that lensing conserves surface brightness or specific intensity. Assuming that the angular scale on which the lens properties change is much larger

than the extent of the source, the lens equation can locally be linearized yielding

$$\boldsymbol{\beta} = \boldsymbol{\theta} - \boldsymbol{\alpha}(\boldsymbol{\theta}) \simeq \boldsymbol{\beta}_0 + \frac{\partial \boldsymbol{\beta}}{\partial \boldsymbol{\theta}} (\boldsymbol{\theta} - \boldsymbol{\theta}_0) \,. \tag{4.30}$$

The local lens properties of the lens mapping are described by its Jacobian matrix $\mathcal{A}$

$$\mathcal{A} \equiv \frac{\partial \boldsymbol{\beta}}{\partial \boldsymbol{\theta}} = \left(\delta_{ij} - \frac{\partial \alpha_i(\boldsymbol{\theta})}{\partial \theta_j} \right) = \left(\delta_{ij} - \frac{\partial^2 \Psi(\boldsymbol{\theta})}{\partial \theta_i \partial \theta_j} \right) \equiv \left(\delta_{ij} - \Psi_{,ij}(\boldsymbol{\theta}) \right) = \mathcal{M}^{-1} \,, \tag{4.31}$$

where an abbreviation for partial derivatives has been introduced and $\mathcal{A}$ is the inverse of the magnification tensor $\mathcal{M}$. This is justified, because a solid–angle element $\delta\beta^2$ of the source is mapped onto the solid–angle element $\delta\theta^2$ on the image, and thus the magnification due to the mapping is given by

$$\frac{\delta\theta^2}{\delta\beta^2} = \det \mathcal{M} = \frac{1}{\det \mathcal{A}} \,. \tag{4.32}$$

The trace of the Jacobian $\mathcal{A}$ describes the isotropic magnification of the source,

$$\mathrm{tr}(\mathcal{A}) = (1 - \Psi_{,11}) + (1 - \Psi_{,22}) = 2(1 - \kappa) \,. \tag{4.33}$$

This also intuitively explains the meaning of the convergence κ, which is a measure for how much the lens focuses light rays isotropically. Subtracting the trace from $\mathcal{A}$ leads to an expression for anisotropic distortion (astigmatism) of the image,

$$\mathcal{A}_{ij} - \frac{1}{2}\delta_{ij}\,\mathrm{tr}(\mathcal{A}) = \delta_{ij} - \Psi_{,ij} - \delta_{ij}(1 - \kappa) = -\Psi_{,ij} + \kappa\delta_{ij} \equiv \Gamma \,, \tag{4.34}$$

where the *shear tensor* Γ has been defined in the last step. This distortion is due to the tidal gravitational field. Particularly, it decomposes in

$$\Gamma = \begin{pmatrix} \gamma_1 & \gamma_2 \\ \gamma_2 & -\gamma_1 \end{pmatrix} \tag{4.35}$$

and

$$\gamma_1 = \frac{1}{2}(\Psi_{,11} - \Psi_{,22}) \equiv \gamma(\boldsymbol{\theta}) \cos\left(2\phi(\boldsymbol{\theta})\right) \tag{4.36}$$

$$\gamma_2 = \Psi_{,12} = \Psi_{,21} \equiv \gamma(\boldsymbol{\theta}) \sin\left(2\phi(\boldsymbol{\theta})\right) \,. \tag{4.37}$$

Here $\gamma = \sqrt{\gamma_1^2 + \gamma_2^2}$ describes the magnitude of the shear and ϕ its orientation, whereas the factor 2 shows that γ is not a vector, but a 2×2–tensor.

4.2.5 Strong and Weak Cluster Lensing

The name of the game in cluster lensing research consists in reconstructing the mass distribution. Depending on the type of lensing – strong or weak lensing – there are different algorithms used.

Strong Cluster Lensing

Using our simplified mass density model of a singular isothermal sphere (SIS, see Section 2.4.1), we can readily work out the relevant strong lensing properties for this model. Recall that the mass density and rotational velocity in this model was given by

$$\rho(r) = \frac{\sigma_v^2}{2\pi G}\frac{1}{r^2} \quad \text{and} \quad v_{\rm rot}^2 = \frac{GM(r)}{r} = 2\sigma_v^2 = \text{const.} \tag{4.38}$$

Upon projection the density along the line-of-sight, we obtain the surface mass density

$$\Sigma(\xi) = \int_0^s \rho(\boldsymbol{\xi}, z)\mathrm{d}z = 2\int_\xi^\infty \frac{\rho(r)r\mathrm{d}r}{\sqrt{r^2-\xi^2}} = \frac{\sigma_v^2}{2G}\frac{1}{\xi}, \tag{4.39}$$

where ξ is the distance from the center of the two-dimensional profile. Using equation (4.17), we obtain the deflection angle

$$\hat{\alpha} = 4\pi\frac{\sigma_v^2}{c^2} \tag{4.40}$$

which is independent of ξ and points to the center of the lens. The Einstein radius of the SIS is given by equation (4.20),

$$\theta_{\rm E} = 4\pi\frac{\sigma_v^2}{c^2}\frac{D_{ls}}{D_s} = \hat{\alpha}\frac{D_{ls}}{D_s} = \alpha. \tag{4.41}$$

The symmetry of the problem reduces the dimensionality of the problem to become one-dimensional. Multiple images are only obtained if the source lies inside the Einstein ring, i.e., if $\beta < \theta_{\rm E}$. If this condition is satisfied, we obtain the following two solutions,

$$\theta_\pm = \beta \pm \theta_{\rm E}. \tag{4.42}$$

The images at $\theta_\pm$, the source, and the lens all lie on a straight line. (The third image with zero flux lies at $\theta = 0$ and only acquires a non-zero flux if the singularity of the lens is replaced by a core of finite density).

Rich concentrated clusters can produce giant arcs when a background galaxy is aligned with one of the cluster caustics. Typically, a parametrized lens model (such as the SIS above or a more complicated functional form) is optimized so as to obtain a good fit to the observed image. If there are many constraints from a number of strongly lensed galaxies such as their position and detailed properties of their distortion (magnitude distribution across their arcs), ray tracing through an adaptive grid is possible. This can even constrain the detailed mass distribution within the cluster including their substructure mass distribution.

Weak Cluster Lensing – The Kaiser & Squires Algorithm

Every cluster weakly distorts images of a large number of background galaxies giving rise to so-called arclets – this phenomenon is referred to as weak lensing. With the development of the Kaiser & Squires (1993) algorithm, weak lensing is being used increasingly to derive parameter-free two-dimensional mass maps of galaxy clusters.

Kaiser & Squires Algorithm:

4.3 X-rays: Astrophysics at High Resolution

4.3.1 Hydrostatic Equilibrium Masses and Biases

4.3.2 Kinematics of Shocks and Cold Fronts

4.3.3 Probing Kinetic Equilibrium with Collisionless Shocks

4.3.4 Width of Cold Fronts – Magnetic Draping

4.4 Sunyaev-Zel'dovich (SZ) Effect: Cluster Calorimeter

4.4.1 Thermal and Kinetic SZ Effect

4.4.2 SZ Scaling Relation and Biases

4.4.3 SZ Power Spectrum

4.5 Radio Emission: Shocks and Plasma Physics

4.5.1 Radio Halos

4.5.2 Radio Relics

4.5.3 Radio Galaxies

Appendix A

Additional Material

A.1 Useful stuff

A.2 Schwarzschild Criterion for Convective Instability

Index